ISTANBUL TECHNICAL UNIVERSITY ★ GRADUATE SCHOOL OF SCIENCE ENGINEERING AND TECHNOLOGY

DESIGN AND IMPLEMENTATION OF ORIGAMI INSPIRED MINIATURE PARALLEL MECHANISMS

M.Sc. THESIS

Hasan SEVİNÇ

Department of Mechatronics Engineering

Mechatronics Engineering Programme

July 2020

ISTANBUL TECHNICAL UNIVERSITY ★ GRADUATE SCHOOL OF SCIENCE ENGINEERING AND TECHNOLOGY

DESIGN AND IMPLEMENTATION OF ORIGAMI INSPIRED MINIATURE PARALLEL MECHANISMS

M.Sc. THESIS

Hasan SEVİNÇ
518171020

Department of Mechatronics Engineering

Mechatronics Engineering Programme

Thesis Advisor: Assist. Prof. Dr. Atakan ALTINKAYNAK
Thesis Co-Advisor: Dr. Merve ACER KALAFAT

July 2020

<u>ISTANBUL TEKNİK ÜNİVERSİTESİ ★ FEN BİLİMLERİ ENSTİTÜSÜ</u>

ORİGAMİDEN ESİNLENİLMİŞ MİNYATÜR PARALEL MEKANİZMALARIN TASARIMI VE UYGULAMASI

YÜKSEK LİSANS TEZİ

Hasan SEVİNÇ
518717020

Mekatronik Mühendisliği Anabilim Dalı

Mekatronik Mühendisliği Programı

Tez Danışmanı: Dr. Öğr. Üyesi Atakan ALTINKAYNAK
Eş Danışman: Öğr. Gör. Dr. Merve ACER KALAFAT

Temmuz 2020

Hasan Sevinç, a M.Sc. student of ITU Graduate School of Science Engineering and Technology student ID 518171020, successfully defended the thesis entitled "DESIGN AND IMPLEMENTATION OF ORIGAMI INSPIRED MINIATURE PARALLEL MECHANISMS", which he prepared after fulfilling the requirements specified in the associated legislations, before the jury whose signatures are below.

Thesis Advisor:	**Assist. Prof. Dr. Atakan ALTINKAYNAK** İstanbul Technical University	....
Co-advisor:	**Dr. Merve ACER KALAFAT** İstanbul Technical University	....
Jury Members:	**Assoc. Prof. Dr. Volkan SEZER** Istanbul Technical University	....
	Assoc. Prof. Dr. Meltem ELİTAŞ Sabancı University	....
	Assoc. Prof. Dr. Erkin DİNÇMEN Işık University	....

Date of Submission : 15 June 2020
Date of Defense : 8 July 2020

To my beloved family,

FOREWORD

I would like to express my genuine gratitude to my advisor, Dr. Merve Acer. Thank you for all your help and guidance during my education in ITU from my bachelor to my master degree. Thank you for being caring, understanding and always supportive.

Furthermore, I would like to thank Assis. Prof. Dr. Atakan Altınkaynak for his most valuable advices, feedbacks, methods and jokes during this project and his efforts to always get us in to the right track. Also, big thanks to Assis. Prof. Dr. Fatma Zeynep Temel for her helps in this project and compelling reviews.

I want to thank my laboratory partner Shahrad Samankan for all the things he has done for me and the valuable moments we created during this time. Likewise, big thanks to Furkan Yıldız for always answering my foolish questions, to Uğur Sarıduran, Atilla Çalışkan and Harun Atasoy for always listening my complainings and thanks to many more friends whom I could not write their names.

Last but not least, I would like to give my most sincere gratitude to my family. Thank you for your love, your sacrifices and your supports for my whole life. I would not be the person I am today without everything you have done for me.

This thesis is financially supported by The Scientific and Technological Research Council of Turkey (TUBITAK) under grant number 216M193.

May 2020

Hasan SEVİNÇ
Mechanical Engineer

TABLE OF CONTENTS

Page

ABBREVIATIONS

DoF	: Degree of freedom
SCM	: Smart Composite Micro-structures
TPU	: Thermoplastic polyurethane
PET	: Polyethylene terephthalate
DAQ	: Data acquisition
MEMS	: Micro-electro-mechanical systems
CAD	: Computer Aided Design
RMS	: Root Mean Square

SYMBOLS

$\boldsymbol{\theta_i}$	: Rotational Input for all three mechanism
$\boldsymbol{\varphi_i}$	: Passive joint angle in Pantograph mechanism
$\mathbf{d_3}$	: Linear input for Pantograph mechanism
$\mathbf{d_i}$	: Link lengths of the Pantograph mechanism
$\mathbf{P_i}$	: End effector's center position
$\mathbf{P_x}, \mathbf{P_y}, \mathbf{P_z}$	: Cartesian coordinate system representation of P_i
$\mathbf{P_0}$	: Inertial reference point
f	: Equilateral triangle's side length of base platform in Delta mechanism
e	: Equilateral triangle's side length of moving platform in Delta mechanism
$\mathbf{r_e}$	: Length of upper arm in Delta mechanism
$\mathbf{r_f}$	: Length of lower arm in Delta mechanism
df	: Distance between the two equilateral triangle in Delta mechanism
u	: Length of upper (long) leg in Stewart mechanism
k	: Length of lower (short) leg in Stewart mechanism
$\mathbf{L_i}$	: Distance between the corners of moving and base platform in Stewart mechanism
$\mathbf{R_s}$	: Rotation matrix of moving platform in Stewart mechanism
$\boldsymbol{\alpha_i}$	: Individual angle between the lower leg and X axis in Stewart mechanism
R	: Resistance
$\mathbf{R_x}$	: Resistance of the embedded sensor
$\mathbf{V_i}$	: Voltage

LIST OF TABLES

Page

LIST OF FIGURES

Page

DESIGN AND IMPLEMENTATION OF ORIGAMI INSPIRED MINIATURE PARALLEL MECHANISMS

SUMMARY

Nowadays, robotic systems are not only used for heavy industries, but also they are used for medicine, agriculture, service sectors or such places that can interact with daily life of people. As it can be expected, each sector has its own unique and different requirements. These differences can be mechanical properties such as scale, material, weight, or it can be new working conditions, workspaces and even physical appearance. However, these new demands cannot be met with the existing traditional methods. Particularly, the design and fabrication of small-scale robotic systems is very difficult. The reasons for this can be said that reduced strength due to the small size of the dimensions, the need for very small fasteners and the difficulty in the assembly of their small structures, which results in time consuming operations and high cost.

In this study, parallel mechanisms with embedded sensor are designed by making use of origami-inspired design methods and 2D monolithic layered production techniques, which is commonly used for small-scale robotic systems. In addition, it is aimed that there are no intermediate steps such as folding and bonding outside of basic steps of the chosen methods that disrupts the planar structure during assembly. The assembly process of the mechanisms to be produced consists only of the cut – bond – repeat cycle that comes from the 2D fabrication methods. The sensor to be embedded in the mechanisms must also be suitable for the manufacturing technique. The fabrication method used in the project has been selected as "Smart Composite Microstructures" (SCM). This fabrication method can basically be described as cutting and joining sheet materials of different properties with certain patterns on top of each other. As a result, a simple five-layered structure emerges. These layers are rigid – adhesive – flexible – adhesive – rigid layers, respectively. The used materials are American Bristol paper with 400 grams for rigid layer, while plastic sheets are called PET for flexible layer and single and two layered 3D printed TPU material. Origami-inspired design methods were used for the patterns to be created (more specifically the joints) for the mechanisms. There are different types of joints present in the designs, which are one, two and three degrees of freedom joints.

The reason for choosing parallel mechanisms is that they are scalable in terms of their structures, that is, they do not lose their properties as their dimension decreases. Even in some cases, the performance increases even if the structure gets smaller. Another reason is the compatibility of parallel mechanisms with closed loop kinematic chains to 2D production techniques. The reason for this is that all the arms are interconnected, have no open ends, and therefore the layers can be designed completely integrated. There are three different parallel mechanisms to be designed in this project. These are called the Pantograph, Delta and Stewart mechanism. The design process started with the Pantograph mechanism with 2 degrees of freedom and continued with the three degrees of freedom Delta mechanism, and finally ended with the six degree of freedom Stewart mechanism. As it can be seen, the aim is to design mechanisms that have

different degrees of freedom; from simple to complex. For all three mechanisms, initially the traditional counterparts are examined. The structure of the mechanisms and the joints types that are going to be used are determined. Then according to those analyses, the kinematic models are obtained. Using these information, 2D pattern designs for the fabrication are created. After that, 3D models of the mechanisms are drawn in order to compare with the kinematic models to see if the behavior of the designed joints are matching with mathematical models. Finally, after validating the mechanisms, the fabrications are realized using the 2D production technique “SCM”.

A sensor must be designed to measure the required angles when calculating the position of the end point of the mechanisms. With the help of this sensor, control of motors and the end effectors can be made using the right dynamic models in the future projects. The sensor designed in this project was made to measure the angle between two rigid arms. A strain gauge is designed for the flexible layer between the rigids to take advantage of the stresses and elongations happening on the surface of the flexible layer due to the rotations between the links. Silver nano-particle ink and inkjet printers have been used since the strain gauges currently on the market are not suitable for integration in between layers. When the printed PET sheet is placed in the joints in the rigid sheets, a connection is formed with the angle between the two rigid sheets and the elongation in the flexible sheet. Detailed studies have been made not only on the design part of the sensor, but also on its location, layouts, cuts and cable connections. Later, sensors were designed and integrated into the production method into the required parts of each mechanism.

Test platforms were designed specifically for each of the mechanisms. These test platforms are produced with 3D printers and contains mechanism’s connection location, motor locations, motor-leg connection equipment and the reference apparatus of the position sensor, which tracks the translational and rotational motions of the end effectors. Robot servo motors are used for the experiments. Carried out experiments can be listed as point tests, continuous motion tests with the circle profile, and rotational motion tests only for the Stewart mechanism. In addition, in order to see the effect of different flexible materials, the same experiments were repeated using the Delta mechanism with different flexible layers. The sensor data is collected using a voltage divider circuit and a DAQ signal processing card.

ORİGAMİDEN ESİNLENİLMİŞ MİNYATÜR PARALEL MEKANİZMALARIN TASARIMI VE UYGULAMASI

ÖZET

Robotik sistemler artık sadece ağır sanayi ve endüstride kullanılmaktan çıkmış olup tıp, tarım ve ya hizmet sektörü gibi insanların hayatı ile etkileşime geçebilecek yerler gibi bir sürü sektör içine girmeye başlamıştır. Tahmin edilebileceği gibi her sektörün kendine özgü istekleri vardır. Bu farklılıklar ölçek, malzeme, ağırlık gibi mekanik özellikler olabileceği gibi yeni çalışma şartları, çalışma alanları ve hatta dış görünüş olarak bile sıralanabilir. Fakat ortaya çıkan bu yeni istekleri, var olan geleneksel yöntemler karşılayamamaya başlamıştır. Özellikle küçük ölçekli robotik sistemlerin tasarımı ve üretimi oldukça zordur. Bunun sebepleri ölçülerin küçüklüğü nedeni ile dayanımın düşmesi, çok küçük bağlantı elemanlarına ihtiyacın olması ve küçük yapılarının birleştirme zorluğu gibi zaman alıcı işlemler ve yüksek maliyet olarak söylenebilir.

Bu çalışmada küçük ölçekli robotik sistemler için yaygın olarak kullanılan origamiden esinlenilmiş tasarım yöntemlerinden ve iki boyutlu yekpare katmanlı üretim tekniklerinden yararlanılarak, içinde gömülü sensörü bulunan paralel mekanizma tasarımı yapılmıştır. Buna ek olarak yekpare üretim tekniğinde sürekli karşılaşılan, montaj sırasında düzlemsel yapıyı bozan ve kullanılan tekniğin temel basamakları dışında katlama ve yapıştırma gibi ara basakların olmaması amaçlanmıştır. Üretilmek istenen mekanizmaların montaj süreci sadece teknikten gelen kes – yapıştır – tekrarla adımlarından oluşmaktadır. Bununla birlikte mekanizmaların içine gömülecek sensörün de kullanılan üretim tekniğine uygun olması gerekmektedir.

Projede kullanılan üretim yöntemi “Akıllı Kompozit Mikro-yapılar” (Smart Composite Micro-structures “SCM”) olarak seçilmiştir. Bu üretim yöntemi temel olarak farklı özelliklerdeki levha malzemelerin belirli desenler ile kesilip üst üste birleştirilmesi olarak tarif edilebilir. Bu yöntem ile yapı içerisine mekanizmalardaki mafsalları taklit eden eklem yapıları yerleştirilebilir. Eklemler iki farklı rijit parçanın birbiri ile esnek bir parça tarafından bağlanması ile oluşturulur. Sonuç olarak ortaya en basit olarak beş katmanlı bir yapı çıkmaktadır. Bu katmanlar sırası ile rijit – yapışkan – esnek – yapışkan – rijit katmanlardır. Rijit katmanların karşılıklı belirli bölgeleri kesilirse ve aralarında sadece esnek katmak kalması sağlanırsa, esnek katmanın özelliklerine bağlı olarak iki ayrı rijit katman birbirinden bağımsız olarak hareket edebilir. Böylece eğer kesilecek desenler doğru bir şekilde tasarlanırsa bu yöntem ile bir mekanizma üretmek mümkündür. Bunların dışında bu çalışmada kullanılan malzemeler rijit katman için 400 gram ağırlığındaki Amerikan Bristol kâğıdı iken esnek katman için PET adı verilen plastik levhalar ve üç boyutlu yazıcıdan tek ve iki katmanlı basılmış TPU malzemesidir.

Mekanizmalarda kullanılacak desenler için origamiden esinlenilmiş tasarım yöntemleri kullanılmıştır. Daha spesifik olarak mekanizmaların eklemleri kastedilmektedir. Tasarlanacak mekanizmalarda bir, iki ve üç serbestlik dereceli olmak üzere farklı eklem tipleri bulunmaktadır. Bu eklem tiplerinin oluşturduğu

desenlerin en temel elemanı aynı olsa bile yerleşimleri farklıdır. Örnek vermek gerekirse bir serbestlik dereceli döner eklemin deseni basit olarak bir kesik çizgidir. Rijit bir levhanın ortasına bir kesik atılırsa ve bu oluşan iki ayrı parça birbirleri ile bir esnek levha ile bağlanırsa, bağımsız olarak tek eksende dönebilirler. Benzer olarak iki serbestlik dereceli üniversal eklem, iki tane bir serbestlik dereceli eklemin 90º derece açı ve bir uç noktaları birleşecek şekilde yerleştirilmesi ile oluşmaktadır. Bunlardan biraz daha karmaşık olarak üç serbestlik dereceli küresel eklem iki çapraz kesik ve ortadan geçen bir düz kesik ile oluşturulabilir. Oluşturulan bu eklemler mekanizmaların geleneksel yapıları göz önünde bulundurularak rijit levha üzerine yerleştirilir. Daha sonra seçilmiş olan üretim yöntemi ile mekanizmalar üretilmiştir.

Bu projede tasarlanmak istenen üç tane farklı paralel mekanizma vardır. Bunlar Pantograf, Delta ve Stewart mekanizmasıdır. Tasarım süreci 2 serbestlik dereceli olan Pantograf mekanizmasından başlayıp, 3 serbestlik dereceli olan Delta mekanizması ile devam etmiş son olarak da altı serbestlik dereceli Stewart mekanizması ile sona ermiştir. Görüldüğü gibi amaç birbirinden farklı serbestlik derecelerine sahip olan mekanizmaların tasarımını gerçekleştirmektir. Paralel mekanizmaların seçilme nedeni yapıları itibari ile ölçeklenebilir olmaları yani boyutları küçüldükçe bulunan özelliklerini yitirmemeleridir. Hatta bazı durumlarda yapı küçüldükçe performansın artığı bile görülmektedir. Diğer bir sebep ise kapalı çevrim kinematik zincire sahip paralel mekanizmaların 2D üretim tekniklerine uygunluğudur. Bunun nedeni bütün kolların birbiri ile bağlı olup, açık bir ucunun olmaması ve dolayısıyla katmanların tamamen entegre bir şekilde tasarlanabilmesidir. Bu bilgiler ışığında origamiden esinlenilmiş yöntemler ve 2D üretim tekniği ile paralel mekanizmalar ortaya çıkarılmıştır.

Pantograf mekanizması projedeki en basit mekanizmadır ve ilk deneylerin yapıldığı başlangıç mekanizmasıdır. Bu mekanizmada istenen tasarım esasları, üretim yöntemi ve gömülü sensörün genel olarak nasıl yapılabileceğinin testleri yapılmıştır. Bir ucu sabitlendiğinde öteki ucu, orta noktasına verilen hareketi belirli bir oran ile tekrar edebilen bu mekanizma eskiden kopyalama işlerinde kullanılmıştır. Bu projede ise sabitlenen kısma bir açısal eyleyici ve mekanizmanın orta noktası ile başka bir nokta arasına bir lineer eyleyici koyularak iki serbestlik dereceye sahip olacak şekilde tasarlanmıştır. Ortaya çıkan yapının kinematik analizleri gerçekleştirilmiştir. Sonra bu yapının desenleri iki boyutlu çizim programları kullanılarak daha önce bahsedilen tekniklere uygun şekilde ortaya çıkarılmıştır. Yapısı gereği sadece döner eklemlerden oluştuğu için ortaya çıkan desenler çok karmaşık değildirler. İki boyutlu tasarımı yapıldıktan sonra mekanizmanın üç boyutlu modeli katı modelleme programları ile oluşturulmuştur. Kinematik model ile oluşturulan bu katı modelin karşılaştırılması yapılarak, tasarlanan kolların rijit olması durumunda bu iki modelin hareketlerinin birbiri ile uygun olduğu görülmüştür. Son olarak tasarlanan mekanizmanın üretimi gerçekleştirilmiştir. Pantograf mekanizması ön deneylerin yapıldığı mekanizma olduğu için detaylı deneyleri yapılmamıştır.

Tasarlanan ikinci mekanizma üç serbestlik derece Delta mekanizmasıdır. Delta mekanizması 1990'larda Clavel tarafından tut – ve – bırak işlemi için tasarlanmıştır. Bir hareketli platform, bir sabit platform, üç paralelogram yapısı ve üç bacaktan oluşmaktadır. İçerisinde bulunan eklemler ise döner ve üniversal eklemlerdir. Mekanizmanın hareketli platformu her zaman sabit platform ile paralel hareket etmektedir. Mekanizmanın tasarımı geleneksel Delta mekanizmasının tasarımı göz önüne alınarak yapılmıştır. Pantograf mekanizmasından elde edilen bilgiler Delta mekanizmasına doğrudan aktarılmıştır. Delta mekanizmasındaki en önemli unsur montaj süreçlerindeki düzlemsel yapıyı bozmadan bir paralelogram tasarımı gerçekleştirmektir. Bu yüzden paralelogram yapısı tasarlandıktan sonra (düzlemsel yöntemlerinde sebep olduğu) ortaya çıkan bir takım yan etkiler detaylı bir şekilde incelenmiştir. Daha sonra mekanizmanın kinematik analizleri yapılmıştır. Bu analizler doğrultusunda istenilen tasarım ve üretim yöntemine uygun iki boyutlu desenler ortaya çıkarılmıştır. Aynı desen yapısı kullanılarak Delta mekanizmasının da üç boyutlu modeli oluşturulmuştur. Kinematik model ile üç boyutlu model karşılaştırılıp mekanizmanın uygunluğu onaylanmıştır. Daha sonra mekanizmanın gömülü sensörlü üretimi yapılıp mekanizma ve sensör üzerine detaylı deneyler yapılmıştır. Yapılan deneylerden sonra üretimi yapılmış Delta mekanizmasının kinematik modeli küçük hatalar ile takip edebildiği kanısına varılmıştır. Bunun yanı sıra kullanılan esnek ve rijit katmanlarının uyumunun mekanizma üzerine doğrudan bir etkisi olduğu sonucu da ortaya çıkmıştır.

Tasarımı yapılan son mekanizma Stewart mekanizmasıdır. Stewart mekanizması üç öteleme ve üç dönme olmak üzere altı serbestlik derecesine sahip bir mekanizmadır. Yaygın olarak hareketli ve sabit platformlar dışında altı tane lineer eyleyicili bacağa sahiptir. Lineer eyleyiciler, kullanılacak olan yöntemler ile düzlemsel yapıyı bozmadan üretilemeyeceği için tek bir bacak yerine aralarında küresel eklem bulunan iki tane bacak kullanılmıştır. Bu bacakların bir tanesi sabit platforma döner eklem, diğeri ise hareketli platforma üniversal eklem ile bağlanmıştır. Eklem tipleri belli olduktan sonra mekanizmanın iki boyutlu tasarımı yani desenleri çıkarılmıştır. İki boyutlu tasarımının yapılabildiği görülünce ortaya çıkarılan bu yapının ters kinematik modeli ve katı modeli oluşturulmuştur. Bu iki model karşılaştırılıp mekanizmanın rijit bacaklar ile düzgün hareket edip etmediği kontrol edilmiştir. Son olarak mekanizmanın gömülü sensörlü hali üretilip üzerinde deneyler yapılmıştır. Bu deneyler üretilmiş Stewart mekanizmasının altı serbestlik derecesine sahip olduğunu ve verilen girişleri küçük hatalar ile takip edebildiğini göstermiştir.

Mekanizmaların uç noktasının konumunun hesaplaması sırasında gereken açıları ölçmek için bir sensör tasarlanması gerekmektedir. Bu sensör sayesinde doğru dinamik modeller kullanılarak motor ve uç nokta kontrolleri yapılabilir. Bu projede tasarlanan sensör iki rijit kol arasındaki açıyı ölçmek için yapılmıştır. Rijitlerin arasında bulunan esnek katmanda, dönmeden dolayı ortaya çıkan katman üzerindeki gerilme ve uzamalardan faydalanmak için bir gerinim ölçer tasarlanmıştır. Hali hazırda piyasada bulunan gerinim ölçerler, katmanlar arasına gömülmek için uygun olmadığıdan farklı bir yöntem olan gümüş nano parçacıklı mürekkep ve inkjet yazıcılar kullanılmıştır. Plastik PET levha üzerine inkjet yazıcılar kullanarak gümüş nano parçacıklı mürekkep ile iletken yollar basılabilmektedir. Bir gerinim ölçer şekli basıldığında, esnek levhadaki uzama ve kısalmalar tespit edilebilmektedir. Basılan PET levha rijit levhalardaki eklem kısımlarına konulduğunda ise iki rijit levha arasındaki açı ve esnek levhadaki uzama arasında bir bağlantı oluşmaktadır. Sensörün sadece tasarım kısmı değil konumu, yerleşimleri, kesimleri ve kablo bağlantıları üzerine de detaylı çalışmalar yapılmıştır. Daha sonra her bir mekanizmanın gerekli yerlerine sensörler tasarlanmış ve üretim yöntemine entegre edilmiştir. Sensörün ilk çalışmaları Pantograf mekanizması üzerinde yapılsa da, detaylı çalışmalar Delta mekanizmasında yapılmıştır. Deneyler sonucunda sensörün 9º ve altındaki açıları ölçebileceği görülmüştür.

Yapılan mekanizmaların denemesi için her birine özel olarak test platformları tasarlanmıştır. Bu test platformları üç boyutlu yazıcılar ile üretilmiş olup içerisinde mekanizmanın oturacağı yer, motor yerleri, motor – bacak bağlantı aparatları ve mekanizmaların uç noktasının hareketini takip etmek için kullanılan altı serbestlik dereceli pozisyon sensörünün referansı bulundurmaktadır. Deneyler için robot servo motorları kullanılmıştır. Mekanizmaların farklılığından dolayı ortaya çıkan spesifik durumlar test platformlarına aktarılmıştır. Yapılan deneyler; noktasal deneyler, çember profili ile sürekli hareket deneyleri ve sadece Stewart mekanizmasında olan dönme deneyleri şeklinde sıralanabilir. Ayrıca farklı esnek malzemelerin etkisini görmek için Delta mekanizması kullanılarak aynı deneyler tekrarlanmıştır. Genel olarak söylemek gerekirse bütün mekanizmalar başarılı bir şekilde deneyleri tamamlamışlardır. Sensör verileri voltaj bölücü devresi ve DAQ sinyal işleme kartı kullanılarak gerçekleştirilmiştir. Delta ve Stewart mekanizması içerisine gömülmüş olan sensörlerden açı değerleri başarılı bir şekilde okunabilmiştir.

1. INTRODUCTION

The robotic field has gradually broadened when they started to enter more common sectors such as medicine, food, service and even our daily life, rather than being single task, large-scale mechanical systems within the industry. Increasing demand in many different field of applications for robotic systems, brought a need for new design and manufacturing methods with itself, in order to be adjusted to the new working conditions that requires different scales, materials etc. However, changing the size of a bulky robotic system, especially from large to small is a challenging problem. Miniature systems (cm or below) require more elegant designs, even smaller fasteners and difficult assembly processes, which then results in time consuming and high cost situations. One of the questions for these problems could be answered with parallel robots. Parallel robots, more definitively parallel mechanisms have inherently very rigid features and can provide fast and precise motion. These features most certainly could help to reduce the size of the mechanisms without losing any motion dependent performance issues. That's why, in spite of the complex nature of their analytical models, which can be solved with modern techniques and limited workspace, the miniaturization of these mechanism could be used in many more fields such as agriculture, space and defense without a doubt.

The 2D monolithic fabrication techniques can be used in order to remedy the manufacturing problem, which is the biggest challenge in the design and production of small-scale robots. These techniques have been inspired and developed by the 2-dimensional origami methods and have many qualities that can help to replace traditional production methods as well as eliminate the difficult assembly processes for robotic systems with a cm and below characteristic size. Ability to create complex systems and mechanisms (which consist different joint types) that have high performance and robustness with a fast, low-cost and scalable features are a couple of benefits of this methods. The basis for this method is basically creating a composite structure that can be turned into a 3D shape by processing many number of sheet materials individually and stacking them on top of each other. There is no limitation for the used sheet material for this methods other than they must be suitable for the mechanisms and the requirements set by the designer. As an example cardboard, polymers and carbon fibers can be given.

Even though they are not new, the origami based designs and 2D fabrication methods is still in open for the development. For example, there are not any universal assembly processes for the known fabrication methodologies. The designed mechanisms in the literature have specific folding and bonding steps during the assembly. These steps generally require additional manual work other that stacking the layers, which results in longer fabrication time and the they disturb the planar nature of the assembly. Also, the sensor integration to the small scale mechanism is still not truly resolved for the matter. Existed sensors started to become unusable as the scale of the mechanisms decrease, because the scale of the necessary sensors also decreased with the scale of the mechanisms. Different kind of novel sensors had to be designed in order to reduce the size using the resistive and capacitive materials, piezo-electricity effect etc. With all that is said, in this research novel origami inspired parallel mechanisms with embedded sensors will be designed for a 2D fabrication method in order to get completely flat assembly processes.

1.1 Purpose of the Thesis

The aim of this project is to design and manufacture novel miniature parallel mechanisms and embedded sensor using origami inspired designs and 2D fabrication methods without adding any additional assembly steps to the basic 2D fabrication operations. Parallel robots are widely used and accepted in a wide range of applications where there is a need for fast, precise and rigid features. However, due to their complex architecture and limited workspace, reducing the size of these robots are very challenging. In this context, the complex architectures of these robots, could be realized in medium and smaller scales (cm and below) by using the existing origami inspired designs and 2D fabrication methods. Generally, these methods are very suitable for small scale manufacturing. In addition to that, differently from already existing designs, in this project the assembly will only consist cut – bond – repeat cycle. Moreover, an embedded strain gauge sensor for these mechanisms will be designed to measure the relative angle between two links. The sensor will measure the strain on the flexible layer at the joint area, caused by the angle between the two connected rigid links. In the fabrication of the sensor, silver nano-particle inks and inkjet printing will be used to ensure that the process is suitable for the 2D fabrication method.

1.2 Literature Review

Over the years, origami inspired designs and 2D layered fabrication methods gained more affinity since they can offer unique and complex systems with various scales. The ability to create 3D shapes out of 2D design techniques becomes more beneficial than the conventional designs as far as small scale systems are considered. Mechanisms and systems developed and manufactured by these methods could have different fabrication names, including Smart Composite Micro-structures (SCM), Printed-Circuit MEMS (PC-MEMS), Printable Robotics and Flexure based designed robots. However, all these methods fundamentally have a common procedure such as layer stacking, material removing and origami inspired designs (Aukes et al., 2014). The systematic structure and working principle of one of these fabrication methods can be seen in detail in a study by Whitney et al. (2011). In this research, he studied mostly "MEMS" and "pop-up systems" and has been able to lay very foundational ideas.

There are already various examples in literature, although these methods are still in their early stages of development. Bioinspired micro scale insect robots are one of the popular topics in this field. For example, micro insects with legged locomotion that needs a stable design and complex joint geometries are manufactured by both the MEMS and SCM fabrication methods (Baisch et al., 2014; Birkmeyer et al., 2009). However, there is not only legged locomotion, but also there are insects that can jump and even fly (Koh et al., 2015; Wood, 2008; Wood et al., 2012). In addition to the insect robots, parallel mechanisms also can be realized by the origami inspired designs and 2D fabrication methods. Due to their closed-loop kinematic chain structures, they became very suitable to be created by these methods (K. Zhang & Dai, 2013). Diverse parallel mechanisms can be manufactured by using prismatic, revolute, universal and spherical joints and can be designed by these methods (Rodriguez Leal & Dai, 2007). Also, there are parallel mechanism examples in the literature that is specifically designed for SCM method, which is the chosen method for this project (Marco Salerno et al., 2017). As an application, combination of parallel mechanism and layer by layer techniques can be found in medical fields. For example, features like high stiffness, performance, efficiency, and precision is highly demanded in minimally invasive surgery, where small scale robots are needed to interact with the human body without causing any harm (M. Salerno et al., 2014). Various surgical parallel mechanisms have been developed utilizing different types of grippers (Gafford et al., 2016; Russo et al., 2016). Other that these works, very recently a novel three degree of freedom parallel mechanism for human – robot interaction research is published (Mintchev et al., 2019). As it can be seen, the origami based designs are very versatile and can be applied to many different platforms.

The most famous of the three parallel mechanisms that is chosen and will be designed in this research is the Delta mechanism. Delta mechanism is one of the most substantial parallel mechanisms in both traditionally and origami inspired designs. Generally, delta robots are widely used in pick and place operations in industries such as pharmaceutical, food, and electronics (Demaurex, 1999; López et al., 2006). The mechanism has beneficial properties such as its capability to reach high speeds and accelerations with a great scalability. For example, delta structure design was used for micro operations by Tanikawa et al. (2002) in the past. Also, there are recent researches on delta mechanism which utilizes the flexure based design and PC-MEMS techniques like Laminated micro-machine with linear guides by Correa et al. (2016) and the MilliDelta by McClintock et al. (2018). However, during the fabrication process, additional steps such as folding and bonding are generally used in these previous works. Although not as famous as Delta mechanism, there are a couple of Pantograph mechanism and origami pattern designs for antennas in the literature (Costantine et al., 2016). On the other hand, information for the proper Stewart mechanism with six degree of freedom created by these methods could not be found in this research.

Even though all these example does not share the exact same fabrication method, they have a similar problem which is out-of-2D manual folding in assembly process. This additional process increases time cost, complexity and difficulty of manufacturing. Using sheet materials to create mechanisms or systems with a standardized fabrication method that has minimum process steps with no manual interaction could result in relatively easier manufacturing and assembly processes, even in the case of mass production (Zhakypov & Paik, 2018). There are methods that tries to eliminate the manual folding in the assembly process. It is possible to build self-folding mechanisms out of sheet materials, which transforms into 3D shapes using soft actuators (Felton et al., 2014; Tolley et al., 2014; Zhakypov et al., 2019). In these examples, initially the systems can be completely flat because the folding procedures are given to the soft actuators. Nevertheless, self-folding and soft actuators are not yet practical enough for various applications.

The ink based printed sensors are one of the focus areas of robotic soft sensors. Even though it is mostly used for angle and bending measurements like a strain sensor, different type of sensors can be made such as structural health monitoring sensors, inductive position sensors or various other transducers, that utilizes the same effects (Andò et al., 2017; Jeranče et al., 2012; Lee et al., 2017). In addition to that, due to their light nature it also found itself a place in the wearable technology (Kramer et al., 2011). Although, the silver nanoparticle ink is the most common conductive ink in the literature, there are other studies using different inks like carbon nanoparticle inks (Pekarovicova & Husovska, 2015). Both of the silver and carbon inks have different properties (Y. Zhang et al., 2017). For example, silver ink has better conductivity than the carbon ink, but it is also more expensive. Furthermore, there are also more than one printing technologies such as inkjet printing and screen printing. Detailed researches and comparison for both printing technologies have been done previously (Ando & Baglio, 2013). However, if the matter comes down to the low-cost side of the things, it can be said that the inkjet printing is better than the screen printing.

The change in resistivity in the terms of an elongation (strain gauge factor) becomes much bigger when it is printed on the plastic sheet rather than gluing into the metal substrate due to lower elasticity of plastic. In order to use this property, traditional shape of strain gauge sensors are started to be printed on the plastic sheets (Sun et al., 2015). Even though the method is relatively new, there are detailed examples in the literature trying to model the nonlinear behaviors and different shapes (Correia et al., 2013). Due to its low cost and precision, generally inkjet technology is used, but there are also examples with the screen printing (Enser et al., 2018). However, in both cases it is found that the sensor has problems like hysteresis and susceptibility to mechanical and ambient effects. In order to protect the sensor against to the environment, it is found that coating the surface with a different layer is helpful (Überblick, 2018). These sensors are usually integrated on the surface or embedded in the structure to measure the angle between two different links.

1.3 Contribution of the Thesis

In the light of the purpose of thesis mentioned before, this work has the following contributions to its research area;

- Novel parallel mechanisms are designed with SCM (smart composite micro-structures) fabrication method. These mechanisms have completely flat initial position, assembly process and an embedded sensor compatible with the same method.
    - The fabrication consists of an iterative process which can be described as cutting rigid and flexible layers, laminating, and releasing cut. It does not consist any additional intermediate steps like folding the sub-layers, which is usually present at other origami inspired mechanisms.
    - Each mechanism uses the same mathematical modeling as their counterpart traditional mechanism. Usually, origami inspired mechanism needs additional kinematic modeling due to their diverse structures. However, in this research they are designed to have the same kinematic structure to eliminate the need for a new mathematical models.
    - In order to design fully integrated mechanisms, an embedded sensor that can measure the angle between two respective links is developed for the mechanisms.
- The effect of different flexible layers in passive joints on position tracking are examined and shown on Delta mechanism. The joints are divided into sections and different flexible material combination is used. By doing so, the errors in position tracking is observed. Importance of the rigid – flexible layer ratio is discussed and shown by experiments.

2. METHODOLOGY: ORIGAMI INSPIRED DESIGN AND FABRICATION METHOD

2.1 Parallel Mechanisms with Origami Inspired Design

Parallel mechanisms are usually very suitable for origami inspired designs and 2D fabrication methods since they have more than one chains connecting different links and forming a robust structure. The robustness becomes convenient if the links themselves are soft which is generally the case for soft robotics. Parallel mechanisms that will be designed in this research are Pantograph, Delta and Stewart mechanism. In order to design and fabricate these mechanisms, the joints must be creatable with origami inspired design, so that they can hold the place of the real joints that is used for traditional parallel mechanisms. There are three different joint types that is needed for this purpose; revolute joints, universal joints and spherical joints. Figure 2.1 shows the common corresponding joints that is used in the origami inspired designs.

Joint Type	Degree of Freedom	Motion
Revolute	1	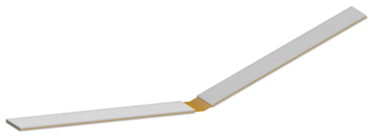
Universal	2	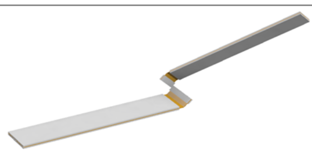
Spherical	3	

Figure 2.1 : Joint types present in origami inspired designs.

Revolute joints in Figure 2.1 are the most common and simple joints that can be created. It has a simple cut between two rigid layers that enables them to rotate in one axis, independent from each other. The Pantograph mechanism will be entirely made up with revolute joints. Delta mechanism and Stewart mechanism will utilize the 1

DoF joints in the connections between base platform and the lower arms. 2 DoF universal joints are generally a combination of two revolute joints placed with a different angle or a different plane between them. Thus, allowing the joints to bend in more than one axis. These joints will be used in the parallelogram structure in the Delta mechanism. Also, a slightly altered version of universal joints is used in Stewart mechanism. Lastly, 3 DoF joints, which is the most complicated joint type, can be created with a combination of two diagonal cuts and a straight cut between them. They are used in between the upper and lower arms connection in Stewart mechanism. A 2D drawings of all of three joints can be seen in Figure 2.2. As a result, fundamentally revolute joint is the basis for all the other joint types and the design of it must be improved. Moreover, also a meaningful combination of revolute joints has to be found in order to mimic the real 2 DoF and 3 DoF joints

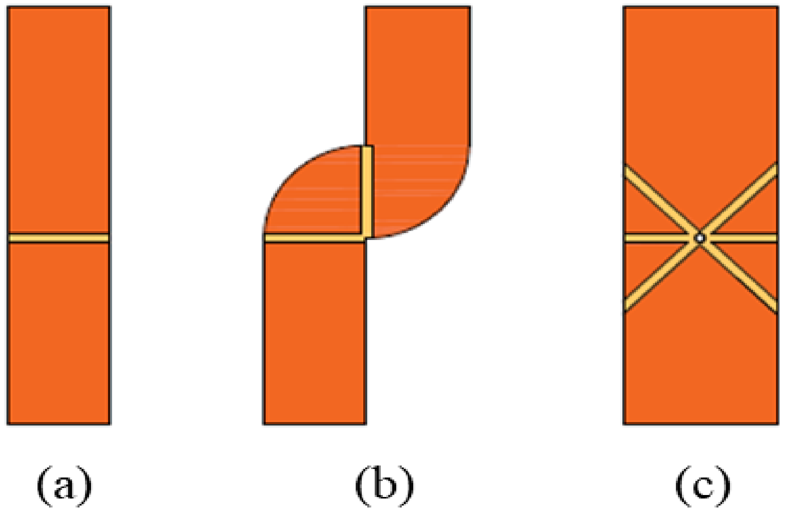

Figure 2.2 : 2D drawing of the joints: (a) revolute joint, (b) universal joint, (c) spherical joint.

The most important factor when designing the 1 DoF joint was to ensure that the rotation axis stays stationary. A straight cut causes an uncertainty on position of the center of rotation as shown in Figure 2.3a. Any force acting on the joints can change the position of the rotation axis. In order to prevent that, castellated joint cuts were used (Doshi et al., 2015). The castellated cuts in which the axis of rotation is a straight line with a stable position are shown in Figure 2.3b. In this design, the rigid materials bend into the spaces in front of them. This behavior mostly ensures the position of axis of rotation stays the same. The castellated design can be used in all three of joint types.

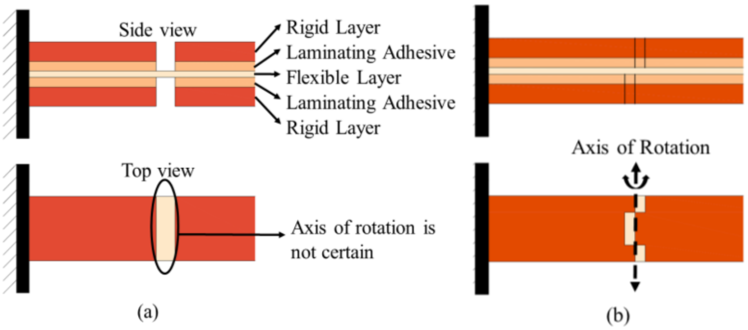

Figure 2.3 : Revolute joint with (a) Uncastellated design and (b) castellated design.

2.2 Fabrication Method and Materials

The fabrication of the origami inspired miniature parallel robots are done by using 2D fabrication technique (layer by layer methods). There are already a couple of different layer by layer fabrication methods in the literature. The name of the method used in this research is Smart Composite Micro-structures (SCM) (it also is addressed as 2D fabrication method or layer by layer technique in this research). This production method consists of a couple of repetitive action. First step is to cut all of the layers using laser cutting machine or with any other proper cutting methods. The next steps consist of aligning and joining the layers that makes up the structure on top of each other. If necessary, cutting, aligning and boning steps can be repeated. Figure 2.4 shows the process steps. Since the dimensional tolerances and alignment effects the geometrical, static and dynamical properties of the mechanism, it becomes a very important issue (Wood et al., 2008).

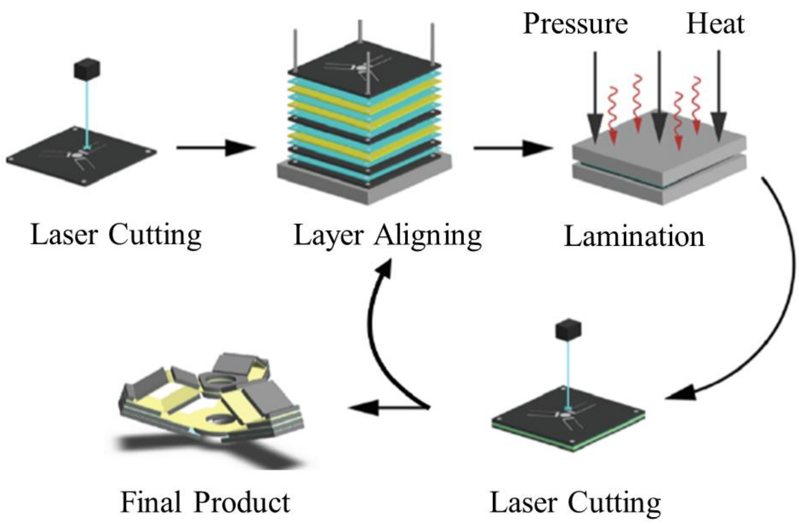

Figure 2.4 : Basic fabrication steps of SCM (Temel et al., 2017).

All three parallel mechanisms (Pantograph, Delta and Stewart mechanisms) has its own alignment platform, that is specifically designed for the specific mechanisms as shown in Figure 2.5.

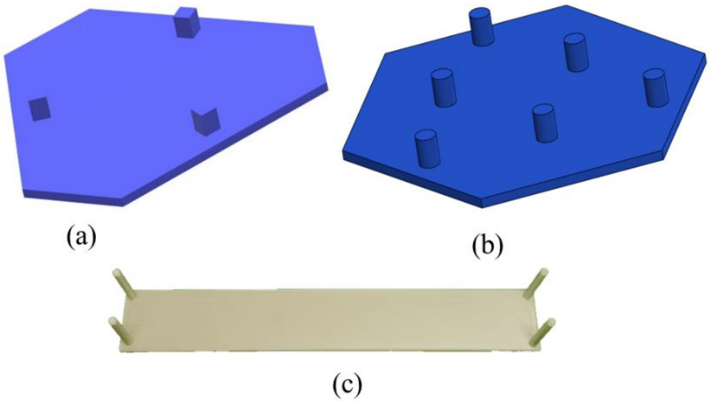

Figure 2.5 : Reference platform for (a) Delta mechanism, (b) Stewart mechanism and (c) Pantograph mechanism.

There are basically two main sublayers in all three mechanisms, which are named rigid 1 and rigid 2. The sublayer rigid 1 represents the two long legs in Pantograph and base platforms in Delta and Stewart mechanisms. On the other hand, the sublayer rigid 2 represents the four short legs in Pantograph and the moving platforms in Delta and Stewart mechanisms. In total there are 11 layers in all three mechanisms; 5 in each sublayer and 1 adhesive layer between the sublayers. Sublayer structure is a sandwich system that is created as follows; rigid layer + lamination adhesive + flexible layer + lamination adhesive + rigid layer as seen in Figure 2.3a. The rigid layer's joint patterns in sublayers are main decisive factor for the overall shape of the mechanism. Patterns are determined according to the joint types that are explained earlier and the specific layout for the mechanisms. The drawing of patterns and individual fabrication processes of mechanism will be given in their own sections.

Aside from the design, there are other factors that effects the fabrication process. First one is the sensitivity of the laser cutting machine. As it is mentioned earlier the dimensional tolerances has a big impact on the mechanisms. In order to have a better performance, the patterns have to be cut very precisely. Calibration of the laser, the cutting board and cutting power tests have to be done initially to have a better cutting without burning the material. Also, since the aligning is done by hand, even if there is an alignment platform, human error can be made. It is necessary to be as sensitive as possible to manufacture the best mechanism.

Materials selected to manufacture the parallel mechanisms are cardboard for rigid layers and plastic sheets for flexible layers. The name of the cardboard is “American Bristol” with a paper weight of 400 gsm. The reasons for using cardboard are that it is easy to obtain, experiment and its low cost. This rigid layer is the same for all the mechanisms whereas there is more than one elastic material used in the flexible layer which are 3D printed TPU, and PET sheets with different thickness. Most important feature wanted in the rigid layer is that it has to be rigid enough to not bend under the force and can hold itself. Also, the castellated joint design requires a good rigidity at the ends of the joint to ensure the thing that is bent is the flexible layer not rigid layer. Cardboard provides these features in this parallel mechanisms. However, more rigid materials like carbon-fiber sheets can be used to get better results.

The flexible sensor layer of each mechanism uses the same PET sheet (Nova centrix - Novelle Printing Media) since it has a special coating for the inkjet printing. However, other flexible layers are changed to see the effects of the flexible layer on the motion of the mechanism. PET sheets with different thicknesses are the main flexible layers that are used. However, in order to test a different flexible layer, 3D printed TPU material is also used. TPU sheets have two different types; one layered TPU sheet where the thickness is usually around 0.2 mm and two layered TPU sheet where the thickness is usually around 0.4 mm. There are couple of properties that is expected from the flexible layer. First one is that it must not allow the laser burn to propagate on itself while the laser cuts and reveals the joints. If the burn propagates to the axis of rotation, the joints split up easily. The other one is that it has to have a good fatigue resistance in order to have longer life span. Lastly, the elasticity must be suitable for the joint to work properly. More detailed explanations of the used flexible layers and experiments is given in the Results Section.

2.3 Embedded Sensor

The parallel mechanisms that will be fabricated with the layer by layer methods generally have revolute joints due to the limitations of the 2D fabrication methods. In order to determine the position of the mechanism, the angles in the joints has to be measured. That’s why the design of an embedded sensor should be able to measure the angle between two links and should not disturb the regular job of the joints.

Main ingredient behind the working principle of the origami inspired joints are the flexible layer. The free bending of the flexible layer between two rigid layer mimics the revolute joint and also connects the rigid layers. At the same time, the bending motion of the rigid layer creates contractions and elongations with a compression and tensile stress on the surfaces of the flexible layer. If the flexible layer is fixed between two rigid layer, the stresses that is created on the flexible layer is expected to be dependent on the angle between the rigid layers. This stress can be utilized to measure the angle of the joints.

One of the most used method to measure the elongation of the materials is strain gauge sensor. However, existing traditional strain gauges cannot be used for the layer by layer techniques since they are being made by very rigid materials. Nevertheless, in the literature there are researches for strain gages printed into the surface of the PET sheets using the silver nano-particle inks and inkjet printing technology shown in Figure 2.6. As it is mentioned earlier PET sheets are the main flexible layer and it is suited for the desired fabrication methods. Using the printed strain gauge sensor at the crucial joints where the position of the end effector can be calculated will be useful for the feedback control systems. That's why a strain gauge sensor for parallel mechanism is designed and fabricated. The detailed sensor design and integration for each mechanism will be explained in their own sections.

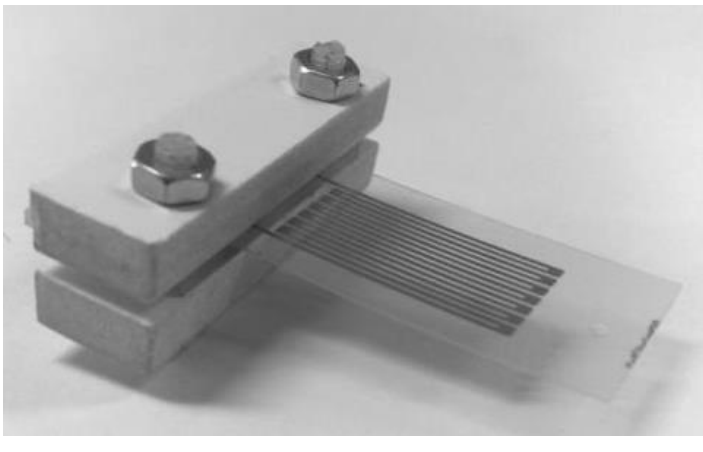

Figure 2.6 : An example of all-inkjet printed strain sensor (Andò et al., 2017).

3. DEVELOPMENT OF PARALLEL MECHANISMS AND EMBEDDED SENSOR

In this section, individual design processes of Pantograph, Delta and Stewart parallel mechanisms and the embedded sensor will be discussed as well as the detailed fabrication process will be given. The designs are going to be done with the methodologies that are mentioned in the previous section; origami inspired design and 2D fabrication method SCM. The same rigid and flexible materials and silver ink are used in all three parallel mechanisms. The most important limitation in the design is that all of these parallel mechanism should be manufactured without any additional processes such as out – of – plane folding or separate bonding steps.

The other limitation is that the mechanisms must be miniature. The definition of miniature is rather vague, but there is a requirement that is set for all three parallel mechanisms. The workspace of mechanisms must be under the 50x50x50 mm^3 volume. Therefore, deciding the dimensions must be done according to this requirement. Although the workspace of the mechanism can be decreased by using the scaled versions designs. That method is very feasible in theory since the parallel mechanisms can be scaled better than serial mechanisms. However, the machinery used in the fabrication becomes very important. The cutting cannot be made smaller if the laser cutting machine cannot reach the desired tolerances.

This research aims to produce a mechanism with a 2 DoF, 3 DoF and 6 DoF movement. That's why the first design will be the Pantograph mechanism with a 2 DoF movement in XY plane. This mechanism is mostly for the proof of concept that a miniature parallel mechanism can be designed by origami inspired techniques and 2D fabrication methods with a complete flat assembly process. Also, the other purpose was initial sensor integration and analysis. After the design of sensor is made in Pantograph mechanism, the sensor is developed further in Delta mechanism. For these reasons experimental results of the Pantograph mechanism will not be given.

The second design is a 3 DoF mechanism, which is the Delta mechanism. The design of the Delta mechanism is much more complex than the Pantograph mechanism because it works in three dimensions. The developed methods and the embedded sensor in the Pantograph will be adjusted to the Delta mechanism and will be improved further. Finally, as a 6 DoF mechanism, Stewart platform will be developed. The complexity of the design increases onward from the Delta mechanism to Stewart mechanism, but already established methods and sensor design will reduce the design load of the Stewart mechanism.

The design, improvement and adjustment of the embedded sensor will be always active because even though the all three mechanisms similar to each other, there is at least the placement problem. However, as a result a general design and common fabrication process will be developed, so that it can be applied to any other angle measurement scheme.

3.1 Pantograph Mechanism

In order to design a Pantograph mechanism with an origami inspired techniques, initially the traditional Pantograph mechanisms must be examined. Generally, the most basic Pantograph mechanisms are four bar linkages like shown in Figure 3.1. The most used property of Pantograph is its copy ability. If one of the end points gets fixed, the other end point follows the movements of the middle point with a certain amplification factor. This factor comes from the internal parallelogram structure and triangle similarities. However, in this work the Pantograph mechanism is wanted to have end effector with a two degree of freedom motion rather than copying the movements of the middle point. That's why the connection point has changed in the new design.

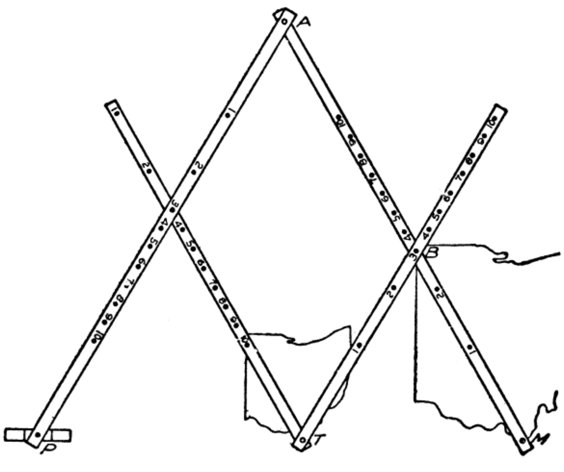

Figure 3.1 : A Pantograph mechanism designed for scaling maps (French, 1911).

Using the set requirements, two points of actuation are defined to have a movement in XY plane. First one is the “A” point that is showed in Figure 3.2 which is the bottom left point of the long leg. In this point, there will be an actuator that can provide an angle input like a servo motor. The other actuation point is the “B” point which is the middle point of the mechanism. There will be a linear actuator between the “B” and “C” points where the position of the “C” point will be determined by using the workspace requirements and the kinematic equations. These actuators will provide a two degree of freedom movement, where “D” point works in XY plane with an amplification factor determined by the length of the legs.

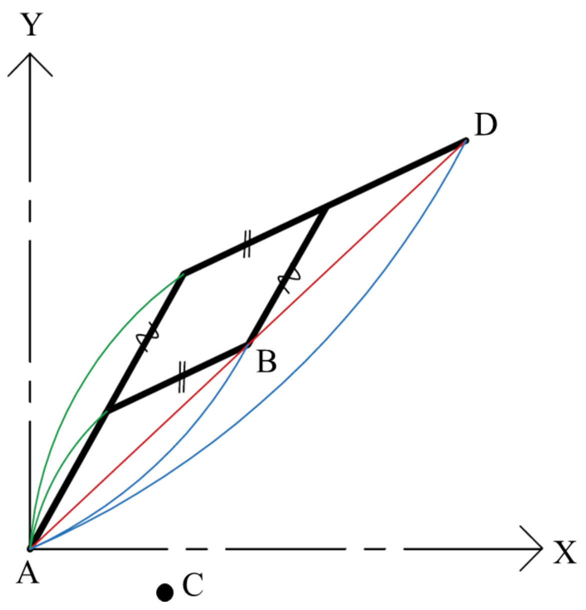

Figure 3.2 : Triangle similarities of the Pantograph mechanism.

The important thing here is the determination of the amplification factor. This amplification factor arises from the positions of the legs, which creates similar triangles. Figure 3.2 shows the triangles similarities with green and blue lines. Due to the parallelogram in the middle and the similar triangles, the red line always stays as a straight line and passes through “A”, “B”, and “D” points. That’s why the amplification factor can be found as a ratio between the length of the long leg and the distance from end point to the connection point of the short leg like shown in Figure 3.2. The amplification factor of the designed Pantograph mechanism has chosen to be 2:1 due to simplifications that comes with the symmetric legs in the design and fabrication steps. However, these processes can be done by using different amplification factors too.

Since the mechanism is designed in flat surface, the total length of the mechanism is determined by two long legs. Total length of the mechanism is chosen to be 160 mm (considering the required workspace of the Pantograph mechanism) which makes the length of the long leg 80 mm and the length of the shot legs 40 mm. This values can be validated using the kinematic equations. Also, a 3D CAD model of the mechanism will be created to compare results with the kinematic model.

3.1.1 Inverse kinematics of the Pantograph mechanism

Pantograph mechanism is a parallel mechanism. Generally, the forward kinematic of parallel mechanisms are harder to solve than inverse kinematic. In both case, initially the closed loop equations must be obtained. Since the Pantograph mechanism is not a complex mechanism, the mathematical equations (3.1) and (3.2) can be obtained easily using Figure 3.3.

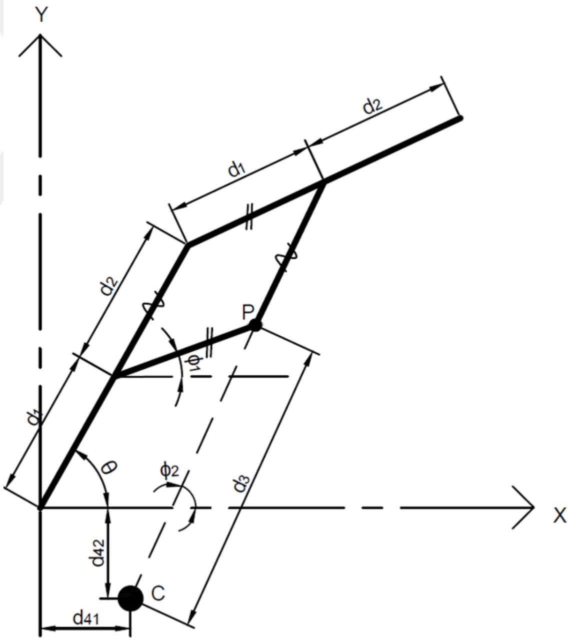

Figure 3.3 : Variable representation and model of Pantograph mechanism.

$$f_1(\theta, d_3) = d_1 \cos\theta + d_2 \cos\varphi_1 - d_3 \cos\varphi_2 - d_{41} = 0 \tag{3.1}$$

$$f_2(\theta, d_3) = d_1 \sin\theta + d_2 \sin\varphi_1 - d_3 \sin\varphi_2 - d_{42} = 0 \tag{3.2}$$

In order to find the inverse kinematic equations, the equations (3.1) and (3.2) can be manipulated and equations (3.3) and (3.4) can be obtained. The d_3 and θ are the two variables representing the actuator inputs. The other values are constants regarding the geometrical properties of the mechanism.

$$P_x = d_3 \cos\varphi_2 + d_{41} = d_1 \cos\theta + d_2 \cos\varphi_1 \quad (3.3)$$

$$P_y = d_3 \sin\varphi_2 + d_{42} = d_1 \sin\theta + d_2 \sin\varphi_1 \quad (3.4)$$

Both left and right sides of the equations (3.3) and (3.4) represent a way to P_x and P_y coordinates, but in a different way. The left side where d_3 is present will be used to find the d_3 variable and the right side with the θ will be used to find the θ variable. Initially, θ variable will be calculated using equations (3.5) and (3.6).

$$P_x - d_1 \cos\theta = d_2 \cos\varphi_1 \quad (3.5)$$

$$P_y - d_1 \sin\theta = d_2 \sin\varphi_1 \quad (3.6)$$

Intermediate variable φ has to be eliminated since it cannot be known in these calculations. That’s why an elimination method will be used, where the both side of the equations will be squared and added like shown in equation (3.7) in order to use the trigonometric property of sine and cosine (Chung & Lee, 2001).

$$(P_x - d_1 \cos\theta)^2 + \left(P_y - d_1 \sin\theta\right)^2 = d_2^2 \cos^2\varphi_1 + d_2^2 \sin^2\varphi_1 \quad (3.7)$$

If the right side are taken into d_2 paranthesis, the squared addition of the sine and cosine becomes 1 and φ_i disappears. After opening the squares of the left side and some simplification steps, equation (3.8) can be obtained.

$$-2P_x d_1 \cos\theta - 2P_y d_1 \sin\theta + +d_1^2(\cos^2\theta + \sin^2\theta) + P_x^2 + P_y^2 - d_2^2 = 0 \quad (3.8)$$

In the equation (3.8), all of the values is known besides the θ variable. Simplifying the equation (3.9), using equations (3.9a) - (3.9c) result in a simple sinusoidal structure where there is a known solution utilizing the tangent half angle trigonometric formulas.

$$\alpha \cos\theta + \beta \sin\theta + \lambda = 0 \quad (3.9)$$

$$\alpha = -2P_x d_1 \quad (3.9a)$$

$$\beta = -2P_y d_1 \quad (3.9b)$$

$$\lambda = \mathrm{P}_\mathrm{x}^2 + \mathrm{P}_\mathrm{y}^2 + \mathrm{d}_1^2 - \mathrm{d}_2^2 \quad (3.9c)$$

If the half angle trigonometric transformations shown in equations (3.10) - (3.12) is applied to the variable, polynomial equation (3.15) and the solution for the second order polynomial equation (3.16) can be obtained, using the steps shown in equations (3.13) and (3.14).

$$\cos\vartheta = \frac{1-u^2}{1+u^2} \tag{3.10}$$

$$\sin\vartheta = \frac{2u}{1+u^2} \tag{3.11}$$

$$u = \tan\frac{\vartheta}{2} \tag{3.12}$$

$$\alpha\left(\frac{1-u^2}{1+u^2}\right) + \beta\left(\frac{2u}{1+u^2}\right) + \gamma = 0 \tag{3.13}$$

$$\alpha - \alpha u^2 + 2\beta u + \gamma + \gamma u^2 = 0 \tag{3.14}$$

$$(\gamma - \alpha)u^2 + 2\beta u + (\gamma + \alpha) = 0 \tag{3.15}$$

$$u = \frac{-\beta \pm \sqrt{\beta^2 - (\gamma^2 - \alpha^2)}}{\gamma - \alpha} \tag{3.16}$$

Finally, using the back transformation of θ in equation (3.16) and arranging the left side, the θ can be found as shown in equation (3.17).

$$\theta = 2\,tan^{-1}\left(\frac{-\beta \pm \sqrt{\alpha^2 + \beta^2 - \gamma^2}}{\gamma - \alpha}\right) \tag{3.17}$$

The most important thing is that there are two different solutions for these equation. The reason for that is there is two different ways to get to point P; internal parallelogram looks down which is the case in Figure 3.3 and internal parallelogram looks up. The real solution can be found and picked by examining the parallelogram. Thus, the first unknown is found. Also, determinant check must be done in order to find a real solution since the mechanism is a real mechanism and cannot have an imaginary solution.

The other unknown d_3 can be found using equations (3.18) and (3.19), which are the left part of the equations (3.1) and (3.2).

$$P_x - d_{41} = d_3\,cos\,\varphi_2 \tag{3.18}$$

$$P_y - d_{42} = d_3\,sin\,\varphi_2 \tag{3.19}$$

Using the same elimination method, the φ_2 variable can be removed from the calculations. If the same square and add steps is applied, the equation (3.20) can be obtained. The equation (3.21) shows the final form, where d_3 can be calculated easily.

$$(P_x - d_{41})^2 + (P_y - d_{42})^2 = d_3^2 \cos^2 \varphi_2 + d_3^2 \sin^2 \varphi_2 \tag{3.20}$$

$$d_3 = \sqrt{(P_x - d_{41})^2 + (P_y - d_{42})^2} \tag{3.21}$$

As a result, if the position P is given, the input values of d_3 and θ can be calculated using equations (3.17) and (3.21) and inverse kinematics is complete. However, this coordinates are the position of the middle point. In order to find the end effector's position, amplification factor must be used. This means, P coordinate of equations (3.17) and (3.21) must be scaled by using the amplification factor.

3.1.2 Forward kinematics of Pantograph mechanism

Forward kinematic of Pantograph mechanism can be calculated using the same elimination methods in the inverse kinematic. However, the solution is not as obvious as the inverse kinematics. The same close loop equations (3.1) and (3.2) can be used in the form of equation (3.22) and (3.23).

$$(d_1 \cos \theta - d_{41}) + d_2 \cos \varphi_1 = d_3 \cos \varphi_2 \tag{3.22}$$

$$(d_1 \sin \theta - d_{42}) + d_2 \sin \varphi_1 = d_3 \sin \varphi_2 \tag{3.23}$$

The values in the parenthesis are completely known since this is forward kinematics, so these values can be represented as a simple variable like shown in equations (3.24) -(3.25a).

$$d_2 \cos \varphi_1 + a = d_3 \cos \varphi_2 \tag{3.24}$$

$$a = d_1 \cos \theta - d_{41} \tag{3.24a}$$

$$d_2 \sin \varphi_1 + b = d_3 \sin \varphi_2 \tag{3.25}$$

$$b = d_1 \sin \theta - d_{42} \tag{3.25a}$$

Squaring the both sides and adding them side by side results in equation (3.26). Using the same sine and cosine trigonometric identities, squared terms can be eliminated and simple equation (3.27) can be obtained.

$$\begin{aligned} d_2^2 \cos^2 \varphi_1 + d_2^2 \sin^2 \varphi_1 + 2d_2(a \cos \varphi_1 + b \sin \varphi_1) + a^2 + b^2 \\ = d_3^2 \cos^2 \varphi_2 + d_3^2 \sin^2 \varphi_2 \end{aligned} \tag{3.26}$$

$$a \cos \varphi_1 + b \sin \varphi_1 + \frac{a^2 + b^2 + d_2^2 - d_3^2}{2d_2} = 0 \tag{3.27}$$

The only unknown variable in equation (3.27) is φ_1 variable, so the other constans can be represented by a simple variable like shown in equation (3.27a). As a result, equation (3.28) can be obtained.

$$c = \frac{a^2 + b^2 + d_2^2 - d_3^2}{2d_2} \tag{3.27a}$$

$$a \cos \varphi_1 + b \sin \varphi_1 + c = 0 \tag{3.28}$$

This structure is the same as the inverse kinematic and it can be solved by using tangent half angle formulations. Finally, φ_1 can be obtained as in equation (3.29).

$$\varphi_1 = 2 \tan^{-1} \left(\frac{-b \pm \sqrt{a^2 + b^2 - c^2}}{c - a} \right) \tag{3.29}$$

As it can be seen, internal φ_1 variable can be found with these elimination method. It has the same problems like there are two solutions and possibility of determinant being smaller than zero. However, just like in inverse kinematic by observing the mechanism, the correct solutions can be chosen. As a last step using equations (3.29) - (3.31), P position can be found.

$$P_x = d_1 \cos \theta + d_2 \cos \varphi_1 \tag{3.30}$$

$$P_y = d_1 \sin \theta + d_2 \sin \varphi_1 \tag{3.31}$$

Using the same method φ_2 can be found, but it is not necessary since one of them is enough the complete the forward kinematic. These kinematic solutions can help to determine the geometrical properties, workspace and they can be used in control problems.

3.1.3 Pantograph mechanism’s 3D CAD model

The 3D model of the mechanism is created with SolidWorks CAD program. The reason for the 3D model is to compare the mathematical models and the 2D design with each other and to check if the joint design is working. The geometrical properties of 3D model are exactly the same with the mathematical model.

The most important factor in creating the 3D model is the joint connections. Since the origami inspired joints fundamentally work with bending of a flexible layer, it cannot be transferred directly to the CAD program. A similar structure has to be created in the model. That’s why using bevels at the end points sharp edges are created. After that two pieces are connected as a line and they are fixed from the sides. Thus, they can only rotate at the connection line and not from any other point as shown in Figure 3.4. However, this model only represents the ideal case for the real life origami inspired design because even if the castellated joints are used, the axis of rotation never becomes a straight line in this technique. Nevertheless, since the purpose is the comparison of two analytical design, this 3D joints is enough for simulations. The results of comparisons will be given in experimental results section.

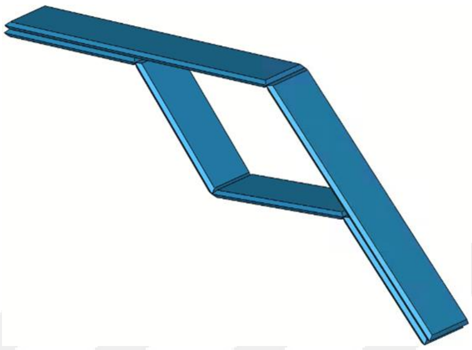

Figure 3.4 : 3D CAD model of the Pantograph mechanism.

3.1.4 The design of Pantograph mechanism for SCM 2D fabrication method

In order to integrate the fabrication method to the Pantograph mechanism, the structure is separated into two main parts named rigid 1 and rigid 2. Rigid 1 is composed of only the long legs, whereas rigid 2 is composed of only short legs. Thereby, rigid 1 and 2 will have different design and fabrication steps. The Pantograph mechanism emerges when these two rigids attached together from end to end. The mentioned main two parts rigid 1 and 2 can be better seen in 3D model in Figure 3.5.

(a)

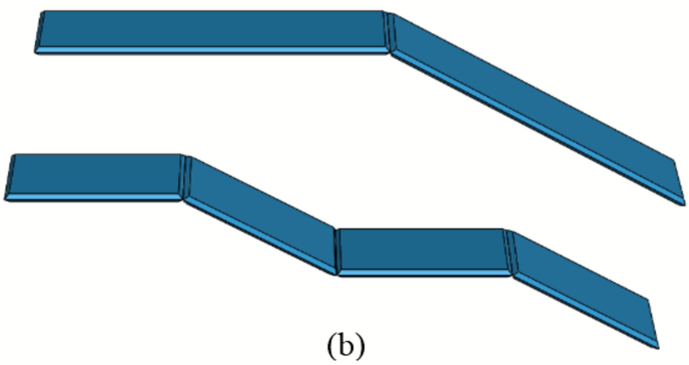

(b)

Figure 3.5 : Sublayers of Pantograph mechanism: (a) long leg sublayer, (b) short leg sublayer.

First of all, number of joints must be determined. Since the rigid 1 will have the long legs, it will have only one joint in the middle and it will act as a main body for the Pantograph. Figure 3.6a shows the lengths of the long legs and the joint cut. Considering the length of the legs, the width is chosen as 15 mm. The width does not directly affect the working principle of the mechanism, but it should not be too low because it determines the rigidity of the legs. The joint cut at the left is for the actuator implementation and to move mechanism with hand. The length of this leg is 10 mm and it does not affect the mechanism. Joint cuts are designed as a rectangle. Since this mechanism is for the proof of concept and the development of the sensor, it does not have the castellated structure that is mentioned in the methodology section. Therefore, in order to joints to work, there have to be at least 1 mm space left, because the rigid material is cardboard and it has a 0.5 mm thickness. If the space is lower than 1 mm, the joint can still work, but the maximum angle before the damage will decrease. Also, the width of the joints is the same as the width of the mechanism. The reason for that is when the final cut in Figure 3.6b is done, there will be no rigid part that holds the two leg together, so the joint will be a revolute joint. The four hole in the corners are for the reference platform to help the layers to be stacked correctly.

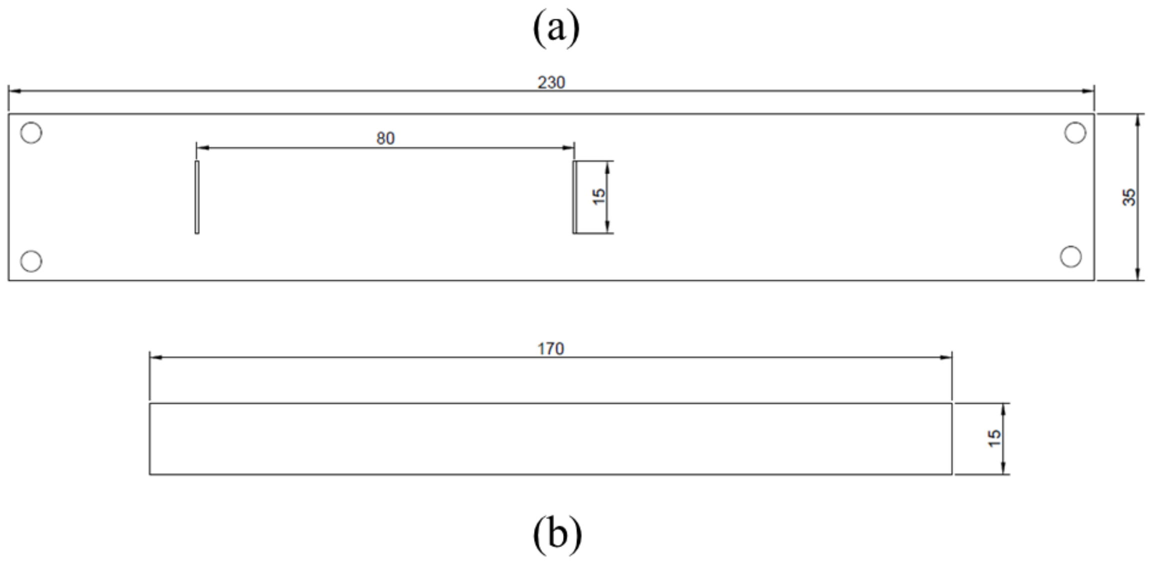

Figure 3.6 : 2D drawing of rigid 1 sublayer. All dimensions are in millimeter. (a) The layer itself with the joint cuts and (b) final cut of the of the layer.

Rigid 2 is mostly the same with rigid 1 except it has three joints. All three of the joints in rigid 2 is to create the parallelogram structure. When the rigid 1 and rigid 2 are attached together, the joints in the rigid 2 still can work because the joints themselves will not have direct connection with rigid 1. The joints and the width of the rigid 2 are exactly the same with rigid 1. Figure 3.7 shows the pattern of rigid 2

(a)

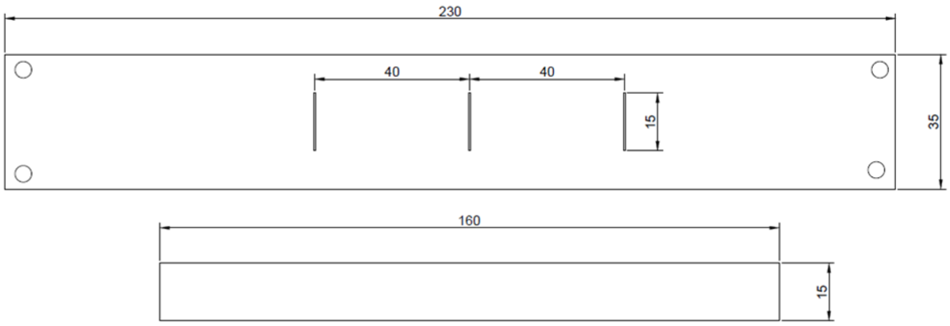

(b)

Figure 3.7 : 2D drawing of rigid 2 sublayer. All dimensions are in millimeter. (a) The layer itself with the joint cuts and (b) final cut of the of the layer.

As a last step, the separate layers will be attached together as a layer + adhesive + flexible + adhesive + layer, respectively. The flexible layers will be applied to the whole surface in both rigids to reduce the work load. Finally, the rigid 1 and 2 will be attached together using a reference platform. The complete process can be seen in Figure 3.8. Also, the manufactured Pantograph mechanism with the SCM 2D fabrication method can be seen in Figure 3.9.

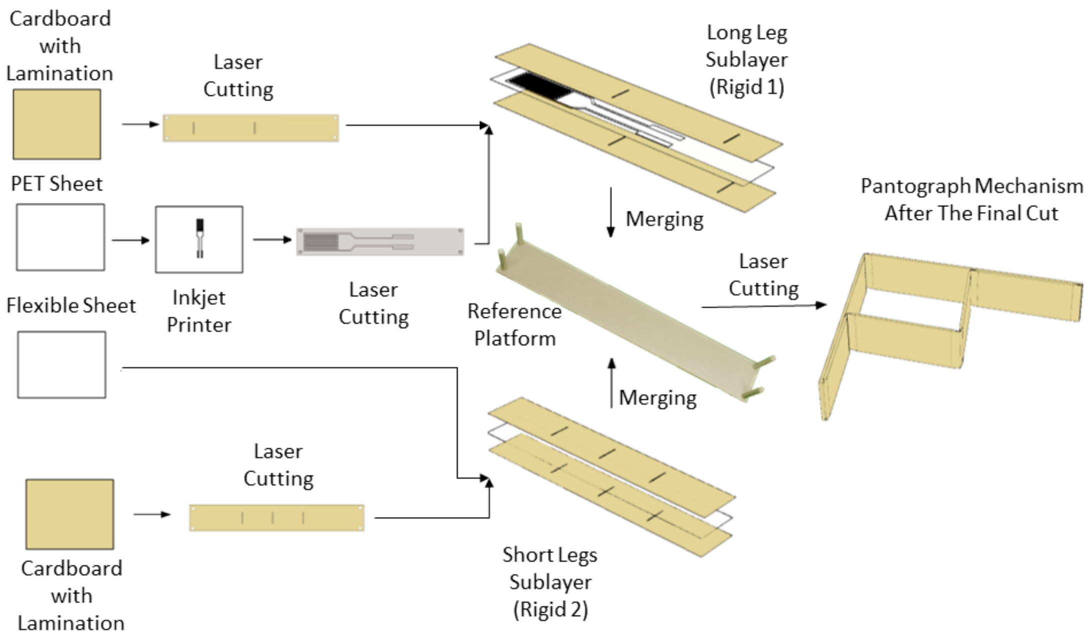

Figure 3.8 : Detailed fabrication and assembly process of the Pantograph mechanism with an embedded sensor.

As a result, using these geometrical properties and kinematic models, the middle points workspace is found as 25x25 mm^2. Using the amplification factor of 2:1, it can be said that the end point of the mechanism has a 50x50 m^2 workspace which is the maximum workspace area that is defined for this work. Thus, the requirements are met with this design.

Figure 3.9 : Fabricated Pantograph mechanism.

3.2 Delta Mechanism

The main idea behind the Delta mechanism is that its moving platforms are connected to the base platform via three different kinematic chains (Kosinska et al., 2003; Rey & Clavel, 1999). These kinematic chains consist of two arms; upper arm, which is connected to the moving platform and lower arm which is connected to the base platform. The joint between the lower arm and base platform is a one degree of freedom (DoF) revolute joint. With this joint, the opposite side of the lower arm will always be parallel to the base platform, making the connection between the upper arm and the lower arm parallel. In order to maintain this parallel motion between platforms, upper arm should be a parallelogram. Parallelogram keeps its opposing links parallel, which then in turn makes the motion of the moving platform to the base platform also parallel. A traditional Delta mechanism can be seen in Figure 3.10.

Just like in Pantograph mechanism, an important design criterion is that design must be suitable for layer by layer fabrication method using 2D processes. However, the design of integrated mechanisms like Delta is very complex because it requires universal joints at the parallelograms. There are parallelograms and Delta mechanisms that are designed and manufactured with origami inspired methods, but all of them requires an assembly process where they have to fold the legs or bond other materials to get the desired mechanism (generally addressed as out-of-plane folding). The challenge is to design the mechanism with a completely flat design method. This kind of design requires 2 DoF joints (initially flat and in the same plane) that can function in 3D space.

Figure 3.10 : A traditional Delta mechanism (Evangelista, 2011).

Basically, design will have two main sublayers; base and moving platform. The leg's connection in base platform will be a revolute joint. A novel parallelogram will be designed and implemented to the moving platform. Parallelograms connection with the lower arm will be done by an extra connection link. Embedded sensors will be placed in the base platform just beneath the legs. Kinematic equations of traditional Delta mechanism will be obtained and a 3D CAD model will be created to validate the design.

3.2.1 Inverse kinematic of the Delta mechanism

Inverse kinematic of Delta robot is relatively more straight forward than forward kinematic. The process consists of finding the positions of connection points and using sphere equations that passes through these connection points to find the angle between the lower arm and base platform. Created spheres and positions can be better seen in Figure 3.11. θ_1, θ_2 and θ_3 variables are the inputs for the lower arms. They represent the angle between the lower arm and the base platform. The moving and base platform are taken as an equilateral tringle. These triangles ensure the 120° shift and make the shifting easier because the distances can be calculated easily. The value "e" is the side length of moving platform, "f" is the side length of base platform, "r_f" is the length of the lower arm and "r_e" is the length of the upper arm. These four parameters are the design parameters, which the designer have control over.

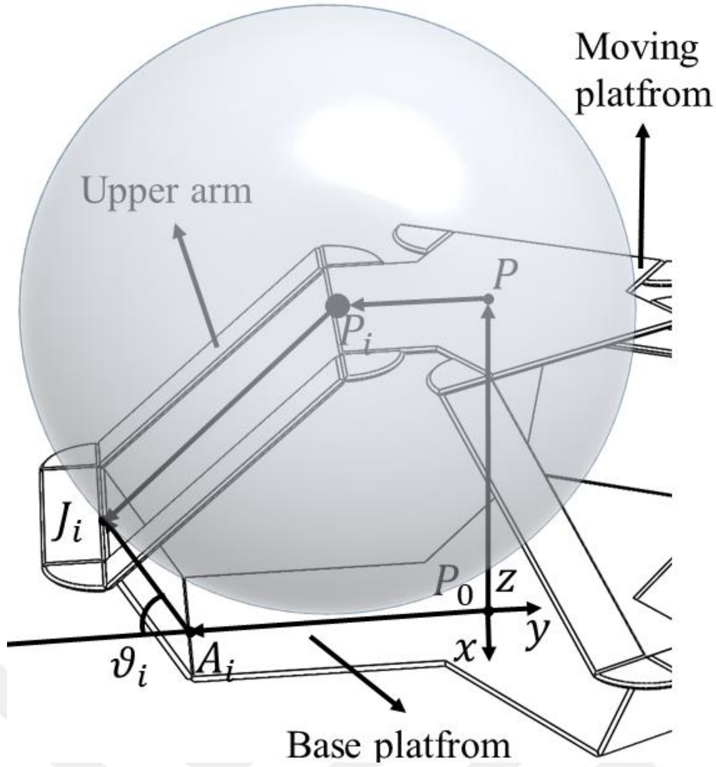

Figure 3.11 : Vector representation of kinematic chain for Delta mechanism's inverse kinematic.

First of all, the position of the connection points of moving platform and upper arm can be described as in equation (3.32). All of the values in this equation (3.32) are known (x, y and z are the positions given to inverse kinematic).

$$P_i = \left[x + \frac{e}{2\sqrt{3}} cos(\varphi_i) \quad y + \frac{e}{2\sqrt{3}} sin(\varphi_i) \quad z\right] \tag{3.32}$$

Since the moving platform is equilateral tringle the φ_i represents the 120º shift between the arms. After that the position of the connection points between the base platform and lower arm can be found as follows. All of the values of the equation (3.33) are known.

$$A_i = \left[\frac{f}{2\sqrt{3}} cos(\varphi_i) \quad \frac{f}{2\sqrt{3}} sin(\varphi_i) \quad 0\right] \tag{3.33}$$

The reference coordinate frame sits on the center of the base platform. That's why the z coordinate is zero. The same 120º shift is also present in the base platform. Using the A_i and r_f values, connection point between the upper arm and lower arm can be found as in equation (3.34).

$$J_i = [r_f \, cos(\varphi_i) \, cos(\theta_i) \quad r_f \, sin(\varphi_i) \, cos(\theta_i) \quad r_f \, sin(\theta_i)] + A_i \tag{3.34}$$

If a sphere with a center of P_i is created, the surface of the sphere have to pass through the J_i. Therefore, if the coordinates of the J_i is substituted in this sphere, the equation must hold. Equation (3.35) shows the sphere equation.

$$(J_{ix} - P_{ix})^2 + \left(J_{iy} - P_{iy}\right)^2 + (J_{iz} - P_{iz})^2 = r_e^2 \tag{3.35}$$

If the substitutions are made and the parenthesis are opened, it results in a very long and complicated equation. However, this equation can be manipulated and simplified to the point which it becomes only dependent of the θ_i unknowns and it resembles the equation (3.9) in the kinematics of Pantograph mechanism. The main equation is shown in equation (3.36). Other equations (3.36a) - (3.36b) shows the real values of the multiplier of equation (3.36) and all of them are known values.

$$a\,cos(\theta_i) + b\,sin(\theta_i) + c = 0 \tag{3.36}$$

$$a = -2r_f(x - A_{ix})\,cos(\varphi_i) - 2r_f\left(y - A_{iy}\right) sin(\varphi_i) \tag{3.36a}$$

$$b = -2r_f z \tag{3.36b}$$

$$c = x^2 + y^2 + z^2 + A_{ix}^2 + A_{iy}^2 + r_f^2 - r_e^2 - 2xA_{ix} - 2yA_{iy} \tag{3.36c}$$

The solution of equation (3.36) can be done using tangent half angle substitution like it is done in Pantograph mechanism. If the same equations (3.10) - (3.12) used, the solution becomes as shown in equation (3.37).

$$\theta_i = 2\tan^{-1}\left(\frac{-b \pm \sqrt{a^2 + b^2 - c^2}}{c - a}\right) \tag{3.37}$$

Same two problems can be seen in equation (3.37), like it is shown in the kinematic equations in Pantograph. The determinant control must be done and the real root has to be chosen as according to the position of the mechanism.

3.2.2 Forward kinematic of the Delta mechanism

Forward kinematic of Delta basically consists of the intersection of three spheres (Rey & Clavel, 1999). One of three closed loop kinematic chain is given in Figure 3.12. The center of the sphere is J which has shifted from point B, with using the vector CP. The coordinates of J can be found in equation (3.38). Other arms have exactly the same mathematical equation, but only shifted 120° and 240° from the first kinematic chain, respectively. The other sphere centers were given in equations (3.39) and (3.40).

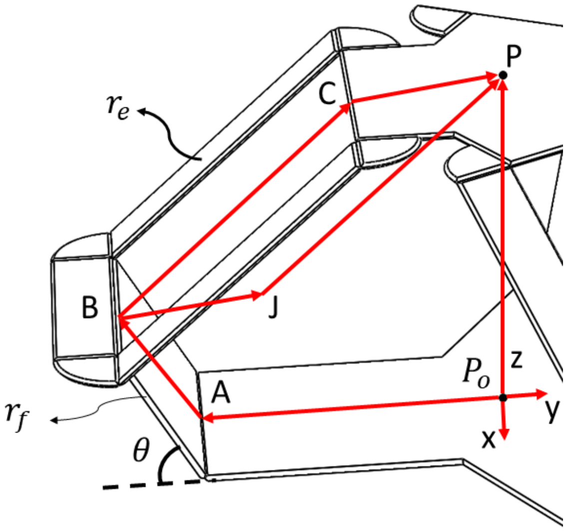

Figure 3.12 : Vector representation of kinematic chain for Delta mechanism's forward kinematic.

$$J_1 = \begin{bmatrix} 0 \\ \frac{e}{2} tan\frac{\pi}{6} - \left(\frac{f}{2} tan\frac{\pi}{6} + r_f \cos\theta_1\right) \\ (-r_f \sin\theta_1) \end{bmatrix} \tag{3.38}$$

$$J_2 = \begin{bmatrix} \left(\left(\frac{f}{2} tan\frac{\pi}{6} + r_f \cos\theta_2\right) - \frac{e}{2} tan\frac{\pi}{6}\right) cos\frac{\pi}{6} \\ \left(\left(\frac{f}{2} tan\frac{\pi}{6} + r_f \cos\theta_2\right) - \frac{e}{2} tan\frac{\pi}{6}\right) sin\frac{\pi}{6} \\ (-r_f \sin\theta_2) \end{bmatrix} \tag{3.39}$$

$$J_3 = \begin{bmatrix} \left(\left(\frac{f}{2} \tan\frac{\pi}{6} + r_f \cos\vartheta_3\right) - \frac{e}{2} \tan\frac{\pi}{6}\right) \cos\frac{5\pi}{6} \\ \left(\left(\frac{f}{2} \tan\frac{\pi}{6} + r_f \cos\vartheta_3\right) - \frac{e}{2} \tan\frac{\pi}{6}\right) \sin\frac{5\pi}{6} \\ (-r_f \sin\vartheta_3) \end{bmatrix} \tag{3.40}$$

To determine the arm positions in base and moving platforms, equilateral triangles were used again. Using these values as center of the spheres, equations (3.41) - (3.42) are obtained.

$$(P_x - J_{1x})^2 + (P_y - J_{1y})^2 + (P_z - J_{1z})^2 = r_e^2 \tag{3.41}$$

$$(P_x - J_{2x})^2 + (P_y - J_{2y})^2 + (P_z - J_{2z})^2 = r_e^2 \tag{3.42}$$

$$(P_x - J_{3x})^2 + (P_y - J_{3y})^2 + (P_z - J_{3z})^2 = r_e^2 \tag{3.43}$$

After that the squared parenthesizes are opened and equations (3.44) - (3.46) are obtained. Since the J_{1x} is zero, it is eliminated from the equation.

$$P_x^2 + P_y^2 + P_z^2 - 2J_{1y}P_y - 2J_{1z}P_z = r_e^2 - J_{1y}^2 - J_{1z}^2 \tag{3.44}$$

$$P_x^2 + P_y^2 + P_z^2 - 2J_{2x}x - 2J_{2y}P_y - 2J_{2z}P_z = r_e^2 - J_{2x}^2 - J_{2y}^2 - J_{2z}^2 \tag{3.45}$$

$$P_x^2 + P_y^2 + P_z^2 - 2J_{3x}x - 2J_{3y}P_y - 2J_{3z}P_z = r_e^2 - J_{3x}^2 - J_{3y}^2 - J_{3z}^2 \tag{3.46}$$

$J_{ix}^2,\ J_{iy}^2\ and\ J_{iz}^2$ squared terms is collected under the same variable as shown in equation (3.47) to simplify the equations.

$$w_i = J_{ix}^2 + J_{iy}^2 + J_{iz}^2 \tag{3.47}$$

After that equation (3.45) is subtracted from equation (3.44) and equation (3.48) is obtained. Then equation (3.46) is subtracted from equation (3.44) and equation (3.49) is obtained. Finally, equation (3.47) is subtracted from equation (3.46) and equation (3.50) is obtained.

$$J_{2x}P_x + (J_{1y} - J_{2y})P_y + (J_{1z} - J_{2z})P_z = \frac{(w_1 - w_2)}{2} \tag{3.48}$$

$$J_{3x}P_x + (J_{1y} - J_{3y})P_y + (J_{1z} - J_{3z})P_z = \frac{(w_1 - w_3)}{2} \tag{3.49}$$

$$(J_{2x} - J_{3x})P_x + (J_{2y} - j_{3y})P_y + (J_{2z} - j_{3z})P_z = \frac{(w_2 - w_3)}{2} \tag{3.50}$$

If equations (3.48) and (3.49) are manipulated, equations (3.51) and (3.52) can be obtained where the P_x and P_y is only dependent on P_z.

$$P_x = a_1P_z + b_1 \tag{3.51}$$

$$a_1 = \frac{1}{d}\left[(J_{2z} - J_{1z})(J_{3y} - J_{1y}) - (J_{3z} - J_{1z})(J_{2y} - J_{1y})\right] \tag{3.51a}$$

$$b_1 = -\frac{1}{2d}\left[(w_2 - w_1)(J_{3y} - J_{1y}) - (w_3 - w_1)(J_{2y} - J_{1y})\right] \tag{3.51b}$$

$$P_y = a_2P_z + b_2 \tag{3.52}$$

$$b_2 = \frac{1}{2d}\left[(w_2 - w_1)J_{3x} - (w_3 - w_1)J_{2x}\right] \tag{3.52b}$$

$$d = (J_{2y} - J_{1y})J_{3x} - (J_{3y} - J_{1y})J_{2x} \tag{3.53}$$

P_x and P_y of equations (3.51) and (3.52) are substituted in equation (3.41). The equation (3.54) is a second order polynomial and only dependent on P_z, obtained by opening the parenthesis squares. All the other values shown in equations (3.54a) - (3.54c) is known. Therefore, solving equation (3.54) will yield the P_z position of the end effector.

$$aP_z^2 + bP_z + c = 0 \tag{3.54}$$

$$a = a_1^2 + a_2^2 + 1 \tag{3.54a}$$

$$b = 2\left(a_1 b_1 + a_2\left(b_2 - J_{1y}\right) - J_{1z}\right) \tag{3.54b}$$

$$c = \left(b_2 - J_{1y}^2\right)^2 + b_1^2 + (J_{1z}^2 - r_e^2) \tag{3.54c}$$

The solution for second order polynomial is shown in equation (3.55).

$$P_z = \frac{-b \pm \sqrt{b^2 - 4ac}}{2a} \tag{3.55}$$

This P_z can be substituted in equations (3.51) and (3.52) to find the P_x and P_y positions to complete the forward kinematic of Delta mechanism. There are two important things to consider here. First one is that there are two different solutions, so the real root must be chosen according to the drawing of the mechanism. The other one is that the determinant of the equation (3.55) must be bigger than zero since this mechanism is a physical system and it must have a real solution. As a result, both of the kinematic solution of Delta can be obtained and they can be used in order to analyze the newly design Delta mechanism furthermore.

3.2.3 Delta mechanism's 3D CAD model

The mathematical equations of the Delta mechanism are obtained using the traditional Delta mechanism's kinematic model. However, the designed and manufactured Delta mechanism has different joints types and fabrication methods than traditional Delta mechanism. This difference mainly comes from the joints that are created for 2D fabrication methods. Since the designed Delta mechanism has a 2 DoF joints that mimics the real universal joints, the effect of these joints has to be taken into consideration rather than only looking in mathematical perspective. Specifically, the parallelogram structure has to be analyzed if it really sustains the parallel motion. That's why a 3D CAD model is developed. The joint connections are done exactly the same as the Pantograph mechanism's CAD model. Because both of them fundamentally have the same type of joints. Figure 3.13 shows the final design of the Delta mechanism.

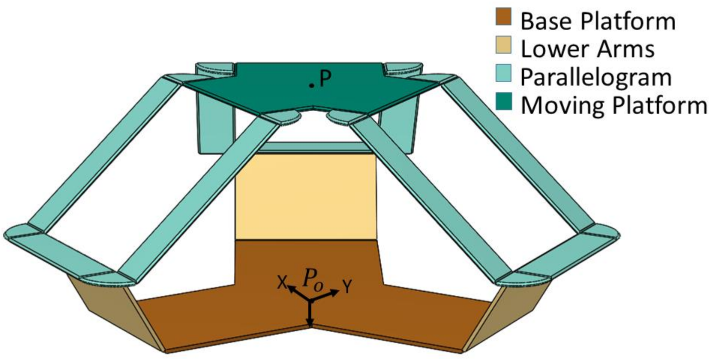

Figure 3.13 : 3D CAD model of the Delta mechanism.

After the model is created, using the same program a motion is given to the lower arms. The movement of the center of the moving platform is recorded. The same motion profile is also given to the kinematic model and calculation are done. Finally, both of these results are compared to see if the CAD model, which is ideal representation of the fabricated Delta mechanism, and mathematical model are the same or not. Result are given in experimental results section.

3.2.4 The design of Delta mechanism for SCM 2D fabrication method

The design of Delta mechanism has been completed by using 2D CAD software. Fundamentally the mechanism has two different laminated piece (sublayers) like the Pantograph mechanism. As it can be seen in Figure 3.14, one of them is for the base platform (rigid 1) and the other one is for moving platform (rigid 2).

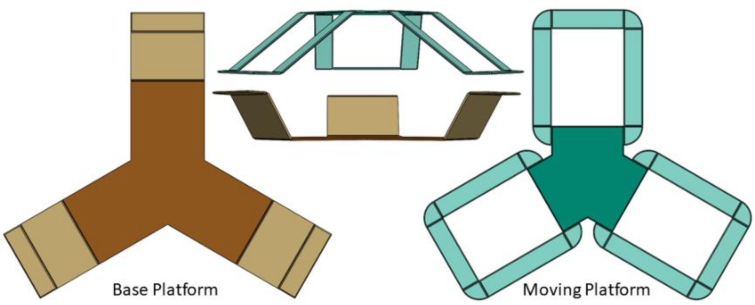

Figure 3.14 : Sublayers of the Delta mechanism.

The design of the base platform is relatively easy because it contains six basic 1 DoF joints that mimics the revolute joints. However, the design of the moving platform is more challenging because of the parallelogram structure. The most important design factor in Delta mechanism is the design of the parallelogram, which provides the parallel motion of the moving platform. Any inconvenience in parallelogram distorts the parallel motion of the moving platform directly.

The design of the base platform consists of six revolute joint, three lower arm and the connection links attached to the lower arms. The 2D drawing of the base platform can be seen in Figure 3.15. Firstly, the revolute joints are designed using the castellated techniques mentioned in the methodology section to ensure the axis of rotation stability. Due to this reason, the rigid layers of the base platform are not symmetric to each other. Therefore, there have to be two different cut has to be made. Secondly, the arms are 120^{o} apart from each other and their length is 25 mm. There are not any cuts in the arms. The actuator (servo motors) will be connected to these lower arms externally without causing any damage. Lastly, the upper and lower arms will be attached to each other by the connection links. The joints between the connection links and the lower arms are again revolute joints. Using the final cut shown in Figure 3.15c, all three of these elements will be finalized.

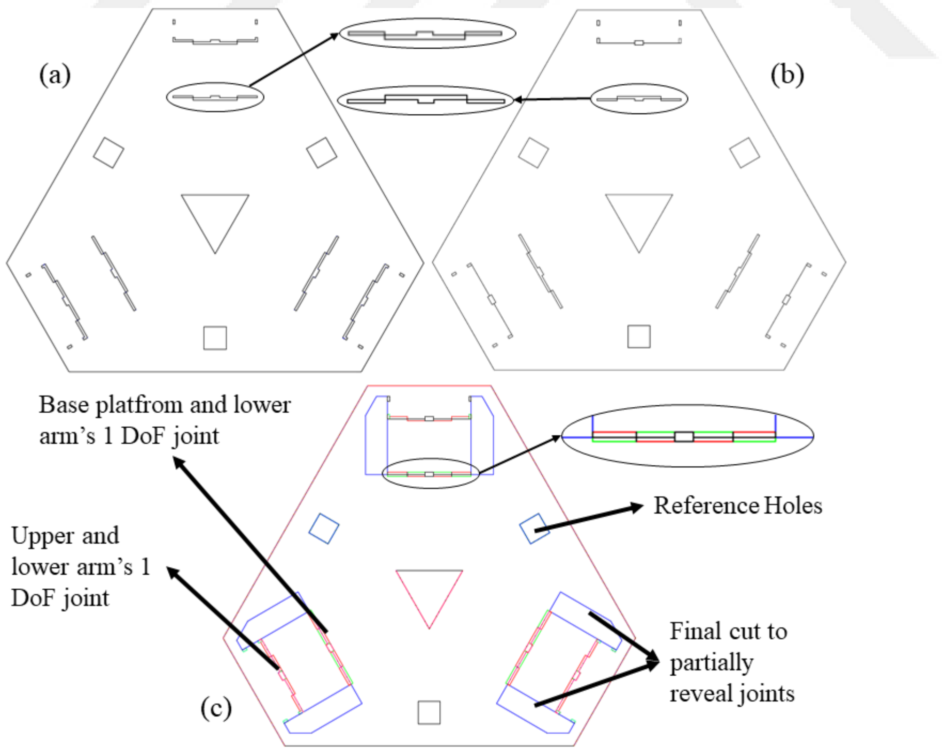

Figure 3.15 : 2D drawings of (a) bottom layer of base platform sublayer, (b) top layer of base platform sublayer and (c) base platform sublayer obtained from merging the bottom layer, flexible layer and top layer, in that order.

As oppose to the base platform, the design of moving platform, where it has three parallelogram structure in it, is a little bit complicated. In order to have a Delta mechanism that does not have any out-of-plane folding in assembly process, a new parallelogram that is suited for the SCM 2D fabrication methods have to be designed. Figure 3.16 shows a new four bar mechanism, a parallelogram that is used for the Delta mechanism. In this mechanism the opposing legs always move parallel to each other. If one leg of the parallelogram is fixed at some line, where it will be the connection link of the base platform in this case, the opposite leg will be forced move parallel to that line. Since the connection link is connected to the lower arm which is connected to the base platform, three parallelogram mechanisms will force the moving platform to work parallel to the base platform.

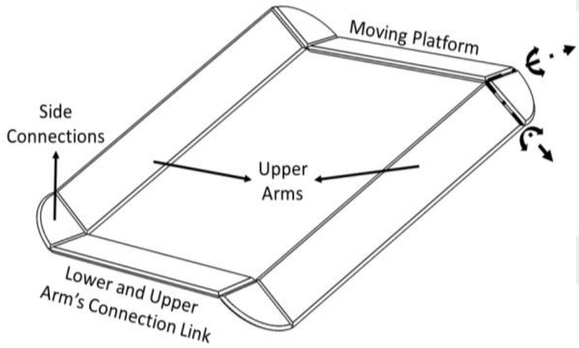

Figure 3.16 : Designed parallelogram mechanism that will be used as upper arms.

The 2 DoF joints used for the four bar mechanism are a combination of two 1 DoF joints that are in the same plane as it can be seen in Figure 3.17. The center of these 1 DoF joints are the same, but there is 90° angle between them. With this set up, the joint could rotate in two axes. The combination of four inner corners (centers of the 2 DoF joints) creates a four bar mechanism, which is a parallelogram in this case. The castellated joint design is used here again to ensure the stability of axis of rotation. However, the intersection between two 1 DOF joints must be taken into consideration. The overlaps resulted in local empty regions on one side and local rigid filled regions on the other side. Generally, this situation does not affect the overall performance. Yet there is a disadvantage, which is the 2 DoF joints have a preferred working direction. As shown in Figure 3.17, when two joint bends in the same direction, there is no place for both of the corners to bend because of the contact. However, the other side is empty, therefore the same problem does not occur. As a result, working area of the joints must be taken into consideration while stacking the layers.

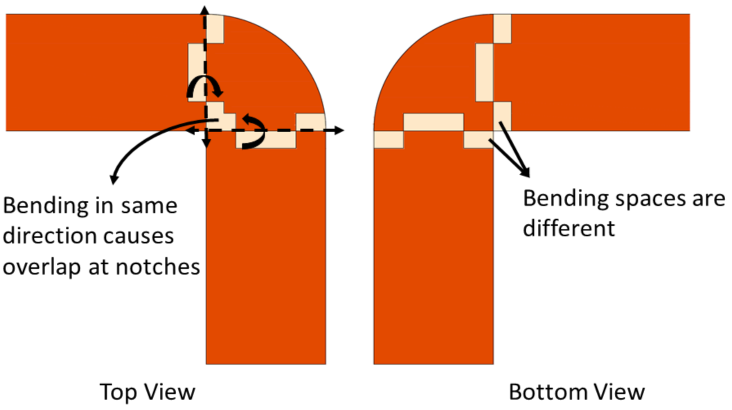

Figure 3.17 : The overlap problem in the joints of Parallelogram.

In conclusion, the final form of the moving platform can be seen in Figure 3.18. Three parallelogram is connected to the moving platform with the same 120º shift. Since the castellated joints are present here, the rigid layers of the moving platform have to be different from each other. Final cut of the moving platform shown in Figure 3.18c will partially reveal the parallelogram structure.

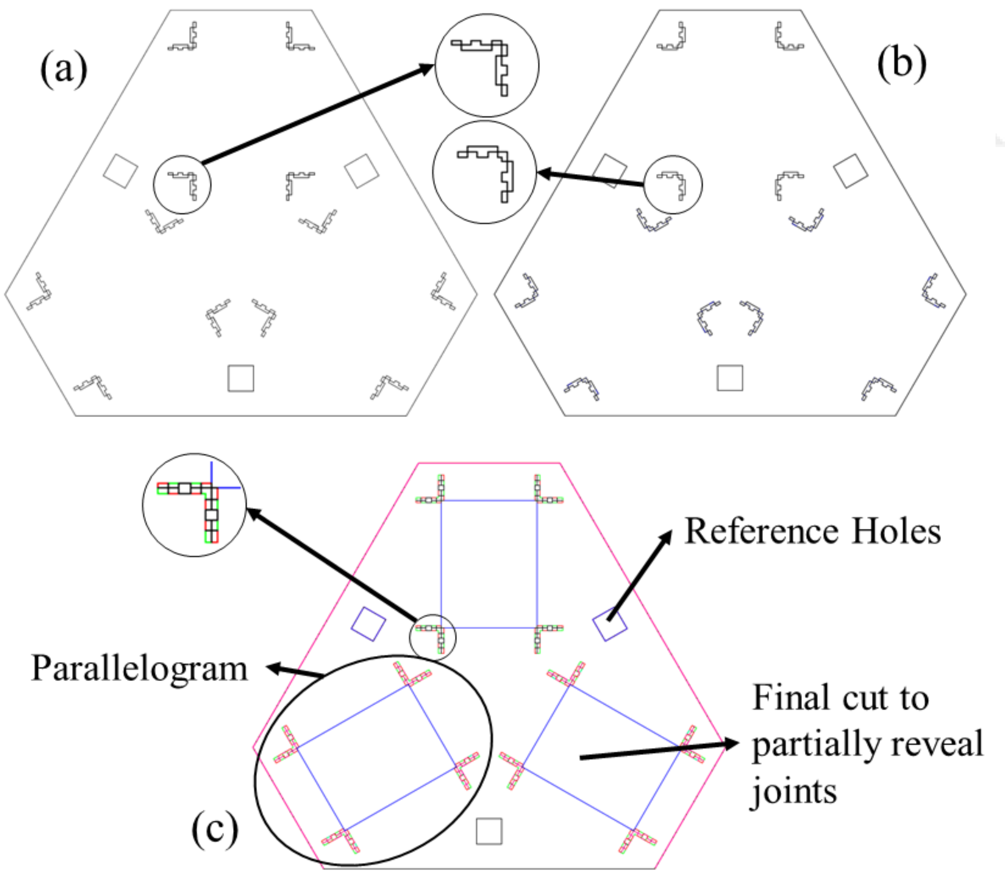

Figure 3.18 : 2D drawings of (a) bottom layer of moving platform sublayer, (b) top layer of moving platform sublayer and (c) moving platform sublayer obtained from merging the bottom layer, flexible layer and top layer, in that order.

Detailed fabrication process for Delta mechanism can be seen in Figure 3.19. The merging of the sublayers (moving and base platforms) happens after the final cut of these sublayers. After that step, the mechanism undergoes an ultimate final cut, where the partially revealed joints before will be fully revealed and the fabrication will be completed.

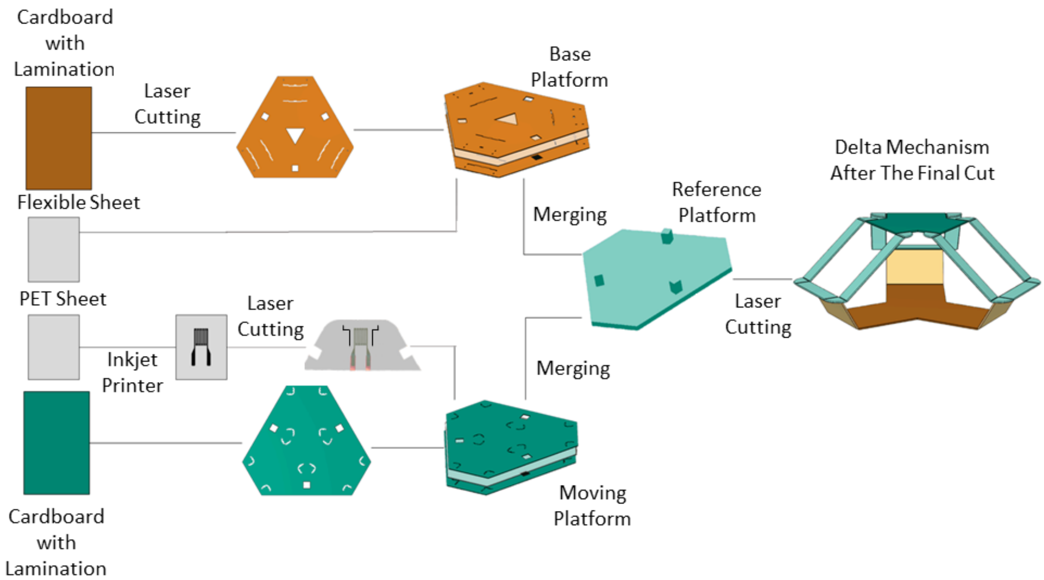

Figure 3.19 : Detailed fabrication and assembly process of the Delta mechanism with an embedded sensor.

As a result, a Delta mechanism with a completely flat fabrication process is designed. The design does not require any additional assembly steps other than fundamental cut – bond – repeat cycle. The mechanism has a stable workspace of 20x20x20 mm^3 where the unwanted non-parallel motions are minimum (in fabricated mechanism). Also, the traditional Delta mechanism's kinematic equations and analyzes can be used without any alteration. The manufactured Delta mechanism can be seen in Figure 3.20.

Figure 3.20 : Fabricated Delta mechanism: (a) closed (folded) form, (b) open form.

3.2.5 Effects of the flat design on the mechanism

When the design methodologies and fabrication methods is realized, it is found out that there arise some side effects. These side effects are coming from the flat form of the mechanism, new parallelogram design and lamination of the two sublayers. By examining these side effects, the design and the performance results can be understood explained better.

3.2.5.1 Dimensional dependencies arising due to flat design

One of the main effect of the 2D fabrication on the designed Delta mechanism, which all of the links are connected to each other (sometimes from more than one points) is it makes the geometrical properties dependent to each other. In this case, since there is no out-of-plane folding in the assembly, initial positions of the arms must be on top of each other and the joint's positions are determined previously and they cannot be changed without effecting solely upper arm or lower arm as it is shown in Figure 3.21.

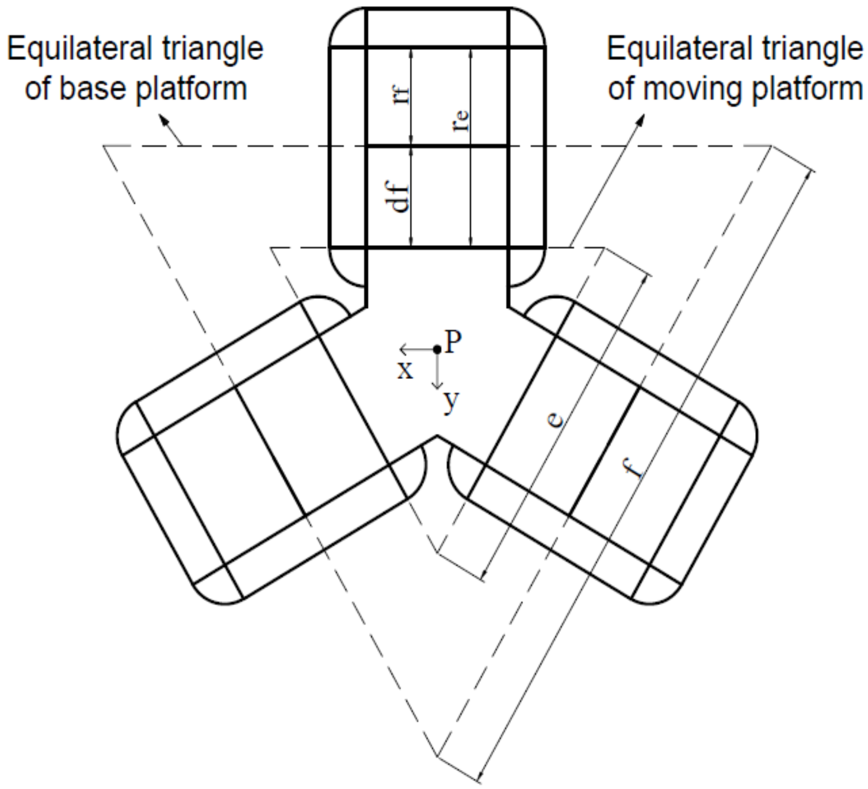

Figure 3.21 : Equilateral triangles and variables of the base and moving platforms.

In addition to that, the platforms and the arms are connected to each other where the dimension of the one will affect the other directly. This situation results in a reduction of the design parameters which are the length of the lower arm "r_f", length of the upper arm "r_e", size of the base platform "f" and size of the moving platform "e". Figure 3.21 is used to mathematically model the effect of flat design.

The base and moving platforms are taken as equilateral triangles as it can be seen Figure 3.21. In this arrangement, the distance between two edges of the triangles "df" and the length of the upper arm can be found using the edge lengths of the triangles in equations (3.56) and (3.57).

$$df = \frac{f}{2\sqrt{3}} - \frac{e}{2\sqrt{3}} = \frac{1}{\sqrt{3}}\left(\frac{f-e}{2}\right) \tag{3.56}$$

$$r_e = rf + \frac{1}{\sqrt{3}}\left(\frac{f-e}{2}\right) \tag{3.57}$$

The value "df" depends on "f" and "e", so at least making the "r_e" a dependent design parameter. "df" variable is used to find the length of the upper arm like given in the equation (3.57). Thus, the ratio of the Delta mechanism's arms can be calculated as in equation (3.58).

$$arm's\ ratio = \frac{r_e}{r_f} = \frac{r_f + df}{r_f} = 1 + \frac{df}{r_f} \tag{3.58}$$

The conventional Delta mechanism has four independent variables "r_f", "r_e", "f" and "e" whereas this design has three, because one parameter is a function others due to flat nature of the fabrication method and design. Also, the ratio of the arms in equation (3.58), that can be used for the singularity analysis in workspace of Delta mechanism, is not only dependent of the upper and lower arm but the dimensions of the base and moving platform as well.

3.2.5.2 Effect of not having a rotation on the rise joints

When there is no rotation on the rise joints, side joints could not rotate to the left or right, because in that position mechanism is flat and in a singular position as shown in Figure 3.22. There has to be an initial level difference between two opposite links to activate the side joints. When the initial level difference is provided, middle connections are forced to work parallel and stay parallel due to the joint symmetricity. These uncertainties do not occur at heights over approximately 10 mm, ensuring the mechanism is not flat.

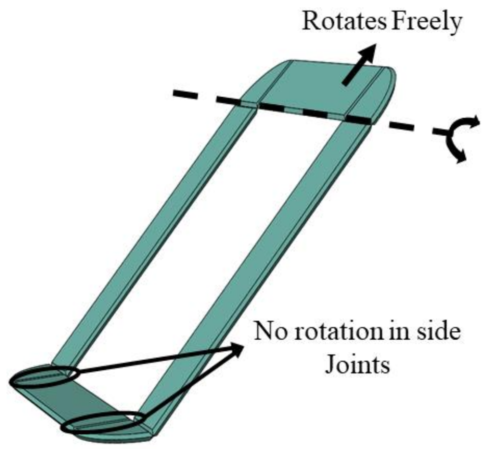

Figure 3.22 : No rotation in side joint state of the parallelogram.

3.2.5.3 Axial misalignment of the connection link

The arms of designed parallelogram itself could move up and down, but they always stay parallel to each other. However, there is a downside with this design; when there is no rotation on the side joints, the position of the connection link does not affect the opposite link of the parallelogram. The line between two joints stays the same ideally, but the link itself can be in any position. Generally, this is not a problem, but for this design it creates an axis misalignment in the connection link.

Fundamentally, the mechanism has two main sublayers; base platform sublayer and moving platform sublayer. These sublayers are bonded together from the upper and lower arm's endpoints (connection link). This connection creates a leveling problem between two joints that are present in the connection link which is not intended in the design. The problem is illustrated in Figure 3.23.

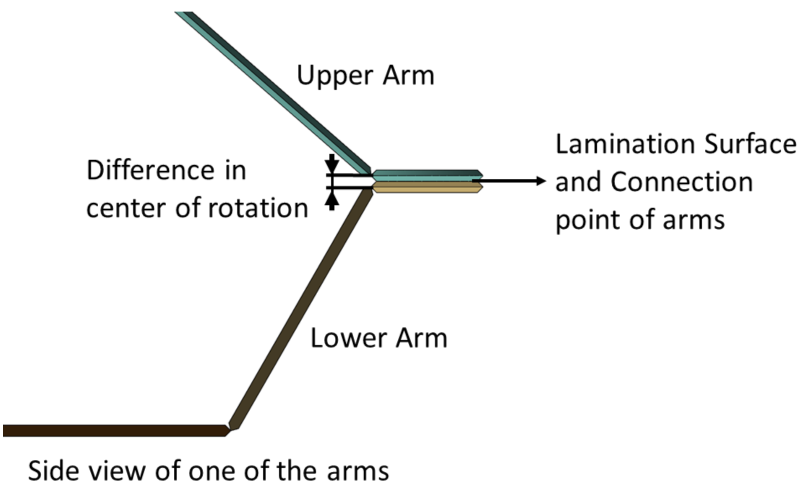

Figure 3.23 : Axis misalignment in the connection link.

This problem generally does not create serious effects on the kinematic model except raising the centers of the spheres perpendicularly to the XY plane. This perpendicularity comes from the parallel motion of the connection point. All three, base platform, moving platform and the connection point of the arms, works parallel to each other due to the nature of the designed parallelogram. Thus, the vectors of the connection point are always perpendicular to XY plane during the movement. However, as discussed earlier, this parallel motion is distorted in some configurations. This situation occurs when there is no rotation at the side joints, which are shown in the Figure 3.22, and these joints do not force the moving linkage to be parallel. Thus, when the mechanism crosses this straight position of parallelogram, the connection linkage loses its parallel motion and bends either up or down depending on the flexible layers.

In the design, this problem is compensated by using different flexible layers. Considering the total width ratios of the arms, less elastic flexible layer is used at the lower arm joints whereas more flexible layer has been used in the upper arm joints. Using flexible layers with a different elasticity creates a situation where the upper arm tries to push the connection point down, but the lower arm holds itself in place due to increased rigidity of the lower arm joint. The force acting on the connection point is not distributed evenly. However, only the maximum magnitude is considered because this effect is only observed when the parallelogram of the upper arm is in straight position. When the side joints are active, they force the connection point to be parallel, overcoming the downward push of the upper arm.

3.3 Stewart Mechanism

Stewart platform mechanism is a parallel mechanism with a 6 DoF motion. It has 6 separate legs with two platforms; base and moving platform. The movements are created by changing the leg's length where the ends of the legs are connected to the platforms by a spherical joint. The leg's connection points can be made with different number of ways and the number of connection points defines the name of mechanisms such as type 6 – 3 Stewart mechanism (six spherical joints in base platform and three spherical joints in moving platform with a group of two legs), type 6 – 6 Stewart mechanism (six spherical joints in both the base and moving platform where six legs are separately connected) and 3 – 3 Stewart mechanism (three spherical joints in base platform and three spherical joints in moving platform with a group of two legs). A traditional 3 – 3, 6 – 3 and 6 – 6 Stewart mechanisms can be seen in Figure 3.24. Different connection yields in different dynamical behavior and equations. Therefore, it is important to pick a Stewart mechanism suitable for the layer by layer techniques.

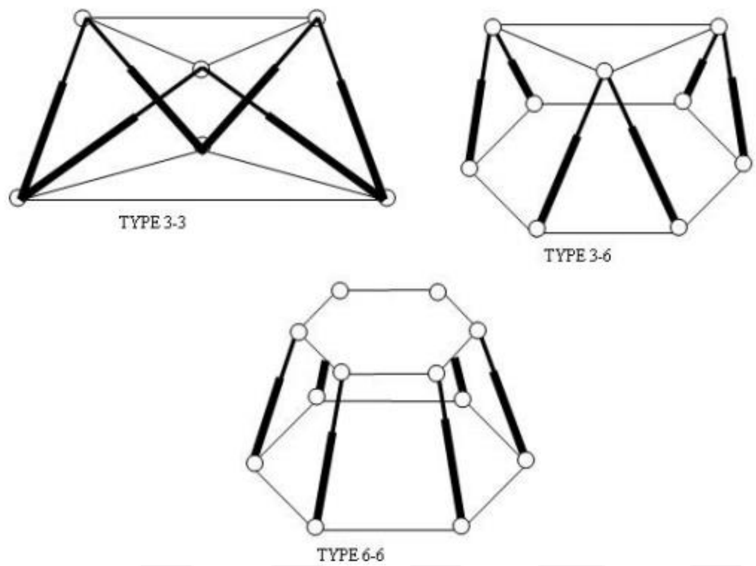

Figure 3.24 : Traditional 3 – 3, 3 – 6 and 6 – 6 Stewart mechanisms (Sonar et al., 2005).

The design in this research is 6-6 Stewart mechanism with a very close 6-3 configuration. Initially, a 6-3 mechanism is considered, but that design requires a spherical three-leg joint, which is a very complex joint to make even in traditional ways. There are not any three-leg spherical joints designed by layer by layer techniques. That’s why the 6-6 Stewart mechanism is designed, where two legs placed very closely in the moving platform creating three main connection areas as seen in Figure 3.25. In addition to that a leg with a linear 1 DoF (contraction and elongation) cannot be made with SCM 2D fabrication methods and origami inspired designs without breaking the monolithic structures, which is the main purpose of this research. That’s why instead of using linear actuator between the platforms, two separate legs are used with a spherical joint between two legs. One of them is connected to the base platform with revolute joint that can be given an angle input, and the other connected to the moving platform with a universal joint. In a nutshell, the design made to be suitable for the origami inspired techniques and the fabrication methods that is mentioned in methodology section and there is no out-of-plane folding or any other additional process in the assembly.

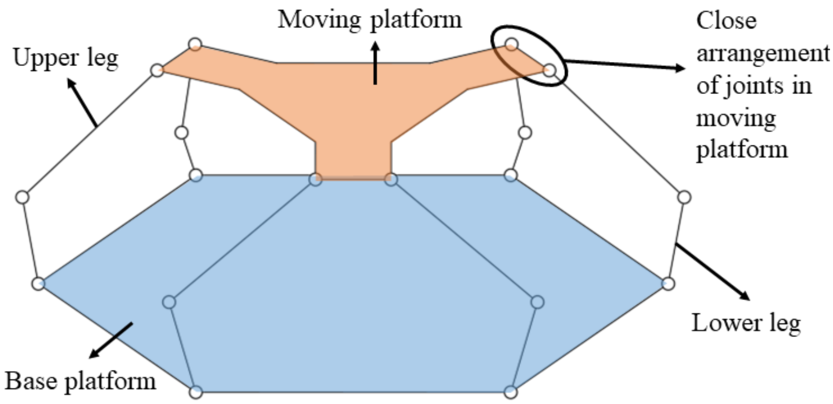

Figure 3.25 : The model of the Stewart mechanism that will be designed.

The mobility analysis of the Stewart platform can be done with Grubler – Kutzbach Criterion shown in equation (3.59). “M” gives the degree of freedom, where the “n” is total number of links, “g” is the number of kinematic pairs and finally “f_i” is the degree of freedom of the ith joint.

$$M = 6(n - g - 1) + \sum f_i \tag{3.59}$$

The number of link in the Stewart mechanism is 14, the number of kinematic pair is 18, where all of the joints connected to the moving platform is universal joint with 2 DoF, all the joints connected to the base platform is revolute joint with 1 DoF and all the joints between two legs are spherical joint with 3 DoF. Therefore, “M” can be found as “6” like shown in equation (3.60), which validates the Stewart mechanism has 6 degree of freedom.

$$M = 6(14 - 18 - 1) + (6 \times 1 + 6 \times 2 + 6 \times 3) = 6 \tag{3.60}$$

There are a couple of examples of the mechanism shown in Figure 3.25 in the literature. Overall shape of the mechanism is very similar to the Delta mechanism with a base and moving platform where they are connected by a number of legs. Therefore, the design process of Delta mechanism can be adjusted to the Stewart mechanism. The mechanism will be separated between two sublayers; base and moving platforms. The leg’s connection to the base platform will be a revolute joint, connection to the moving platform will be a universal joint and the connection between the legs will be a spherical joint. The legs that are connected to the base platform will be actuated using a servo motor just like in the Delta mechanism. The embedded sensors will be placed in the base platform, beneath the legs. In order to test the Stewart platform, an inverse kinematic and 3D CAD model will be developed, so that it can be validated by two different models.

3.3.1 Inverse kinematic of Stewart platform

Since the Stewart platform is a parallel mechanism, obtaining the inverse kinematic is rather simple. All six legs of the Stewart mechanism form a closed loop kinematic chain with its platforms. Therefore, the solution of one leg will be applicable to the other legs, only changing the coordinates of the initial points.

As seen in Figure 3.26, there are two different chains that can be created. The first one is $\mathrm{ACPP_0}$ loop that is the normal 6-6 Stewart loop with the linear actuator $\overrightarrow{\mathrm{CA}}$ vector, the second one is $\mathrm{ABCPP_0}$ loop which is two leg version of the mechanism with a revolute actuator. In order to find the angle between the base platform and the lower leg, initially the length of the $\overrightarrow{\mathrm{CA}}$ vector will be found using the $\mathrm{ACPP_0}$ loop. Then two spheres will be created, where the first one will be a sphere with the center "A" and radius $|\overrightarrow{\mathrm{CA}}|$. The second one will be a sphere with a center of "B" and radius $|\overrightarrow{\mathrm{CB}}|$. The center B can be found using the "θ" input. Surface of the both of the spheres must cross the point "C" due to the kinematic chains that are created. All of the mentioned parameters is already known as a design parameter, or can be found using the loops like vector $\overrightarrow{CA}$.

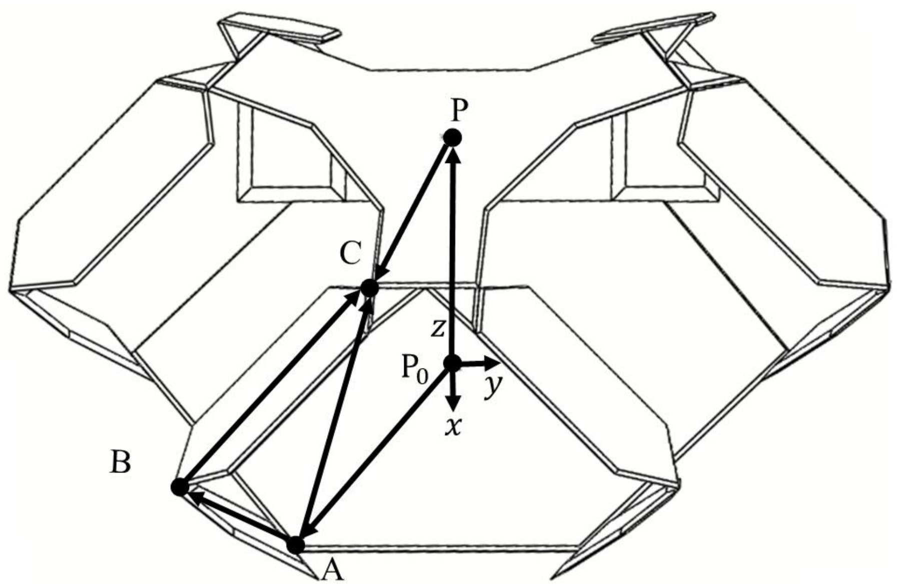

Figure 3.26 : Vector representation of kinematic chain for Stewart mechanism's inverse kinematic.

In order to find the $|\overrightarrow{CA}|$, first the coordinate of point "C" has to be obtained in respect to coordinate frame of P_0 by the position and rotation inputs. $\overrightarrow{PP_0}$ is the position input of the mechanism and it will be given, whereas $\overrightarrow{CP}$ vector will be calculated with the given rotation input of the moving platform "R_s" with respect to the base platform as shown in equation (3.61). $C'$and P' is the coordinates of the original points in the moving platforms coordinate frame. End position of sum of these vectors will give the "C" point's position as seen in equation (3.62).

$$\overrightarrow{CP} = R_s(C' - P') \tag{3.61}$$

$$\overrightarrow{CP_0} = \overrightarrow{PP_0} + \overrightarrow{CP} \tag{3.62}$$

At the same time the position of the "C" point can be found using the other side of the loop as seen in equation (3.63). $\overrightarrow{AP_0}$ is basically points the connection of the lower leg and the base platform and it is known by design, and $\overrightarrow{CA}$ is the vector to be found.

$$\overrightarrow{CP_0} = \overrightarrow{AP_0} + \overrightarrow{CA} \tag{3.63}$$

By using the equation (3.62) and (3.63), the equation (3.64) and then equation (3.65) can be obtained. At this point the vector $\overrightarrow{CA}$ can be found because all the other vectors are known. However, the necessary variable is the length of the vector $\overrightarrow{CA}$ rather than the vector itself. Equation (3.66) shows the calculation of the length of the vector $\overrightarrow{CA}$.

$$\overrightarrow{AP_0} + \overrightarrow{CA} = \overrightarrow{PP_0} + \overrightarrow{CP} \tag{3.64}$$

$$\overrightarrow{CA} = \overrightarrow{PP_0} + \overrightarrow{CP} - \overrightarrow{AP_0} \tag{3.65}$$

$$|\overrightarrow{CA}| = \left|\overrightarrow{PP_0} + \overrightarrow{R_s(C' - P')} - \overrightarrow{AP_0}\right| \tag{3.66}$$

As a next step, two spheres can be formed since the radius of the sphere with the center of "A" is obtained. From now on $|\overrightarrow{CA}|$ will be addressed as L_i, where "i" shows the number of the leg. The position of the point "B" can be found using the desired unknown "ϑ" as shown in equations (3.67) - (3.69). The α_i represents the angle between the vector $\overrightarrow{PP_0}$ and the x-axis in the XY plane that lies at the base platform and "k" is the length of the lower legs.

$$B_x = A_x + k \cos\theta_i \cos\alpha_i \tag{3.67}$$

$$B_y = A_y + k \cos\theta_i \sin\alpha_i \tag{3.68}$$

$$B_z = A_z + k\,sin\,\theta_i \tag{3.69}$$

The equation of the two spheres can be seen in equations (3.70) and (3.71). The variable "u" is the length of the upper legs.

$$(C_x - A_x)^2 + \left(C_y - A_y\right)^2 + (C_z - A_z)^2 = u_i^2 \tag{3.70}$$

$$(C_x - B_x)^2 + \left(C_y - B_y\right)^2 + (C_z - B_z)^2 = L_i^2 \tag{3.71}$$

The next three step is to substituted the open from of "B" in equation (3.71), open the parenthesis squares of equations (3.70) and (3.71), and the subtract the equation (3.70) from (3.71). If these steps are done the equation (3.72) can be obtained.

$$\begin{aligned} 2k\,cos\,\alpha_i\,(A_x - C_x)\,cos\,\theta_i + 2k\,sin\,\alpha_i\,\left(A_y - C_y\right)cos\,\theta_i \\ +2k(A_z - C_z)\,sin\,\theta_i + L_i^2 + k^2 - u^2 = 0 \end{aligned} \tag{3.72}$$

In order to shorten the equation (3.72) and to see the equation better, "α", "β", "γ" and "δ" variables are used in equations (3.73a) - (3.73d). As a result, similar to Pantograph and Delta mechanism, equation (3.73) with sine and cosine terms are obtained.

$$(\alpha + \beta)\,cos\,\theta + \gamma\,sin\,\theta + \delta = 0 \tag{3.73}$$

$$\alpha = 2k\,cos\,\alpha\,(x_A - x) \tag{3.73a}$$

$$\beta = 2k\,sin\,\alpha\,(y_A - y) \tag{3.73b}$$

$$\gamma = 2k(z_A - z) \tag{3.73c}$$

$$\delta = L_i^2 + k^2 - u^2 \tag{3.73d}$$

The solution for this equation structure are done with a half angle trigonometric formulation before as shown in equations (3.10) - (3.17). If the same solution process is used here, the final equation (3.74), which gives the desired angle can be found.

$$\theta_i = 2\,tan^{-1}\left(\frac{-\gamma \pm \sqrt{(\alpha + \beta)^2 + \gamma^2 - \delta^2}}{\delta - (\alpha + \beta)}\right) \tag{3.74}$$

As a result, given the position and the rotation of the moving platform, the lower leg’s angle can be found and the inverse kinematic can be solved. The equation (3.74) has two solutions. The correct solution can be picked according to the physical condition of the mechanism. Also, the determinant control has to be made. The equation represents a real mechanism’s position, so there have to be real solution. Imaginary solutions mean that the moving platform cannot go to the given positions.

The forward kinematic of the Stewart mechanism is much more complex than the inverse kinematic. There are analytical solutions for specific configurations. However, since the inverse kinematic is enough to analyze and test the mechanism, forward kinematic will not be found. Instead of the forward kinematic, the comparison will be made with 3D CAD model which will also represents the joints mechanical situation too.

3.3.2 Stewart mechanism's 3D CAD model

In order to validate the design of the Stewart mechanism, a 3D CAD model is created as shown in Figure 3.27. Even though the same universal joints of Delta mechanism are used, there is no parallelogram mechanism in the Stewart mechanism, so the six legs can move independent from each other. Also the consecutive revolute – spherical – universal joints that took the place of linear actuator, must be tested to see if it is really working even if the mechanism is completely rigid not flexible.

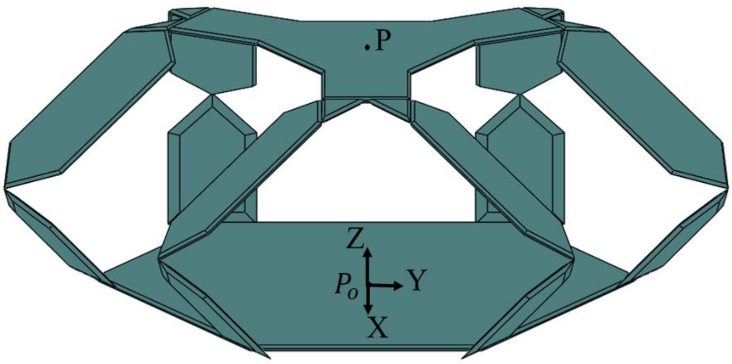

Figure 3.27 : 3D CAD model of the Stewart mechanism.

Since the Stewart mechanism has six degree of freedom movement, the forward kinematic equations have very high degree nonlinearities in it. That's why the workspace and the singularities inside the workspace are a hard challenge and they are not obtained in this research. Therefore, the 3D CAD model of the mechanism will be used as a forward kinematic. The angle values that are calculated from the inverse kinematic will be used in the CAD model, then the position of the center of the moving platform will be measured in respect to the base coordinate frame. After that, the result will be compared with the inputs of the inverse kinematic to see if they match. The one advantage of this method is that it also includes all the joints structure inside the results, so this is not solely an analytical comparison. It is the comparison between the mathematical model and the rigid physical representation of the mechanism. Results can be seen in experimental results section.

3.3.3 The design of Stewart mechanism for SCM 2D fabrication method

The same method of separating the mechanism's design into two sublayers (rigid 1 and 2) is also used in Stewart mechanism as shown in Figure 3.28. Rigid 1 sublayer will represent the base platform of the mechanism. It has a hexagon configuration where each leg sits on one corner. Again the joints between the lower leg and base platform will be 1 DoF revolute joint just like modeled in the kinematic equations. On the other end, rigid 2 sublayer will represent the moving platform. It has three main joint areas, where areas consist of two very close joints. Six legs coming from base platform will be connected to the moving platform with a 2 DoF universal joint. These joints will be similar to the joints used in the parallelogram design. The connection between upper and lower leg will be 3 DoF spherical joint. 3 DoF joints will be created by bonding two of the same pattern on top of each other, where half of it will be on the base platform and the other half will be on the moving platform. Alignment of these 3 DoF joints will be very important because 3 DoF joints consists of many small parts. Since the Delta mechanism's design methodology, fabrication and assembly steps are very similar, the design of the Stewart mechanism becomes a lot easier.

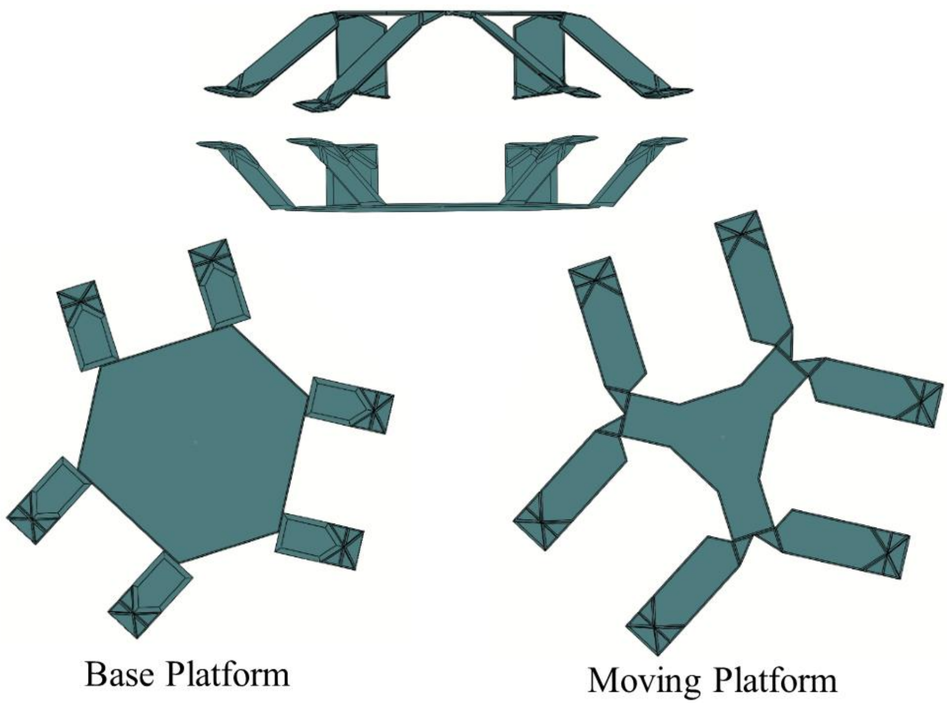

Figure 3.28 : Sublayers of the Stewart mechanism.

Rigid 1 sublayer has six revolute joints connected to the six lower legs and six 3 DoF joint halves that is attached at the end of the legs. The patterns of the base platform can be seen in Figure 3.29. Castellated joint technique is used in both the revolute joints and the 3 DoF joints. That's why the problem of having a preferred working direction and necessity of two different layers for rigid 1 sublayer occurs in Stewart mechanism too. The legs are gathered together by two by two, creating three groups where each group has different angles with the X – axis; leg 2 and 3 have 60º angle with the X – axis, leg 4 and 5 have 180º angle with the X – axis and leg 6 and 1 have 300º angle with the X – axis. The length of the legs is 25 mm. There are not any structural cut in the legs. The servo motor will be connected with the same method in Delta mechanism. Finally, the upper legs will be connected to the lower leg's 3 DoF joint half by their own 3 DoF joint half. The final cut of the base platform can be seen in Figure 3.29c.

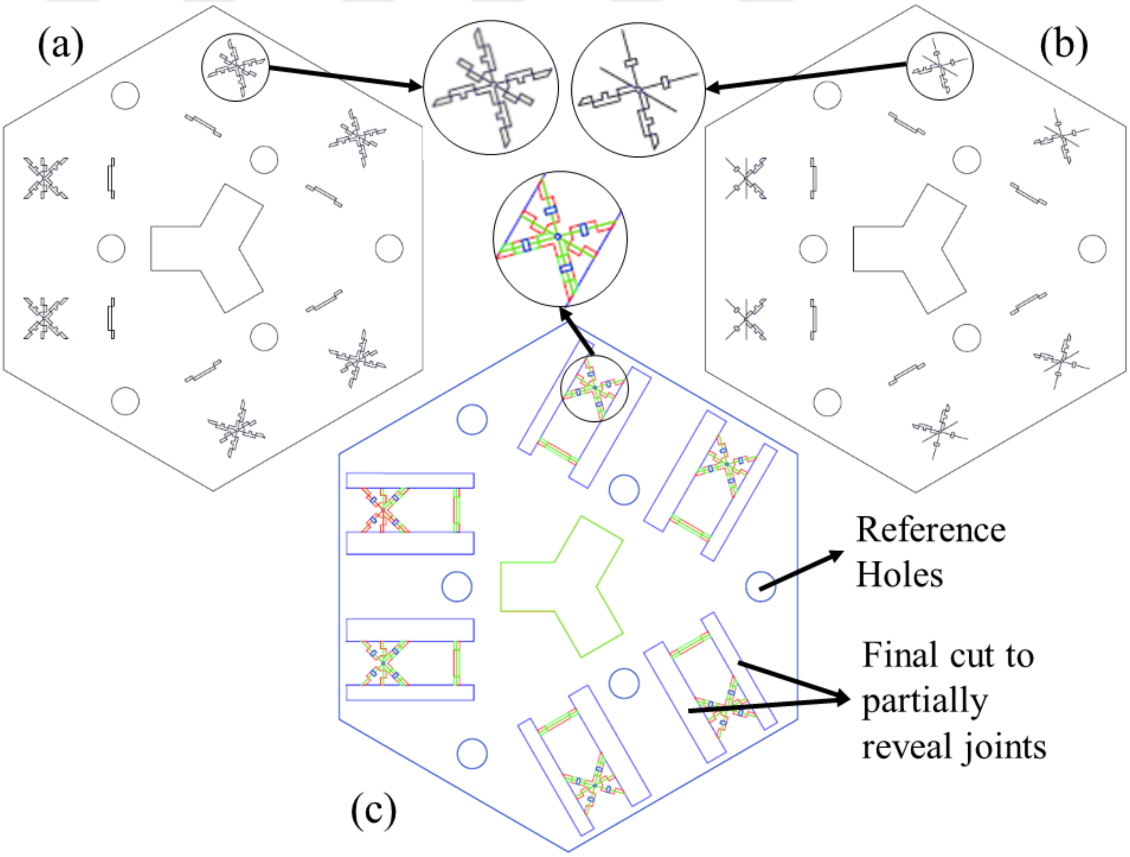

Figure 3.29 : 2D drawings of (a) bottom layer of base platform sublayer, (b) top layer of base platform sublayer and (c) base platform sublayer obtained from merging the bottom layer, flexible layer and top layer, in that order.

The design of the rigid 2 sublayer has six upper legs connected to the moving platform with an altered version of 2 DoF joints and other half of the 3 DoF joints. The patterns of the moving platform can be seen in Figure 3.30. The 2 DoF joints are the same joints that are used in the Delta mechanism with one difference. The angle of connection of the 2 DoF joints are 90º in Delta mechanism whereas the angle between the edge on the moving platform and the upper legs has 120º as seen in Figure 3.30c. That's why the joints also have to have the same angle in order to maintain the monolithic structure of the mechanism. These joints are still 2 DoF joints, but the rate of motion and the acting forces inside joints will definitely change. However, this research is on the design and fabrication of parallel mechanism, not the dynamical behavior. That's why the joints can be used here. The 3 DoF joints are the counterparts of the ones used in the base platform. The final cut of the rigid 2 sublayer can be seen in Figure 3.30c.

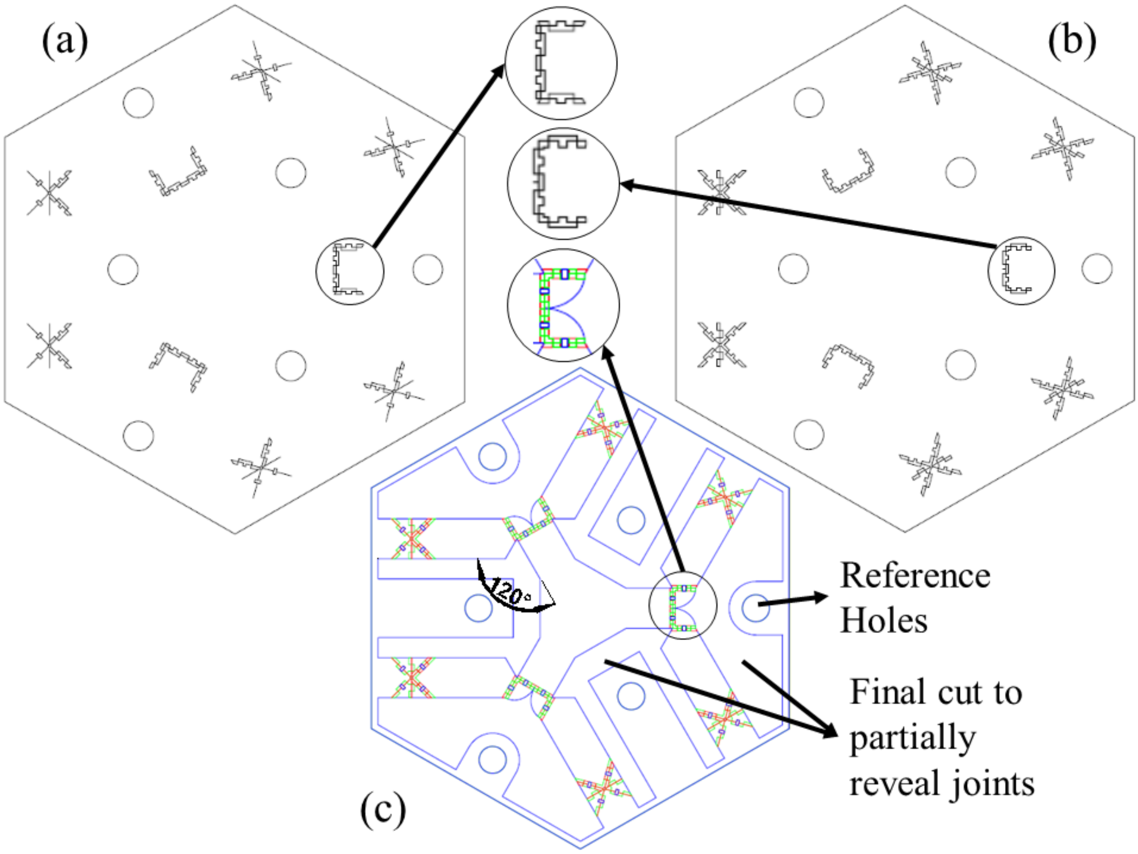

Figure 3.30 : 2D drawings of (a) bottom layer of moving platform sublayer, (b) top layer of moving platform sublayer and (c) moving platform sublayer obtained from merging the bottom layer, flexible layer and top layer, in that order.

Figure 3.31 shows the fabrication process of the Stewart mechanism. As always first the cuts of the sublayers have to be done. Then the next step is the assembly of the layers of sublayers and final cuts. After that two sublayers will be joined together and undergo an ultimate final cut. As a result, the Stewart mechanism will be completed.

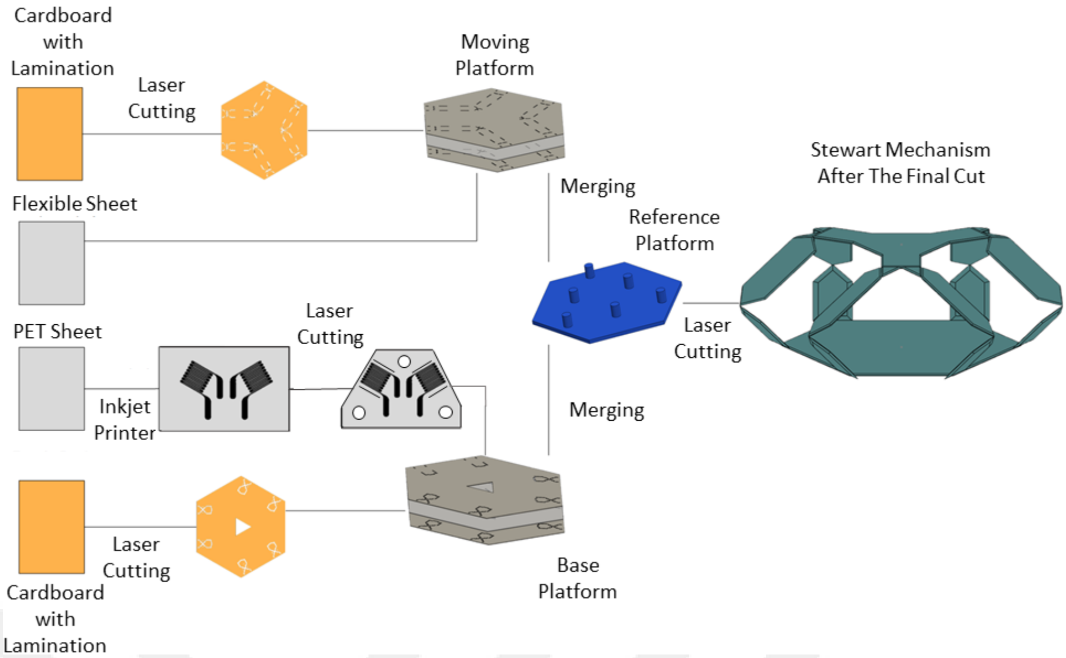

Figure 3.31 : Detailed fabrication and assembly process of the Stewart mechanism with an embedded sensor.

In conclusion, a design for a Stewart mechanism that is achieved by origami inspired and 2D fabrication method with a completely flat assembly process. The process only consists of cut – bond – repeat cycle. Since the forward kinematic of the mechanism is not obtained, the exact workspace is not known. However, using inverse kinematic and actual fabricated mechanism, it is estimated that the mechanism has a 20x20x20 mm^3 (the design is made with this goal) translational workspace. Inside this volume, the rotational movement of the mechanism is ±10º in X and Y axes, and ±7.5º in Z axis. If there is not any translational motion, the rotations in X and Y axis can be up to ±20º and rotation in Z axis can be up to ±15º. Thereby, the design of the Stewart mechanism is successfully done and fabricated mechanism can be seen in Figure 3.32.

Figure 3.32 : Fabricated Stewart mechanism: (a) open form, (b) closed (folded) form.

3.4 Design of Embedded Sensor

The most important parameters of the strain gauges are the leg length, leg thickness, leg number and the distance between the legs. All of these parameters decide the initial resistance of the strain gauge. The appropriate values can be determined by the requirements and the limitations. The leg number can be adjusted according to the desired width for the mechanism. The leg length is directly connected to the available space at the base platform. The distance between legs and the leg thickness depend on the resolution of the inkjet printer. Therefore, these design parameters are different for all three mechanisms except the leg thickness and the distance between the legs. Initial experiments showed that 0.4 mm leg thickness and distance between the legs is optimum, because the inkjet printer can easily print in that scale and there is no connection between the separate legs after the printing is done. The 2D drawing of the sensor can be seen in Figure 3.33.

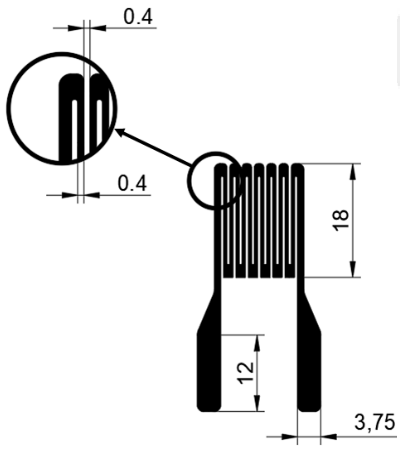

Figure 3.33 : Strain gauge sensor for inkjet printing. All dimensions are in millimeter.

Since the strain gauge sensor works due to the elongation in the materials that they are printed on, it is crucial to place the sensor into the correct measurement zone and secure their position that it works as it intended to work. If the mechanism's legs are analyzed, it can be seen that there are two distinct position that the sensor can be placed. The sensor can be placed right beneath the joint as shown in the Figure 3.34a or it can be placed at the middle of the joints as shown in Figure 3.34b. If the sensor is place at the middle of joint, after a couple of movement, the connection of the legs of the sensor breaks off and it becomes completely dysfunctional. Because the silver nano-particle ink lines cannot resist the repeated movements and loses its connection.

That’s why the middle of the joints it not a good place for the sensor. If the sensor is placed just beneath the joints, the problem goes away. However, in this place since the relative elongation due to the angle between the legs are small, the flexible movements in the rigid legs effects the measurements. This problem can be avoided by increasing the rigidity of the legs or by fixing the stationary leg to eliminate the flexible movements. Using the placement position in Figure 3.34a and placing the sensor in the surface that compression stress occurs, guarantees the sensor will be not broken easily by the mechanical affects.

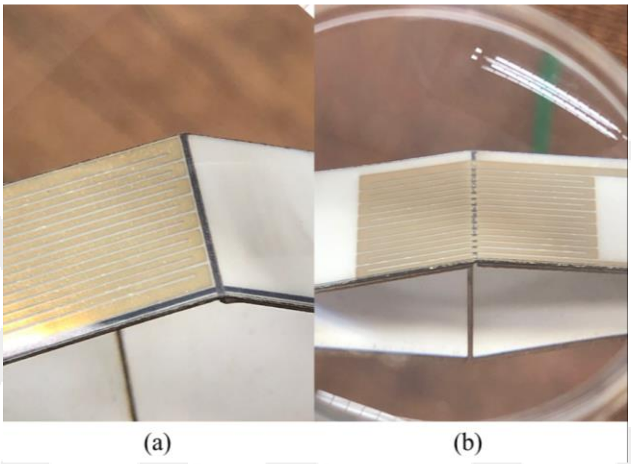

Figure 3.34 : Sensor placement in (a) beneath the joint and (b) on top of the joint in the Pantograph mechanism.

The other important factor to improve the signal quality of the sensor is to give it a freedom in the movement inside the layers. As it mentioned in earlier sections, there is always an adhesive layer between two separate layers. Since the sensor will be placed in the flexible layer, it means both surfaces of the sensor will be exposed to the adhesive layer. However, when the sensor is fixed strongly to the rigid layer, the elongation becomes very much dependent of the properties of the adhesive layer. Thus, removing the adhesive layer just in the active working area of the sensor by placing a really thin plastic film will distribute the input to the whole sensor rather than only the edge. In addition to that, cutting and releasing the sensor from the surrounding flexible layer in order make only the sensor area to be exposed to the input angle will improve the output furthermore reducing the uncertainties that comes from the placement. Figure 3.35 shows the deactivation of adhesive layer and the sensor cutting. However, the important matter to be considered here is that the flexible sensor layer is not only there for the measurement, but also it has to fulfill its duty as a joint too. That’s why the cut that can be seen in Figure 3.35c is not goes to the axis of rotation and weakens the joint. The cut expands when it gets close to the joint to the sides becoming exactly the length of the arm.

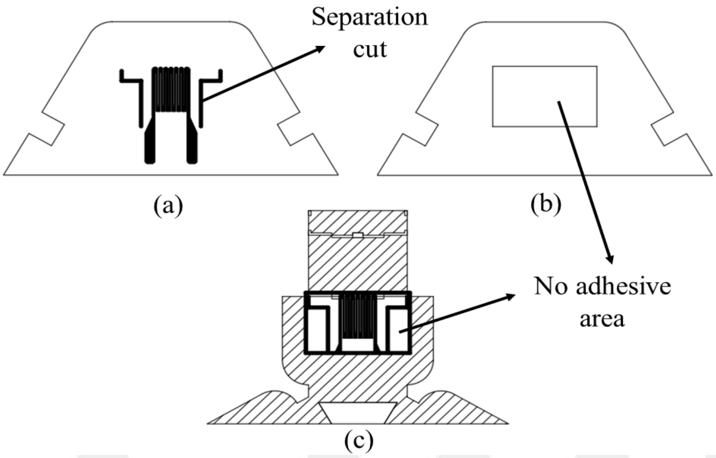

Figure 3.35 : (a) Separation cut to isolate the sensor from its environment, (b) rectangular cut in adhesive layer to prevent the sensor contact with adhesive and (c) the sensor integration in Delta mechanism.

The output voltage of the sensor is collected by a voltage divider circuit as shown in Figure 3.36. Voltage divider helps to convert the resistance change into to voltage that will be measured by a DAQ card (NI USB-6003). Since the circuit is very simple, the recorded voltage can be transformed back to the resistance value using the equation (3.75).

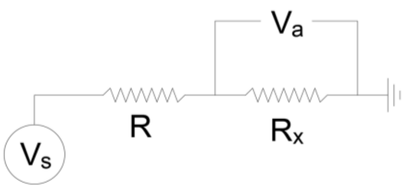

Figure 3.36 : Voltage divider circuit to collect data from the embedded sensor.

$$V_a = \frac{R_x}{R + R_x} V_s \tag{3.75}$$

3.4.1 Sensor layout in the parallel mechanisms

After the general placement position, isolation and cutting design steps are done, the sensors position on each individual parallel mechanism has to be decided. Since the Pantograph mechanism is for the proof of concept and the initial sensor design, the position of the sensor is in between the two long legs as shown in Figure 3.37. This joint represent the intermediate angle φ_i in equation (3.3) in forward kinematic. Therefore, designing a test setup where that angle can be measured and comparing the sensor output voltage will give an information about if the sensor is working or not.

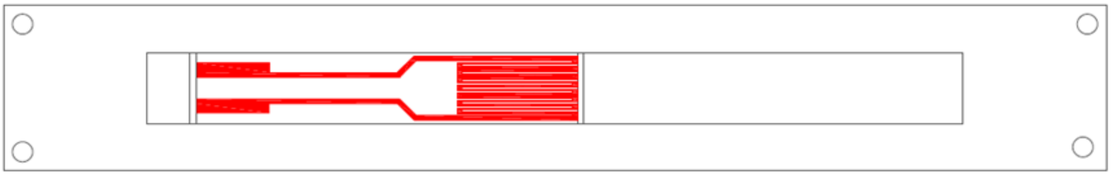

Figure 3.37 : Sensor layout of the strain sensor in the Pantograph mechanism.

The sensor position of the Delta mechanism can be seen in Figure 3.38. Since the Delta mechanism has three separate legs, there have to be three different sensors. Each sensor is independent from each other. The sensors are embedded in the base platform's flexible layers, so they cannot be seen from the outside. After the Pantograph mechanism's tests, it is realized that crossing the axis of rotation a little bit with the edge of the sensor improves the signal quality. Also, the crossed part does not include the legs, so that even if the connection is lost at the edge, the legs connection is not broken and sensor continues to work.

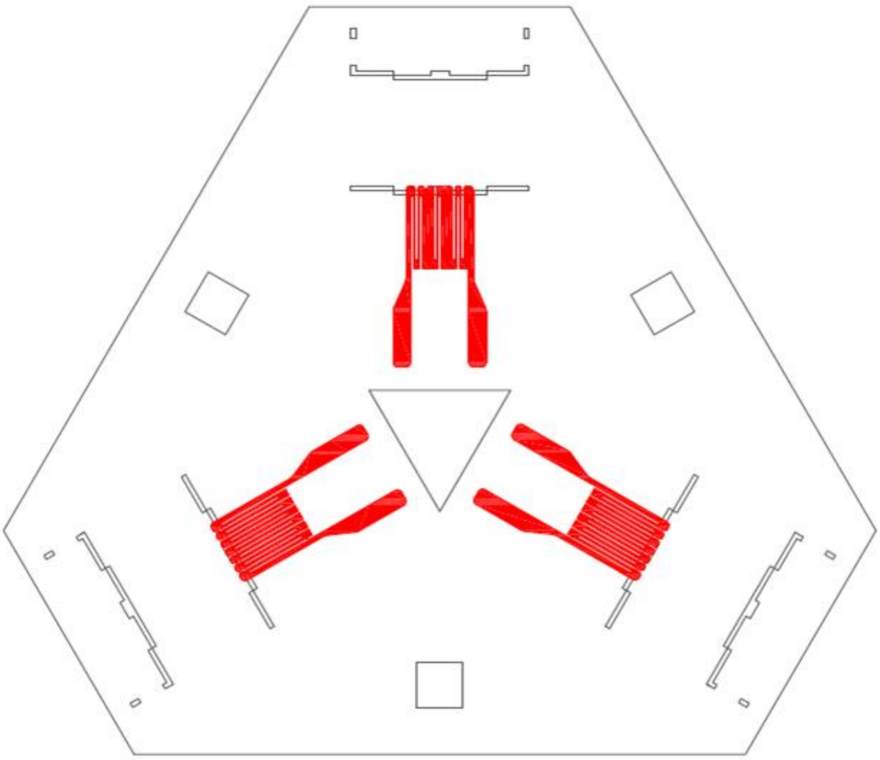

Figure 3.38 : Sensor layout of the strain sensor in the Delta mechanism.

The placement of the sensors in the Stewart mechanism became rather easy due to the collective information from Pantograph and Delta mechanisms. As it can be seen in Figure 3.39, the legs and the placement of sensors of the Stewart mechanism and Delta mechanism is very similar. The big difference is that size of the sensors and the number of legs. Having six legs at the base platform, where the embedded sensor is present, means six sensors will be placed in a small place. That's why the number of the legs and the sensors are little bit smaller than Delta mechanism. Other than that the isolation layers and cutting lines at the sensor layers adapted to the Stewart mechanism exactly.

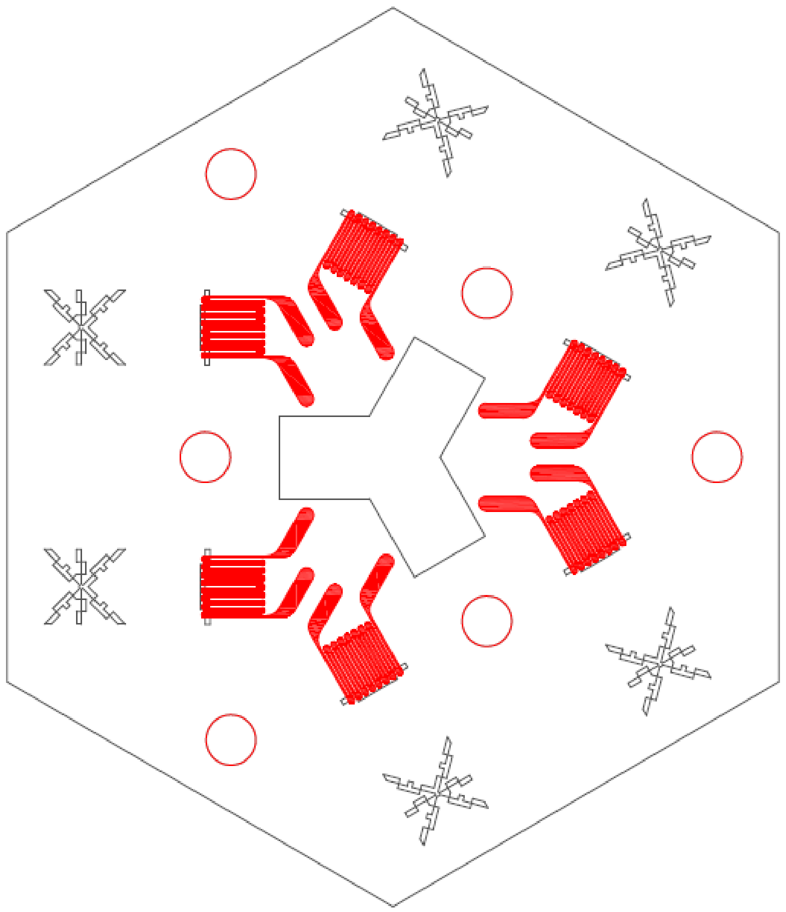

Figure 3.39 : Sensor layout of the strain sensor in the Stewart mechanism.

3.4.2 Connections between the sensor and the cables

One of the very challenging problem of the embedded sensor is the cable connections. The strain gauge sensors are made of silver ink. Any friction, heat or mechanical impact, removes the ink from the surface making the sensor ineffective. Thus, a copper cable cannot be soldered to the ink. Also, a method where there will be a bumps and bulges cannot be used because it will disrupt the flat shape of the sublayers and over all mechanism. That’s why three similar but different method are develop for the cable connection.

Figure 3.40 shows the three developed methods. The first one is to gluing the cable using a conductive epoxy. The connection becomes very strong and stable, but the bulges that are created due to the epoxy is not small and is noticeable. The second one is to use a flat middle connection like a copper-kapton film to spread the conductive epoxy to a larger area and reduce the size of the bulge and then solder the cables to the copper-kapton film. However, even if the bulge is reduced, it still disrupts the flat shape. The final one is to use only the middle connection copper-kapton without the conductive epoxy. Since the layers are attached together very strongly with an adhesive layer, that compression and friction between the layers can be used to hold the copper-kapton film in place. This method does not leave bump and bulge due to absence of any filling media. Also, the connection becomes very strong and stable even if there is not any direct adhesive between the film and the sensor. That’s why the last method is chosen to be applied to all of the mechanisms.

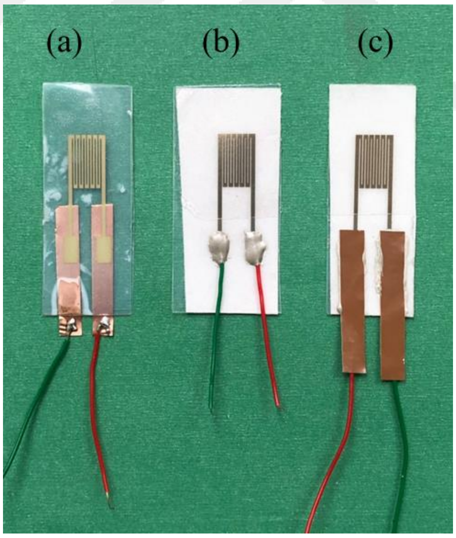

Figure 3.40 : Cable connection with (a) copper – kapton and friction between the layers, (b) only conductive epoxy and (c) conductive epoxy and copper – kapton.

3.4.3 Sensor fabrication with layer by layer techniques

If there is no sensor in the flexible layer, fabrication is rather straight forward because the flexible layer is just applied everywhere between the rigid layers. However, embedding a sensor in the flexible layer changes the process. There are a couple of extra step to prepare the sensor layer as seen in Figure 3.41. Even if the patters are different, the process steps are exactly the same in all three parallel mechanisms. The example in the figure shows the Delta and Stewart mechanism’s sensor layer preparation.

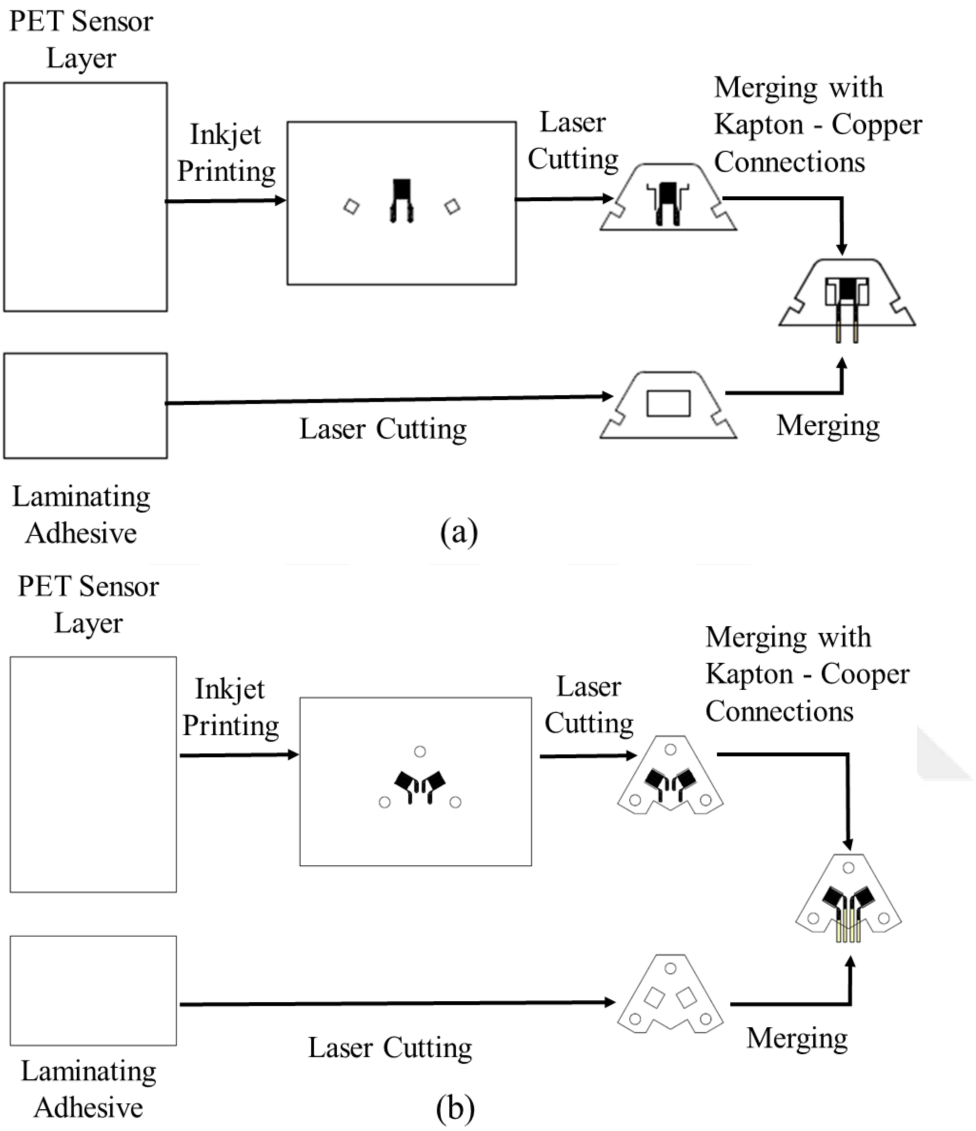

Figure 3.41 : Sensor layer preparation of (a) Delta and (b) Stewart mechanisms.

As it can be seen in Figure 3.41, the sensors have to be printed on the PET sheet (Nova centrix - Novelle Printing Media) with a silver nano-particle ink (Novacentrix-metalon JS-B25P) using an inkjet printer (Epson L382). After that the sensors have to be taken out of the sheets, reference holes and isolation cuts have to be opened by cutting with laser. Before placing the sensors to their respective areas, a thin plastic films are placed on the effective working areas in the base platform. Also, the copper-kapton film integration is done in this step. As a result, and flexible layer with a sensor and cable connection integration is done and ready to be placed to the rigid layers.

4. EXPERIMENTAL RESULTS AND DISCUSSIONS

There will be three separate experiments conducted. The first one will be the comparison between kinematic models and the 3D CAD models in order to validate the mechanisms if they are suitable for the traditional mathematical equations ideally and to check if the joints are working as they are intended to work. The second one will be the tracking performance of the fabricated Delta and Stewart mechanisms. The motion of the moving platforms will be compared to the input. The third one will be the sensor experiments. Sensor output will be examined to see if the sensor detects the angle input chance in the legs.

4.1 Experimental Setup

The test platforms will be designed and manufactured for each individual mechanism with 3D printer Ultimaker S5. The design will be done by a CAD program, considering the real dimensions of the mechanism. The actuation will be done by Dynamixel (XL430 – W250 – t) robot servo motors. The motors and the lower arms will be connected to each other by a custom design connection shown in Figure 4.1. The position of the moving platform will be measured by a 6 DoF Polhemus Patriot position sensor. PATRIOT sensor has 6 Degrees of Freedom with a resolution of 0.0381 mm, 0.01 degree, and a static accuracy of 1.52 mm RMS for the X, Y and Z position and 0.4 degrees RMS of orientation. The measuring point of the sensor will be placed right in the center of the moving platforms. The reference of the position sensor will be fixed right next to the test platforms and the X, Y and Z axis of both platforms will be aligned. Output of the embedded sensor will be collected by NI – USB6003 data acquisition device and a simple voltage divider circuit.

The experimental setup of the Delta mechanism can be seen in Figure 4.2 and 4.3. It has three servo motor connected to three lower arms. The trajectory test of the Delta mechanism will be done in ±10 mm in X and Y axis, and between 40 – 60 mm in Z axis. Sensor calibration will be done before the tests to get more accurate results.

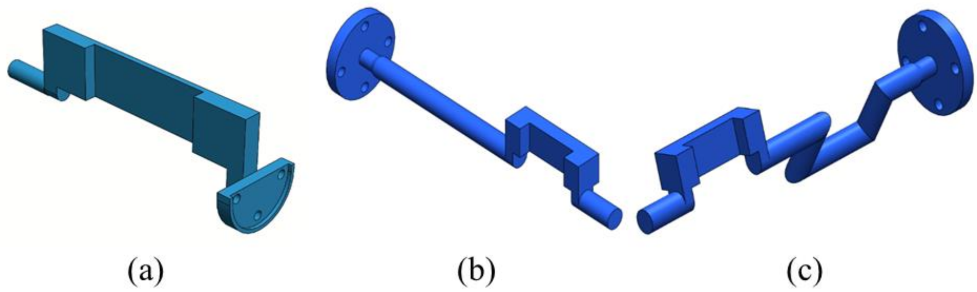

Figure 4.1 : Mechanism – motor connections: (a) Delta mechanism’s connection part, (b) and (c) Stewart mechanism’s connection part.

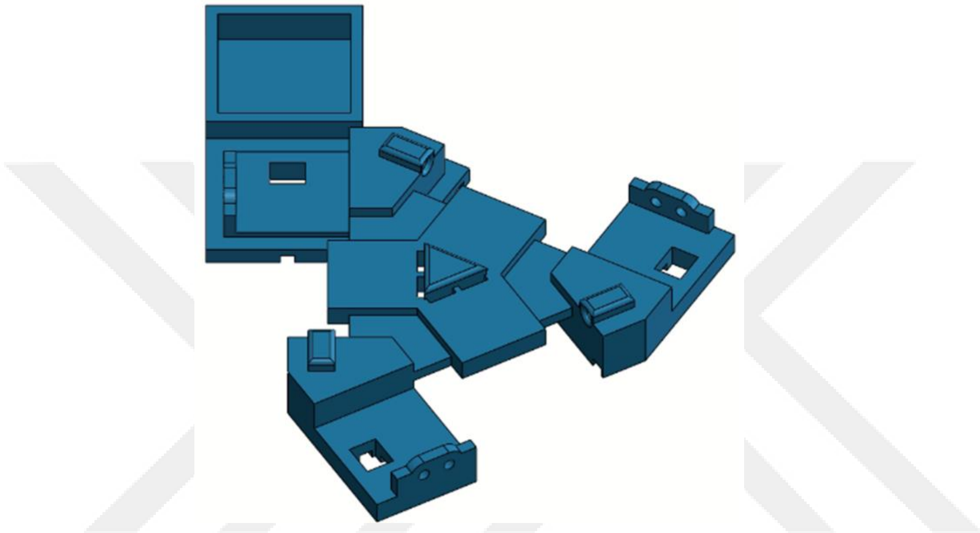

Figure 4.2 : 3D model of test platform for Delta mechanism.

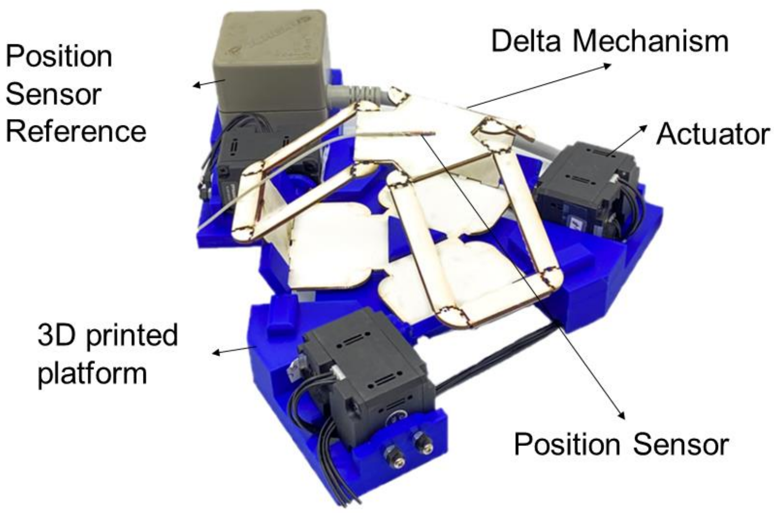

Figure 4.3 : Delta mechanism and equipment placements in the test platform.

The experimental setup of the Stewart mechanism can be seen in Figure 4.4 and 4.5. There are six motors actuating six legs of the Stewart mechanism. The tests will be conducted in ±10 mm in X and Y axis, and in 30 – 50 mm in Z axis. The sensor connection and the axis alignment is more important in here due to the rotational motion that will be measured. The rotation in one axis will influence the others if there is any inaccurate positioning in the alignment. In addition to that differently from the Delta mechanism, there are two separate motor – leg connection part in this platform as seen in Figure 4.1b and 4.1c. The driving axis of two nearby motors of the Stewart mechanism overlaps with each other because the motors are wanted to be connected directly to the arms without using any secondary parts. One of the connection part has a straight axis whereas the other one has an axis eccentricity in it. That eccentricity allows the part to rotate a ±90º from the zero position of the mechanism. However, in order to be safe two different precautions are taken. First one is to prevent the motor to move in software more than the desired angles. This method is also used in Delta mechanism. The second one is choosing the diameter of the connection axis according to the maximum tork that the motor can have with simple stress and torsion calculations. By doing so, it is ensured that the connection part will be broken if it crashes on the platform before the motor reaches its maximum tork.

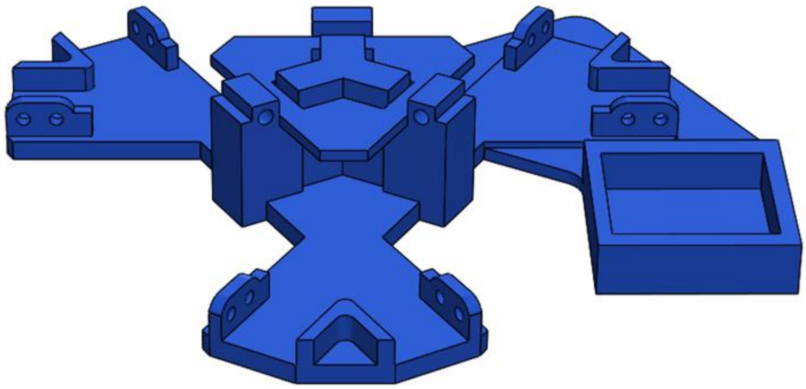

Figure 4.4 : 3D model of test platform for Stewart mechanism.

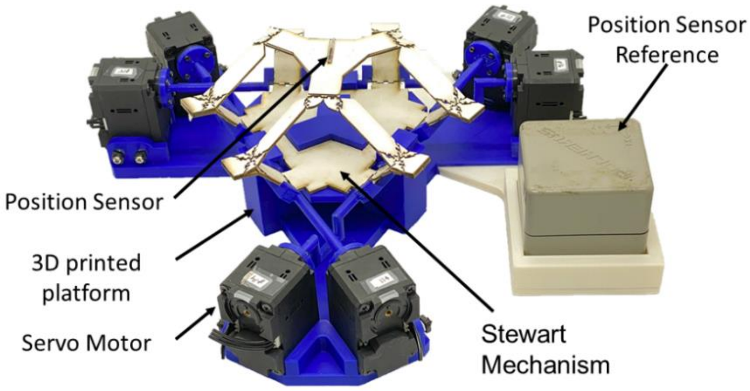

Figure 4.5 : Stewart mechanism and equipment placements in the test platform.

4.2 Comparison Between the CAD Models and the Kinematic Models

The comparison tests are done by using the motion analysis tool of Solidworks CAD software and MATLAB software. The previously obtained 3D models are used. Firstly, the tests for Pantograph mechanism are conducted. There is only one test for Pantograph mechanism. The mechanism has two different input; rotational input and linear input. The linear input is chosen as a fixed value as 7 cm. On the other hand, a sinusoidal input with a magnitude of ±22.5° degree whose center is 67.5° degree is given as a rotational input for 5 seconds. The frequency of the wave was 1 hz. Then, both solutions are compared with each other. Figure 4.6 shows the results in X axis and Y axis.

As it can be seen, both the CAD model and kinematic model have given very close solutions. The error is on the level of one in ten thousand in both graphics. The error is very likely caused by the difference between the numerical and analytical solutions. Therefore, it can be said that the pantograph's design is consistent with the mathematical model.

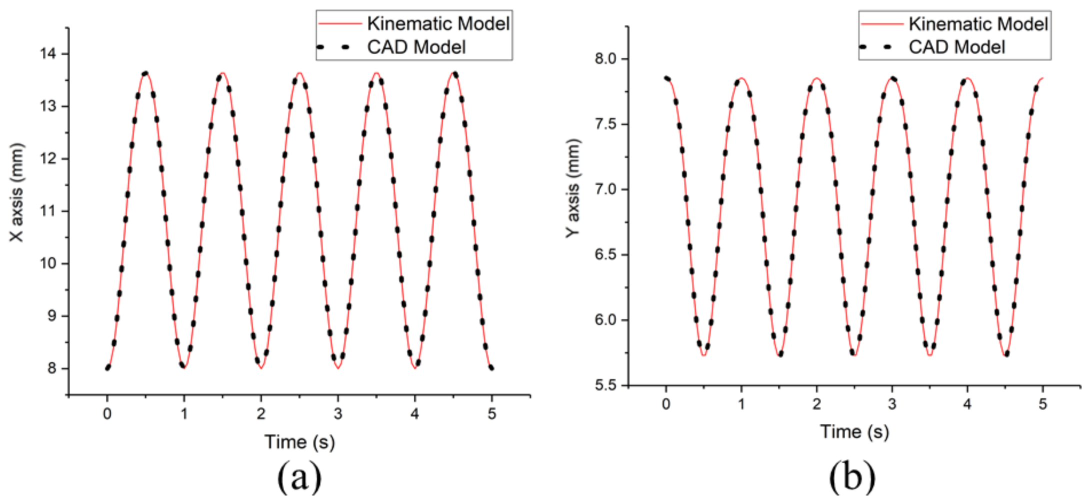

Figure 4.6 : Comparison between the CAD and kinematic model of Pantograph mechanism in (a) X axis and (b) Y axis.

In Delta mechanism, there are two different test that are conducted; one arm is fixed in position whereas the other two is moving and all three arms are moving at the same time. Both tests are conducted for five seconds and mechanisms move in all directions. The used model is same with the model that is shown in Figure 3.13. The axes are aligned according to the axes orientation that is taken in the kinematic model the with one to one comparison. The obtained kinematic equations are solved by MATLAB and recorded.

In the first test, arm 1 has a sinusoidal motion with a magnitude of ±15º and 0.5 Hz frequency starting from 30º, in the 0º direction whereas arm 2 has a sinusoidal motion with a magnitude of ±22.5º and 0.25 hz frequency starting from 30º, in the 90º direction. Arm 3 is fixed at the 45º. The results of moving platform's trajectory following in X, Y and Z axes for both the analytic and CAD model can be seen in Figure 4.7.

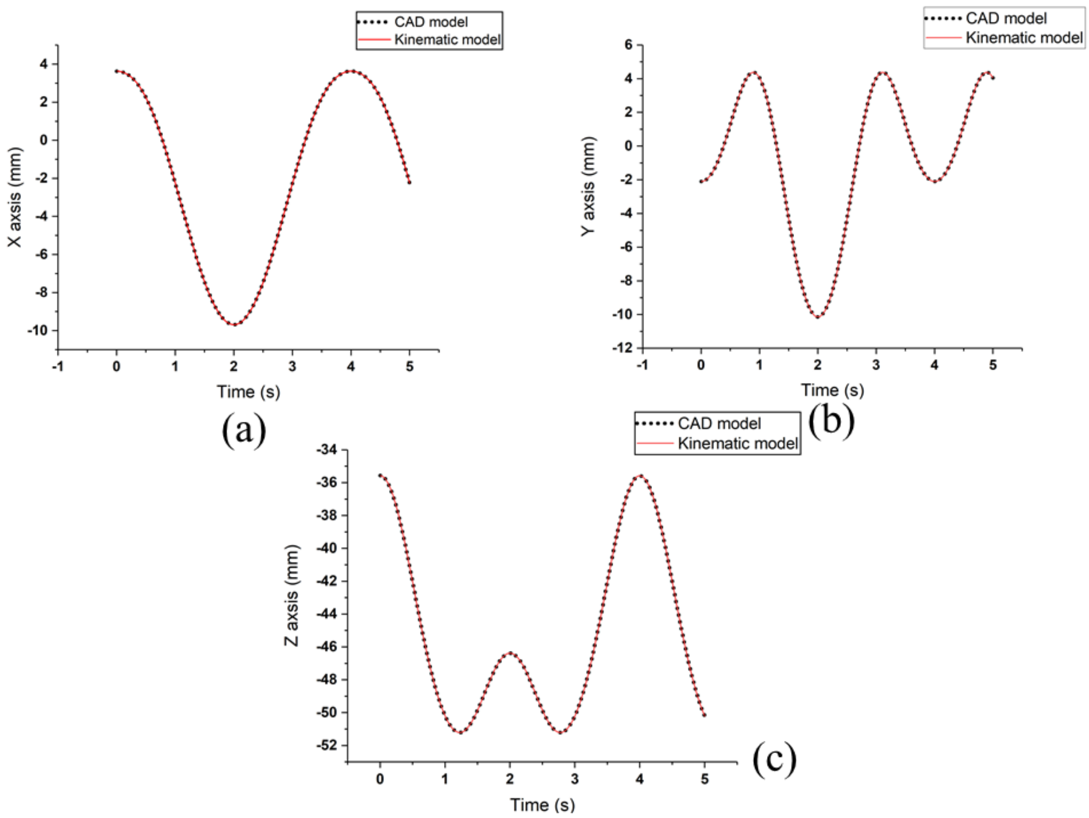

Figure 4.7 : First test of comparison between the CAD and kinematic model of Delta mechanism in (a) X axis, (b) Y axis and (c) Z axis.

The second test is conducted in the same way except this time all three arms had sinusoidal motion. The magnitude and the directions of the arm 1 and arm 2 is kept the same. However, this time the arm 3 had an input sine wave the magnitude of ±30º rotation. The starting point of the arms were 20º, 30º and 40º whereas the frequencies were 0.6, 0.4 and 0.2 hz, respectively. The results can be seen in Figure 4.8.

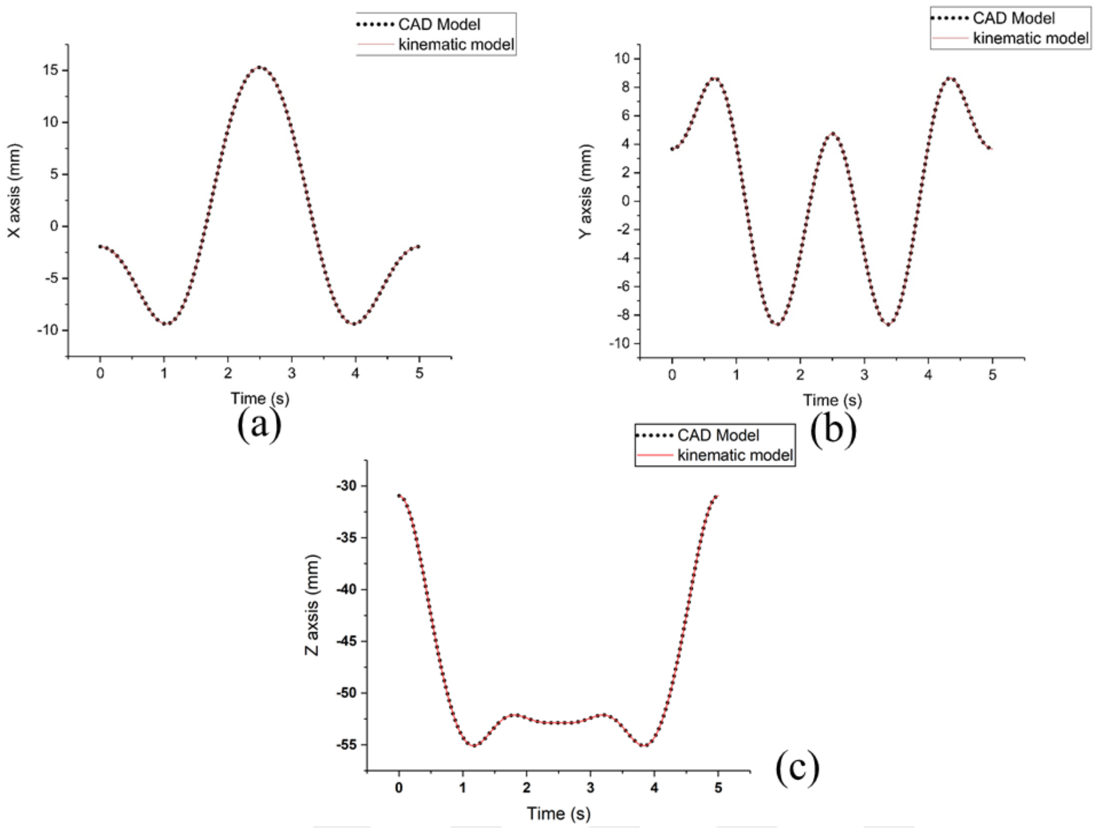

Figure 4.8 : Second test of comparison between the CAD and kinematic model of Delta mechanism in (a) X axis, (b) Y axis and (c) Z axis.

As it is shown in Figure 4.7 and 4.8, both models have a consistent result with each other. Both of them followed the same trajectory. The error is zero in the 10^{-4} scale. After that there becomes little differences between the models. However, the reason for that can be said as the CAD model equation solver has numerical calculation whereas the mathematical model is analytical and exact. In order to reduce the error to this scale, maximum allowable part interaction and sensitivity is set to the program. In light of these information, it can be said that the kinematic equation of the traditional Delta mechanism can be used to control and analyze the mechanism that is design with the origami inspired techniques and SCM 2D fabrication methods.

The test for the Stewart mechanism is conducted differently from the Delta mechanism. Since the Stewart mechanism has 6 DoF movement and six legs and a lot of little connection part of the joints, the CAD program's motion solver could not simulate the mechanism properly for continuous motion. That's why the comparison is done point by point. A reference position and orientation is given to the mathematical model to get the angle between the lower legs and base platform. After that the position and the orientation of the moving platform will be measured and compared with analytical solution. The result can be seen in Table 4.1.

Table 4.1 : Comparison between the analytical and CAD model of Stewart mechanism.

Position						Rotation					
Analytical Model			CAD Model			Analytical Model			CAD Model		
X axis [mm]	Y axis [mm]	Z axis [mm]	X axis [mm]	Y axis [mm]	Z axis [mm]	X axis [º]	Y axis [º]	Z axis [º]	X axis [º]	Y axis [º]	Z axis [º]
8	-8	40	8	-8	39.99	0	0	0	0	0	0
1	5	30	1.99	4.99	30	0	0	0	0	0	0
-5	2	50	-5	2	50	0	0	0	0	0	0
0	0	40	0	0	40	0	0	5	0	0	5
0	0	30	0	0	30	-5	-5	0	-4.98	-5	0
0	0	40	0	0	40	4	6	2	3.98	5.99	1.98
-3	1	45	-3	1	45	5	-10	2	-4.92	-9.9	1.98

As it can be seen from the Table 4.1, seven different point is tested. Three of them are for the pure position test. The CAD model and the kinematic model are exactly the same or very close to each other when there is no rotation in the moving platform. The following three test are for pure rotation in 0, 0 and 40 mm position. These tests shows that the Stewart mechanism CAD model can perform pure rotational movements with extremely small errors. The last test shows the combination of both position and rotation. The CAD model of Stewart mechanism can do pure translational and rotational motions as well as combination of them. The little differences can be coming from the difference between the analytical and numerical solutions and the round properties of two different program. However, the results are enough to continue to use the traditional Stewart mechanism's kinematic equations on the newly designed Stewart mechanism with origami inspired techniques and 2D fabrication methods.

4.3 Tracking Performance of Designed Mechanisms

4.3.1 Tracking performance of the Delta mechanism

The validation of kinematic equations is done with the 3D CAD model and very good results are obtained. However, in order to observe the mechanism, real experiments must be done. It is very well known that the mechanism with flexible material performs differently that the rigid mechanism. Also, this is confirmed by the initial tests that are done with the Pantograph mechanism. That's why the designed Delta mechanism is fabricated to conduct several tests are done using the Delta mechanism's test platform. The first test is to compare the real Delta mechanism to analytical model point by point. After that, a circular trajectory motion is given to the Delta mechanism. It should be noted that there is no control action in software or hardware in these tests.

4.3.1.1 Point by point test of the Delta mechanism

The point by point test are performed to test if the mechanism can reach the same points as the analytical model. A reference position is given to the inverse kinematic of the mechanism to obtained the corresponding lower arms angles. Then these three angle is given to the actuator of the real mechanism and the position of the center of moving platform is measured with the position sensor. The results can be seen in Figure 4.9. The Figure 4.9a shows the results where the motion in Z axis is fixed at 47 mm whereas there are 5 different position on X and Y axis starting from -10 to +10, with a 5 mm increments. On the other hand, in Figure 4.9b this time the X and Y positions are fixed at the zero (origin), where the position in Z axis is changed from -37 to -57 mm with 5 mm increments. Finally, in Figure 4.9c, X and Y is fixed at a different place than zero ($X = 7$ and $Y = -4$) and the Z axis is again changed from its lower point to highest to point. The motive of the last test was to see if there will be a different behavior in the positions other than zero in X and Y axis. The test shows a consistency between the analytical and the real delta mechanism. The mechanism can follow the reference positions with small errors. The main source of the error is the different nature of the flexible and rigid systems where the flexible systems can change shape due to external or internal forces and cannot imitate the movements of the rigid systems. The other error sources could be the imperfections at the test platform and the resolution of the motors. Lastly, it is observed that the error in higher Z positions is lower than the lower Z positions. The reason for that can be the more defined rotation of axis since the higher the mechanism goes, the more the joints are bent.

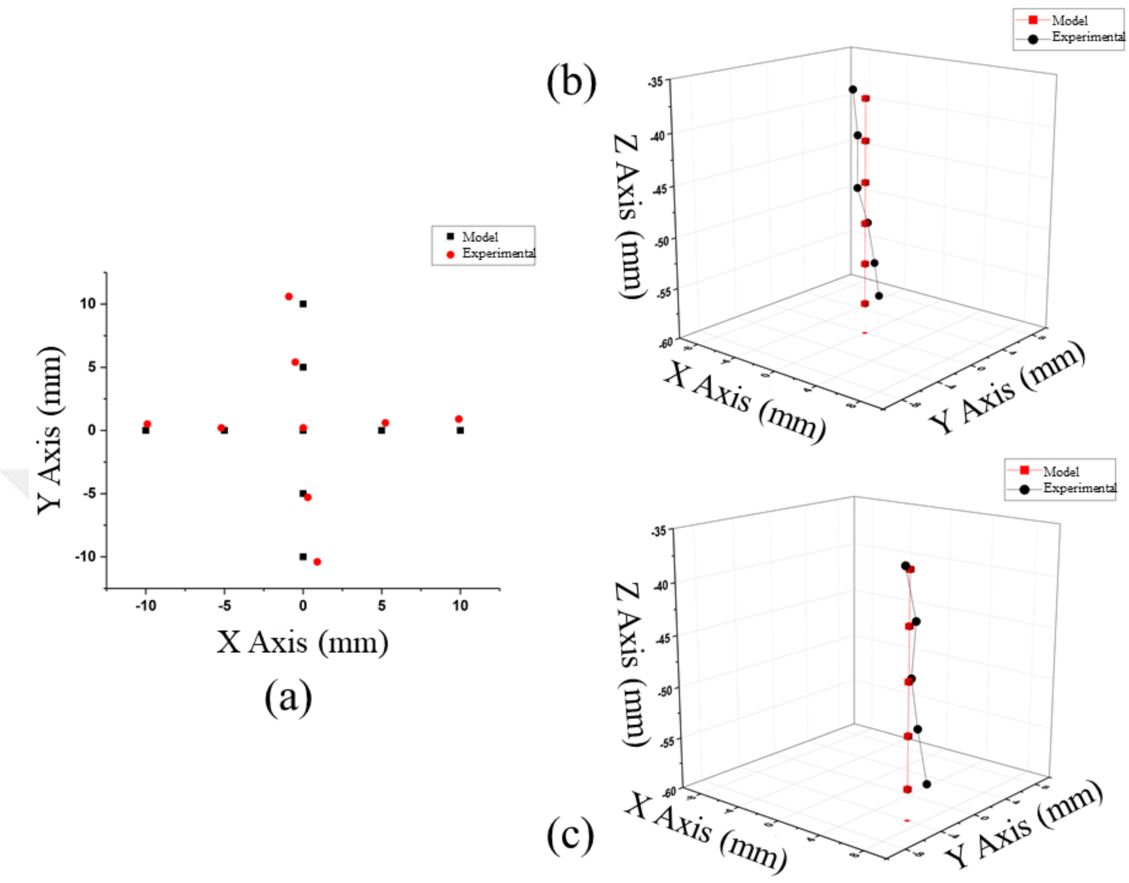

Figure 4.9 : Point test of the Delta mechanism, (a) Z = 47 mm plane with X and Y changing, (b) X = Y = 0 with Z changing and (c) X = 7 mm and Y = -4 mm with Z changing.

4.3.1.2 Circular motion tests of the Delta mechanism

The second test is performed to analyze the continuous motion of the Delta mechanism. As a continuous motion, a circular trajectory with a 10 mm radius is given as an input. Also, in these tests the moving platform has to move parallel to the base platform, so the rotation of the moving platform will be measured with the position sensor. The circular motion profile will be given with 5 mm increments in Z axis, starting from 40 mm to 60 mm. The results can be seen in Figure 4.10a and 4.10b. The Delta mechanism can follow the circular trajectories with a certain error. Generally, the errors in the Z = 50 mm plane (the calibration position) is smaller than the other end positions and the errors in the highest plane (Z = 60 mm) has smaller errors than the lowest plane (Z = 40 mm). The motion profile of the Delta mechanism resembles to an egg shaped figure. This profile is present not only in this mechanism, but also in all of the fabricated and tested Delta mechanisms. Overshoot in the position is generally in the Y axis where one arm is directly placed on. The reason for this could be the layout of the legs. Theoretically, 120º difference between the arms ensures that the forces acting on the origin eliminates each other. However, it seems like there is an unbalance of forces since there are fabrication errors and test platform's imperfections. These problems can be solved by better equipment.

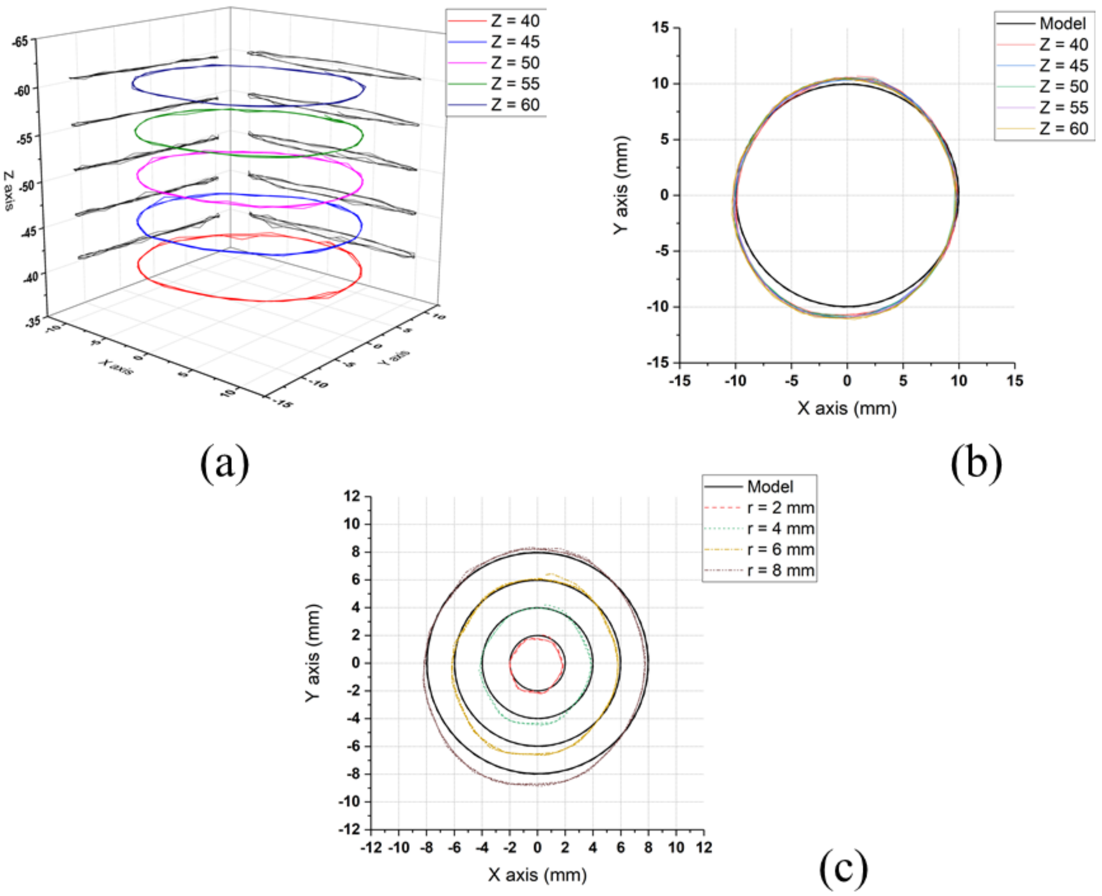

Figure 4.10 : Circular motion test of the Delta mechanism with (a) r = 10 mm in different Z planes, (b) top view of the circles in different Z planes and (c) Z = 50 mm plane with r chancing from 2 mm to 8 mm.

Figure 4.10c shows the results of the other test where the Z axis is fixed at 50 mm and the radius of the circular motion is decreased from 8 mm to 2 mm with 2 mm increments. The mechanism can follow the smaller circular trajectories too. Even if the error seems to be decreasing, it is still similar to 10 mm circles relatively to its diameter. The egg shape is still present in the smaller circles. The maximum non parallel angle error is around ±4º degree for both test cases. As a result, it can be said that using the origami inspired techniques and SCM 2D fabrication processes, a parallel Delta mechanism can be designed and fabricated, where the assembly process is only consisting of cut – bond – repeat cycle with no additional steps. Also, the Delta mechanism's traditional kinematic equations and analysis can be used because the mechanism is designed to have the same characteristics as the traditional Delta mechanism.

4.3.2 Tracking performance of the Stewart platform mechanism

The designed Stewart mechanism is fabricated with the proposed fabrication methods and materials in order to test the trajectory following performance. Even though the design is validated to some point using 3D CAD model, the real mechanism will have different behavior because it will be flexible, not rigid like the CAD model. That's why three group of tests are conducted using the test platform designed for the Stewart mechanism; point measurements, circular motion with no rotation, and rotations in X, Y and Z. All the tests have no control action in the software or hardware. Therefore, the results will show the plain motion of the mechanism.

4.3.2.1 Point by point test of the Stewart mechanism

In these tests, input to the legs will be given from the inverse kinematic equation with a specific position. Then the position of the mechanism will be measured with the position sensor and compared. In Figure 4.11a, the mechanism's Z position is fixed to 40 mm whereas the X and Y positions are changed from -10 to +10 with 5 mm increments. In Figure 4.11b, this time the X and Y positions are fixed at 0 whereas the Z positions are changed from 30 to 50 mm with 5 mm increments. Finally, the Figure 4.11c shows the Z position change from 30 mm to 50 mm with X position at 7 mm and Y position at -4 mm. The last test is conducted in order to test the change in the Z planes with different than zero positions at X and Y. As a result, it can be said that fabricated Stewart mechanism follow the kinematic model with small errors. The errors could be coming from the flexible nature of the mechanism as well as the errors that is present at the test platform and the resolution of the motors. Also, it is known from the initial Pantograph and Delta mechanism's tests that the inaccuracies in alignment and any other handmade problems in the fabrication can cause this error too.

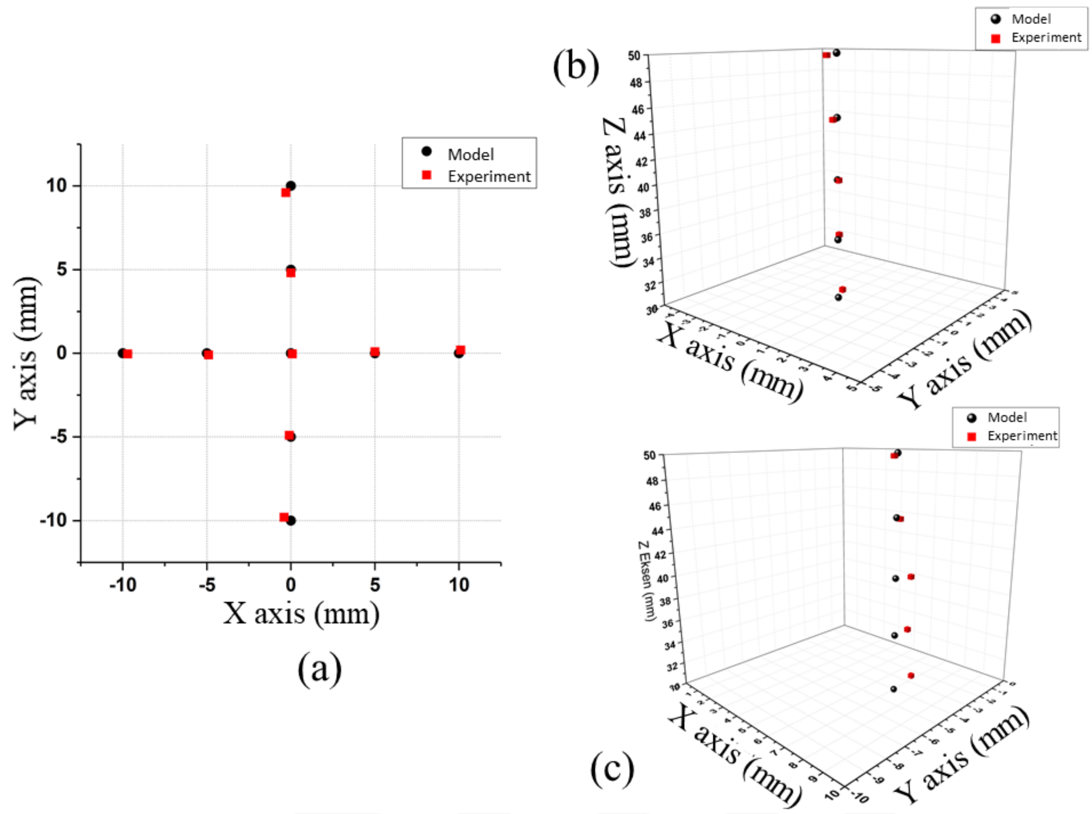

Figure 4.11 : Point test of the Stewart mechanism, (a) Z = 40 mm plane with X and Y changing, (b) X = Y = 0 with Z changing and (c) X = 7 mm and Y = -4 mm with Z changing.

4.3.2.2 Circular motion tests with no rotation

The second test is conducted with a circular trajectory, where the rotation in X, Y and Z axis are zero in order to test the continuous motion performance of the mechanism. In this test, the Stewart platform basically moves parallel to the base platform like a Delta mechanism. Two different tests are done; a circle with a 10 mm radius in Z planes changing from 30 to 50 mm with 5 mm increments and circles with a radius changing from 8 to 2 mm with 2 mm increment in a fixed Z = 40 mm plane. Figure 4.12a and 4.12b show the results of the first test. The mechanism responded better in higher Z planes. These results are seen in Delta mechanism too, where the planes far from the origin has smaller errors, because the joints have a better determined axis of rotation. Nevertheless, the Stewart mechanism can follow a circular trajectory in different Z planes. Figure 4.12c shows the result of the second test. It is observed that the mechanism can follow the same circular paths with smaller radiuses without breaking the circular shape. As a result, it can be said that the Stewart mechanism can follow continuous translational trajectories in different Z planes with changing X and Y positions without any control action.

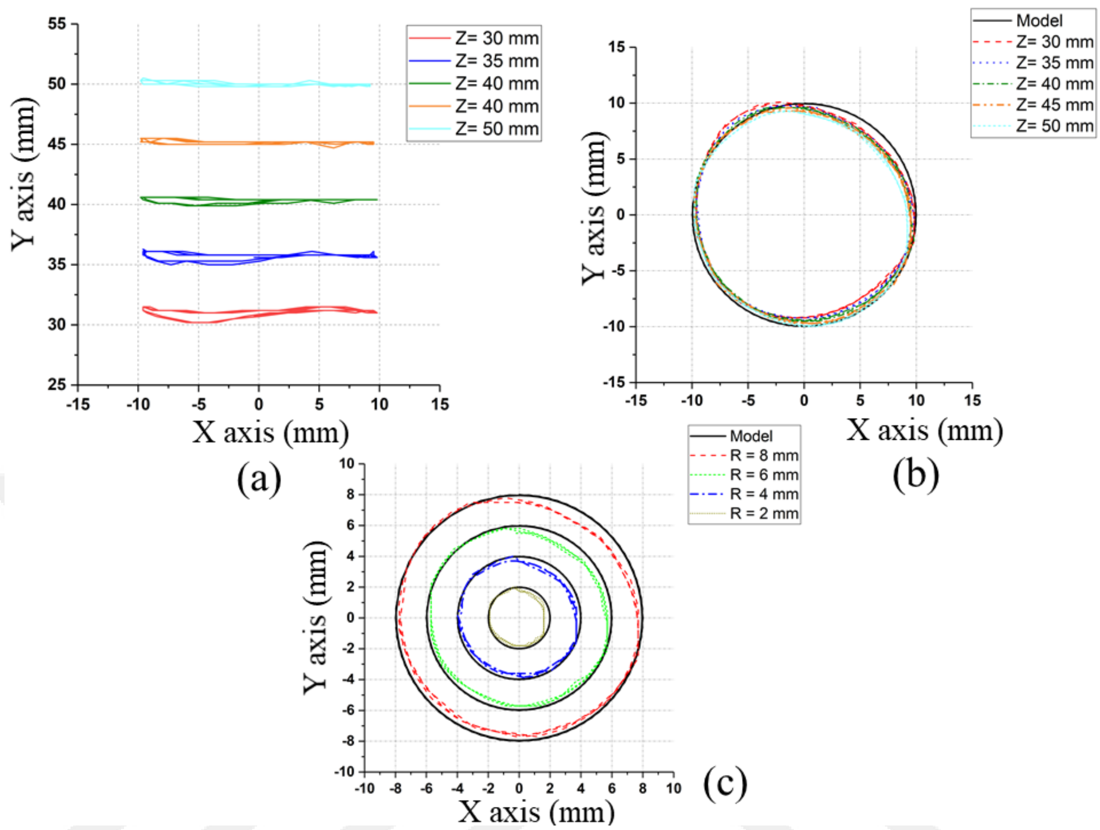

Figure 4.12 : Circular motion test of the Stewart mechanism with (a) r = 10 mm in different Z planes, (b) top view of the circles in different Z planes and (c) Z = 50 mm plane with r chancing from 2 mm to 8 mm.

4.3.2.3 Rotational motion in X, Y and Z axis

Finally, the rotational motion performance of the Stewart mechanism is tested. Five different tests are conducted.

1. Rotation on the X axis with X, Y and Z translational motion
2. Rotation on the Y axis with X, Y and Z translational motion
3. Rotation on the Z axis with X, Y and Z translational motion
4. Rotation on the X and Y axis with X, Y and Z translational motion
5. Rotation on the X, Y and Z axis in the origin

All of these tests are with sinusoidal input. Magnitude of wave in tests 1 – 4 is ±10^o degree whereas the magnitude of the test 5 will be changed between ±2^o, ±4^o, ±6^o, ±8^o, ±10^o degree. General idea behind these tests is to see if the mechanism can perform the combination of continuous translational and rotational motion as well as the rotation in all axes at the same time.

Figure 4.13 shows the results of the test 1. The Stewart mechanism can follow the rotation in X axis while there are translational movement. Specifically, the error in the X and Z axis is small as ±1º degree. Since translation motion in Y axis and rotation in X axis creates a wave like profile, the biggest error has occurred here. Figure 4.14 shows the results of the test 2. This time the mechanism can follow the sinusoidal rotational motion with a general ±2º degree error. The behavior of the mechanism is very consisted with each other in this test. Lastly, the Figure 4.15 shows the final test 3 of the single axis rotation tests. Differently, from the other two test, the rotations on the Z axis never reached the maximum magnitude of ±10º degree. Instead it has an ±8º rotation. However, the rotation is more accurate than the other axis even if the motion is in ±8º degree range.

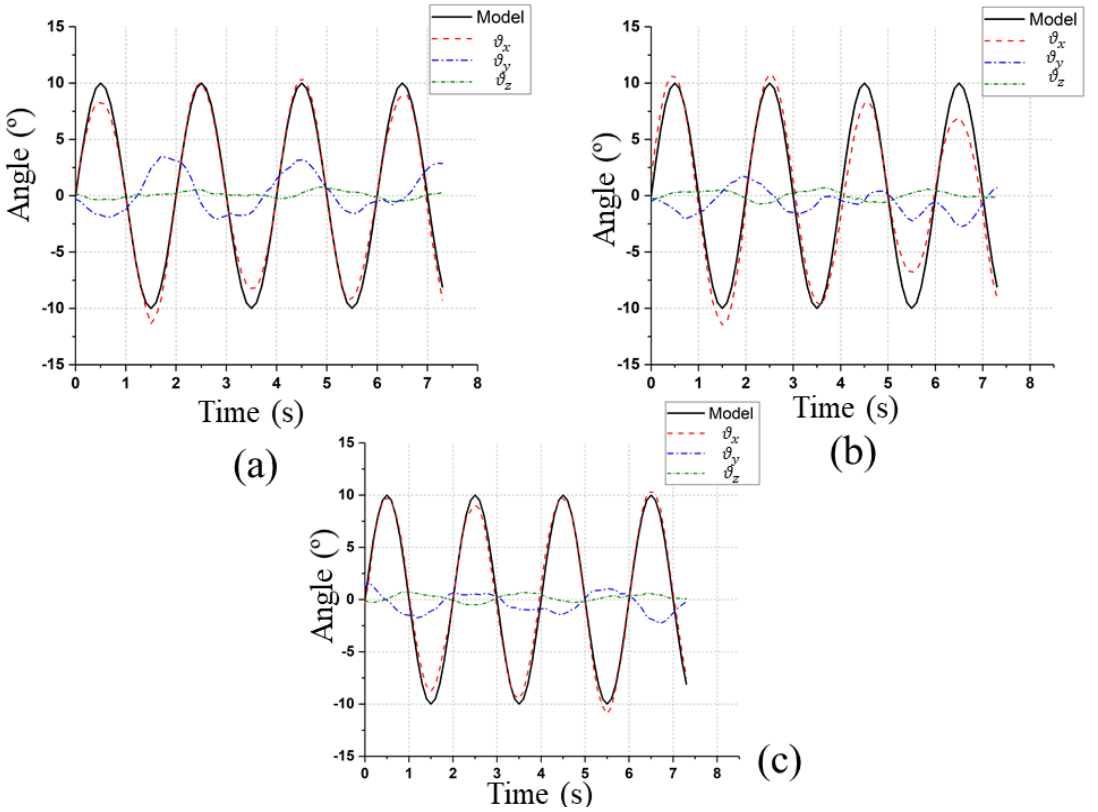

Figure 4.13 : Rotation on the X axis with translational motion in (a) X axis, (b) Y axis and (c) Z axis.

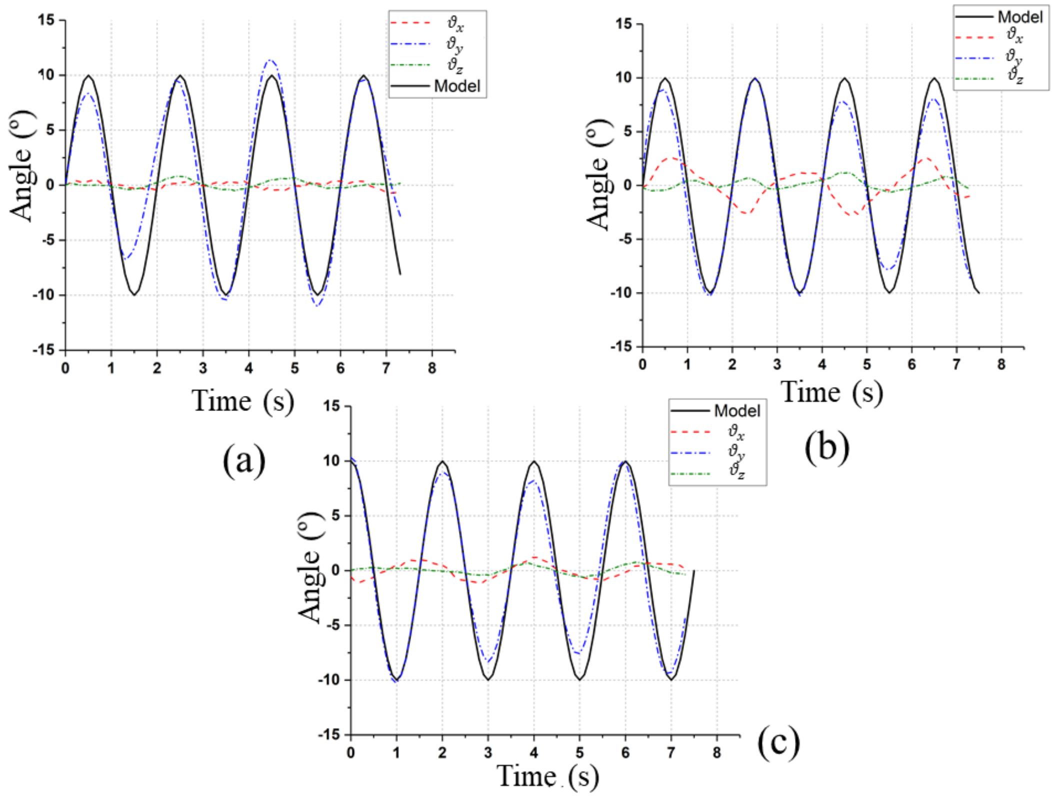

Figure 4.14 : Rotation on the Y axis with translational motion in (a) X axis, (b) Y axis and (c) Z axis.

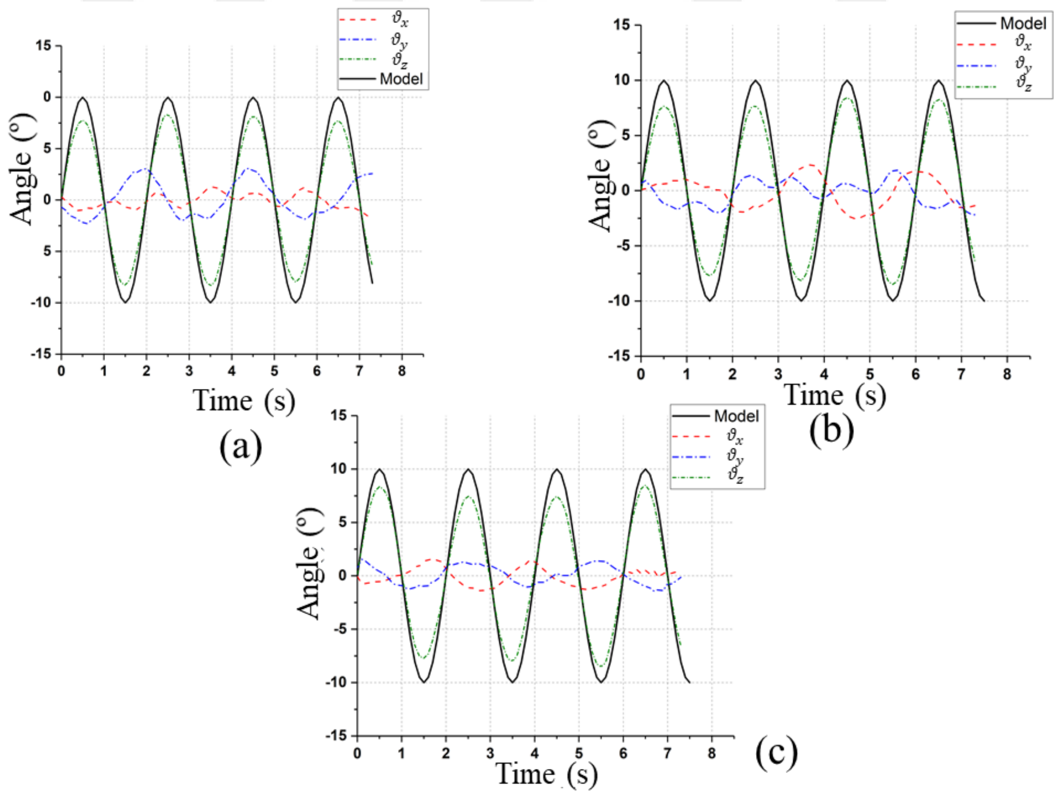

Figure 4.15 : Rotation on the Z axis with translational motion in (a) X axis, (b) Y axis and (c) Z axis.

Figure 4.16 shows the combinational rotation in X and Y axis with a translational motion. This test is harder than the first three test because rotational motion generally makes the motion difficult for the mechanism. However, the Stewart mechanism still can follow the input with a certain error. Sometimes the error becomes maximum at the peaks of the sine wave and these points are the X and Y translational motion's maximum points. This means at these points, the mechanism stretches very far and the joints does not allow the motion. This problem is expected because it is known that the flexible mechanism does work properly when they are at the end of their workspaces and lose their joint stability.

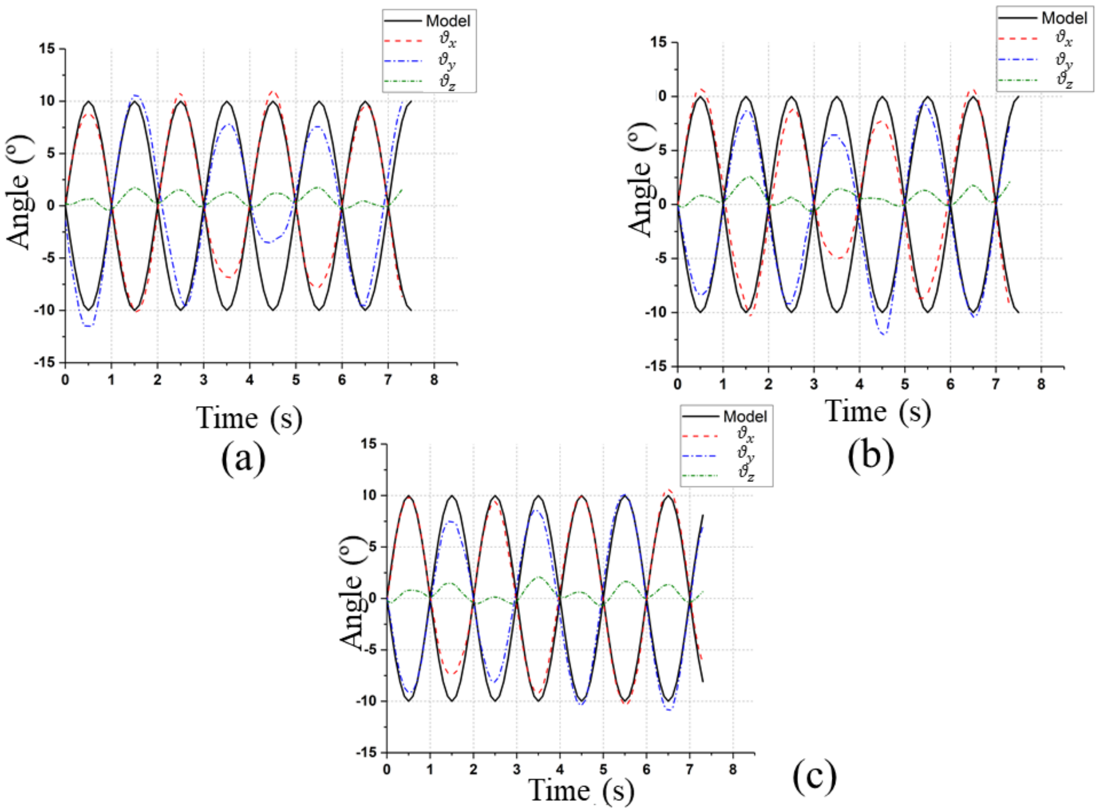

Figure 4.16 : Rotation on the X and Y axis at the same time with translational motion in (a) X axis, (b) Y axis and (c) Z axis.

Finally, Figure 4.17 shows the results of the test 5, where there is rotational motion in all axis at the same time in origin. The first thing to say it that the rotation in Y axis follows its trajectory very good, but the rotation in X and Z axis has always an ±2° degree error. The reason for that can be the X and Z axis effects each other very much in the flexible mechanism, so that they both cannot move to their desired positions, or the position sensor's position could be in a way that it mixes the rotation on the X and

Z axis. Also, the error becomes small when the angle range gets smaller because mechanism gets closer to the origin from the workspace's ends. Anyway, even if there is a small error, it can be said that the motion of the profile is followed very accurately in Stewart mechanism.

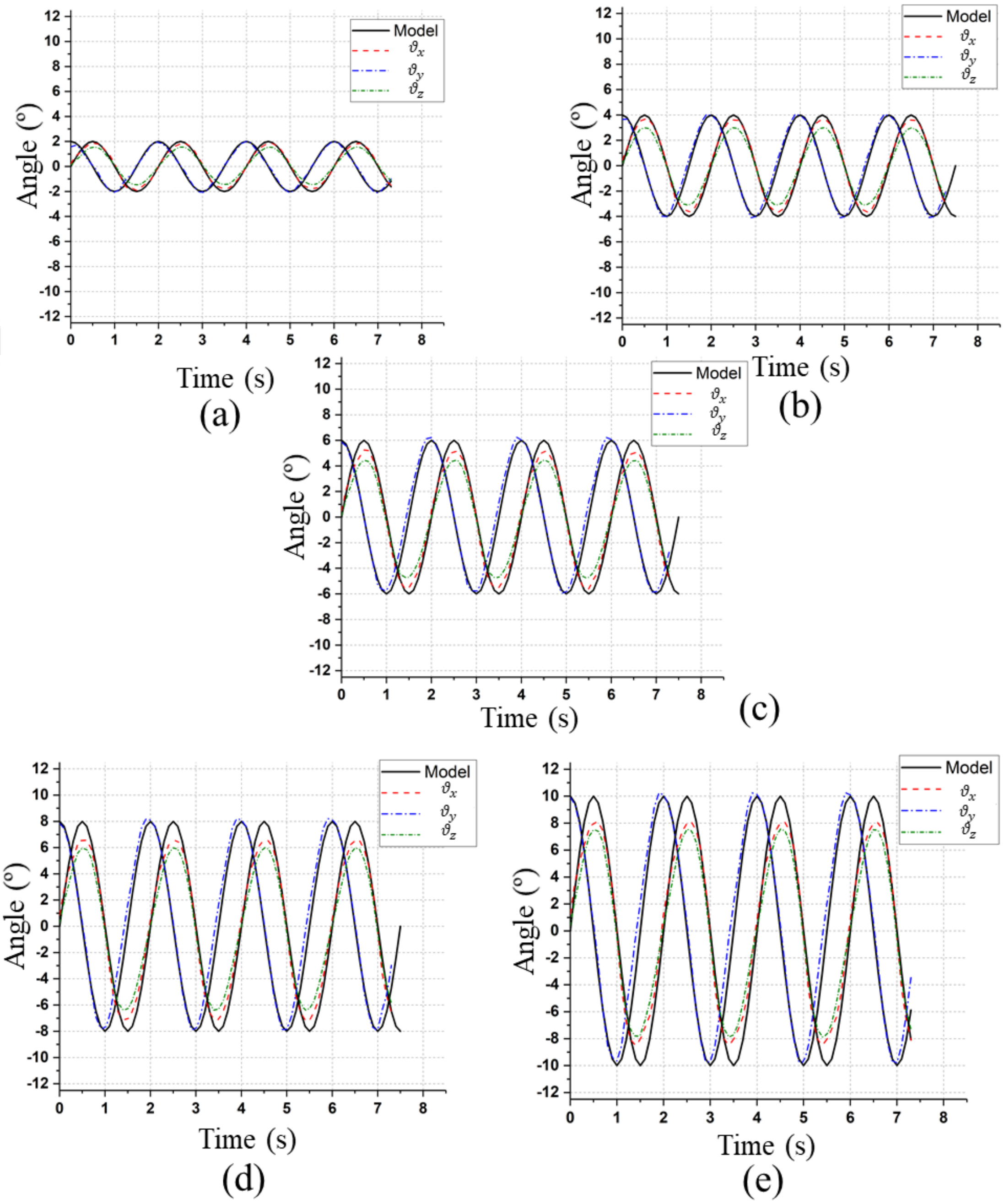

Figure 4.17 : Rotation on the X, Y and Z axis at the same time in the origin with magnitude of (a) ±2º, (b) ±4º, (c) ±6º, (d) ±8º and (e) ±10º degree.

The reason for the maximum errors to generally shows up in the peaks of the sine wave could be the gear backlash of the motors. After some examination, it is found that the motors have backlash in the gears up to 10 tick, which converts into 0.87º error. Using the controller of the motor, this effect is tried to be reduced, but it could not have made to be zero. This effect is present in all the experiments.

As a result, a Stewart mechanism can be designed with origami inspired techniques and SCM 2D fabrication method with a completely flat assembly process, which can use the traditional kinematic analysis and follow the given translational and rotational motions.

4.3.3 Effects of materials on the tracking performance

The elasticity of the flexible layer had a great impact on the joints. If the flexible layer is too elastic, the joints do not carry the weight of the moving platform and they shear off easily when subjected to a force or whilst cutting with the laser machine. If the elasticity module of the flexible layer is too high, bending curvature increases and the tips of the rigid layer deforms. When the joints do not bend, they push the moving platform up or to the sides, depending on the position, which disturbs the general motion of the mechanisms. This disruption becomes obvious when mechanisms reach the boundary of their workspace where there are a lot of upward force acting upon the moving platforms. That's why it is suggested to stay as far as possible from maximum distances for this reason too. Experimental results suggest that there is an optimum range of ratio between flexible layer and rigid layers.

In order to analyze this relation and understand effects of different flexible materials, six Delta mechanisms with different flexible layers are fabricated. Since the detailed experiment on this subject is done on the Delta mechanism, the tests will be conducted on the Delta mechanism. However, this problem is also present in the Stewart platform. Since the joints structure is very similar in both mechanism, the foundings can be applied to the Stewart mechanism.

Different flexible layers are used in four crucial flex sections of the Delta mechanism that is shown in Figure 4.18. Properties of flexible materials used in these sections of the mechanisms were given in Table 4.2. Flex material in flex section 1 was kept the same in all mechanisms because the embedded silver-ink sensor and the flexible layer of the sensor is constant in all three parallel mechanisms. There was a correlation between thickness ratio of flexible material in flex section 2 and 3 with the parallel motion of the Delta mechanism. This ratio should be in the range of 1 – 2 considering the ratio of lower and upper arm widths from delta mechanism's design.

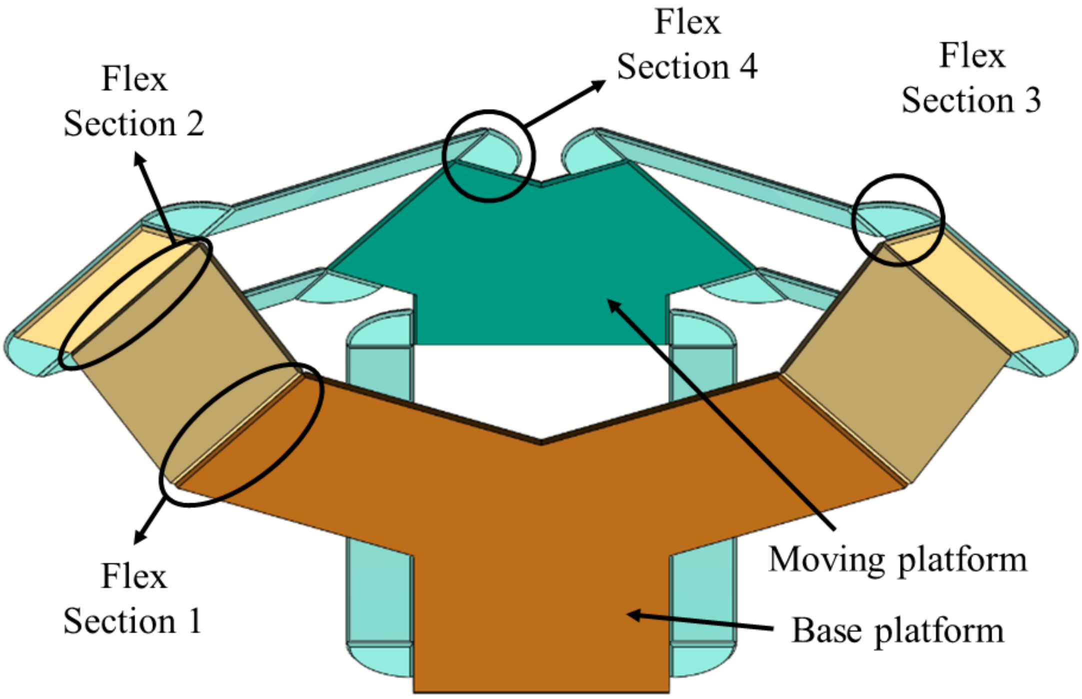

Figure 4.18 : Flex sections of the Delta mechanism.

Table 4.2 : Flex section materials of each individual Delta mechanism.

Mechanism	Material of Flex Section [mm]	Material of Flex Section [mm]	Material of Flex Section 3 [mm]	Material of Flex Section 4 [mm]
1	PET (0.14)	PET (0.08)	PET (0.08)	PET (0.08)
2	PET (0.14)	TPU (0.2)	TPU (0.4)	TPU (0.2)
3	PET (0.14)	Nylon (0.03)	TPU (0.2)	TPU (0.2)
4	PET (0.14)	TPU (0.2)	TPU (0.4)	TPU (0.4)
5	PET (0.14)	TPU (0.2)	TPU (0.4)	PET (0.08)
6	PET (0.14)	Nylon (0.03)	TPU (0.4)	TPU (0.4)

In order to test these mechanism, same circular trajectories are given just like in the

Delta mechanism. After all the tests, the RMS position error for each mechanism is found using the classic RMS equation. The sum of RMS (mm) position errors in x, y and z directions are provided in Table 4.3. Lower RMS errors shows more accurate trajectory following and the closeness of the RMS results means stability of the mechanism in different heights. The accuracy of the mechanisms was compared and concluded that mechanisms Number 1 and 5 performs better than others. In other word mechanisms with 0.08 mm thickness in flex section 4 have lower RMS results. Different radiuses were tested while keeping the height at Z=50 mm for all mechanisms.

Table 4.3 : RMS values of each individual Delta mechanism in different Z planes and with different radiuses.

Mech.	Z = 60 [mm]	Z = 55 [mm]	Z = 50 [mm]	Z = 45 [mm]	Z = 40 [mm]	R = 8 [mm]	R = 6 [mm]	R = 4 [mm]	R = 2 [mm]
1	2.13	2.04	2.01	2.01	2.04	1.6	1.18	0.75	0.41
2	2.4	2.14	2.05	2.24	2.42	1.72	1.32	0.89	0.51
3	2.35	2.36	2.44	2.47	2.47	1.99	1.59	1.27	1.01
4	2.11	2.09	2.11	2.28	2.4	1.74	1.28	0.85	0.51
5	1.51	1.53	1.54	1.55	1.57	1.25	0.93	0.61	0.44
6	2.83	2.81	2.87	3.01	3.17	2.43	1.98	1.42	0.88

Also, the trajectory following graphs of these mechanism can be seen in Figure 4.19 and 4.20. Just like in the table, the graphs of mechanism number 1 and 5 shows a very consistent trajectory in all Z planes and radiuses. As a results, not only the design and fabrication methods, but also the materials used effects the kinematic behavior of the mechanisms. Therefore, in order to have the best results, the material selection becomes very important. A PET sheet with 0.08 mm seems to be working for the rigid cardboard in this research. However, using different rigid materials will definitely require less flexible layers, and/or a combination of multiple layer.

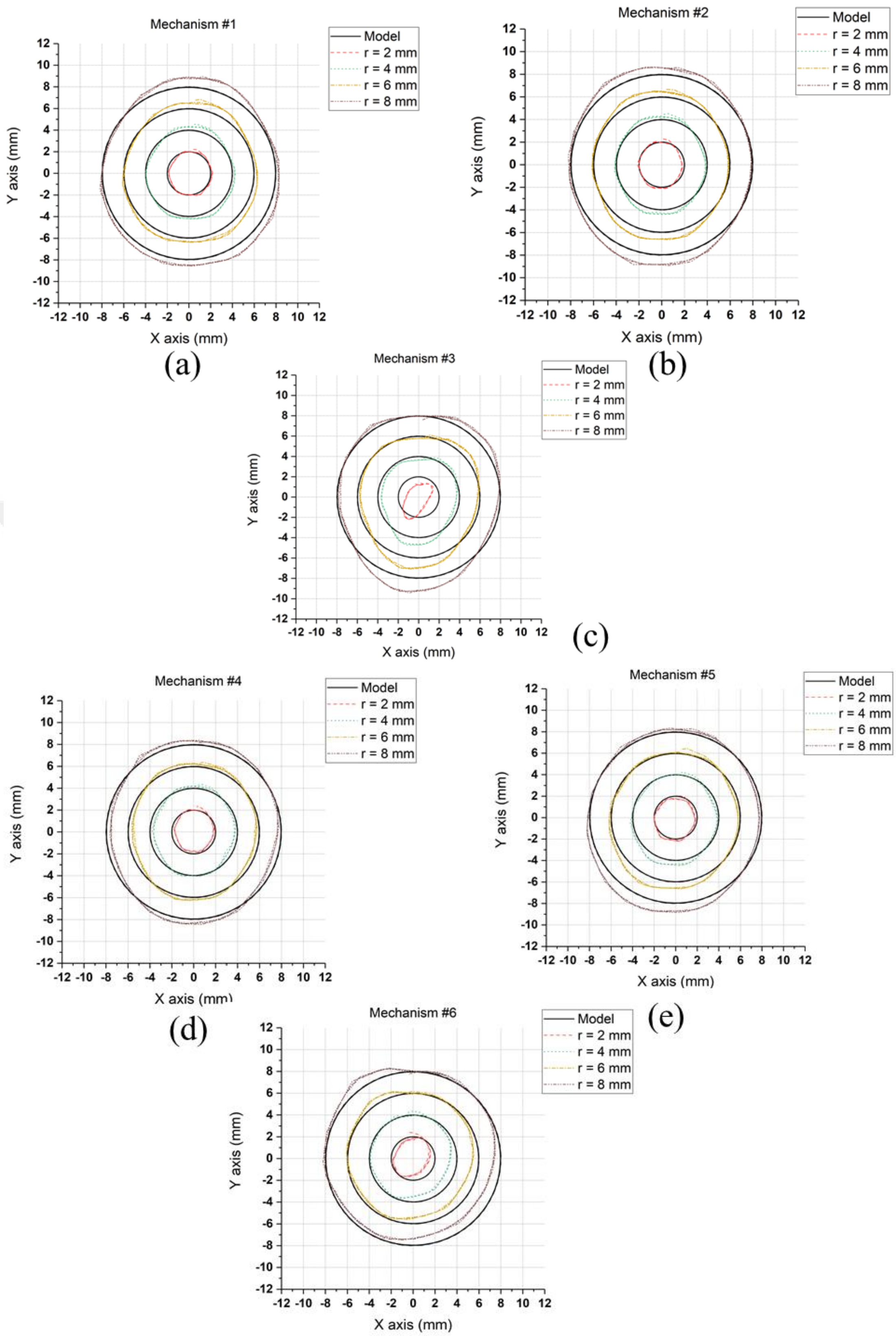

Figure 4.19 : Six different Delta mechanism test with radiuses from 2 mm to 8 mm at Z = 50 mm plane. Mechanism 1 and 5 have the best input following elliptic shapes. The performance of the mechanism 4 could be looking better than other two, but table 4.3 shows that Z performance of mechanism 4 is worse than other two.

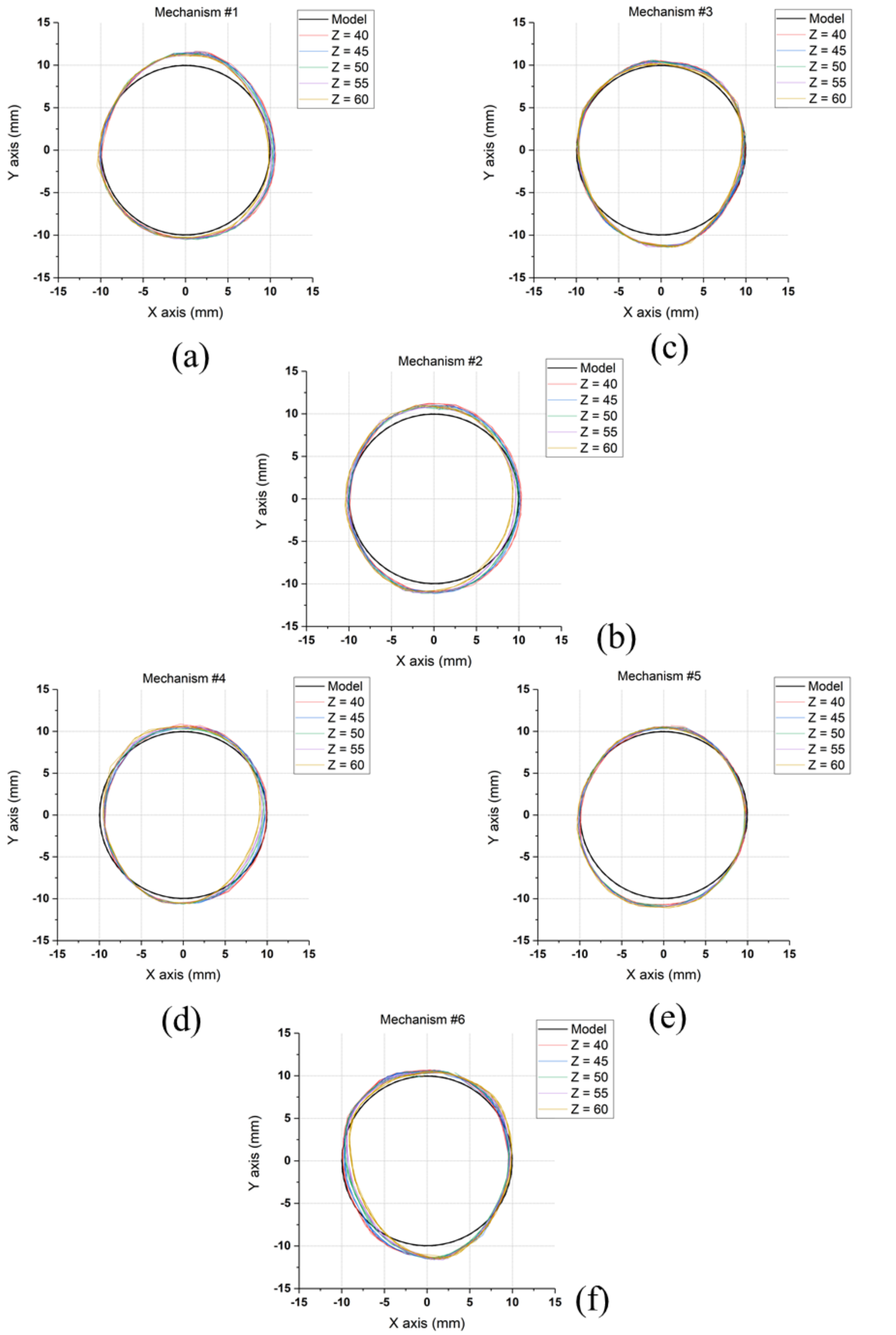

Figure 4.20 : Top views of six different Delta mechanism test with r = 10 mm circular profile at different Z planes. Overall input following is very consistent in all six mechanisms. However, if the Z plane performance is taken into account the mechanism 1 and 5 seems better than others.

4.4 Embedded Sensor Results

Sensor with a cut in the flexible layer and non-adhesive surface is mentioned in the embedded sensor design section. Experimental results with these sensors are given in the Figure 4.21 – 4.23. As the experiments will be conducted in the Delta mechanism, the sensors are embedded into the delta mechanism's base platform with one sensor per lower arm. Angle inputs ranging from 0-90º degrees are given to the joints by the robot servo motors and the voltage outputs are measured with the voltage divider circuit and a DAQ card. The Figure 4.21 shows the hysteresis curves of the sensors against 0-90º degree sinusoidal angle inputs. The Figure 4.22 shows the responses of the sensors to the angle inputs given in 11 steps between 0-90º degrees. The Figure 4.23 shows the sinus responses of the sensors between 0-90º degrees. Each experiments contains 5 different measurements of the sensor and they are taken one after another in a row.

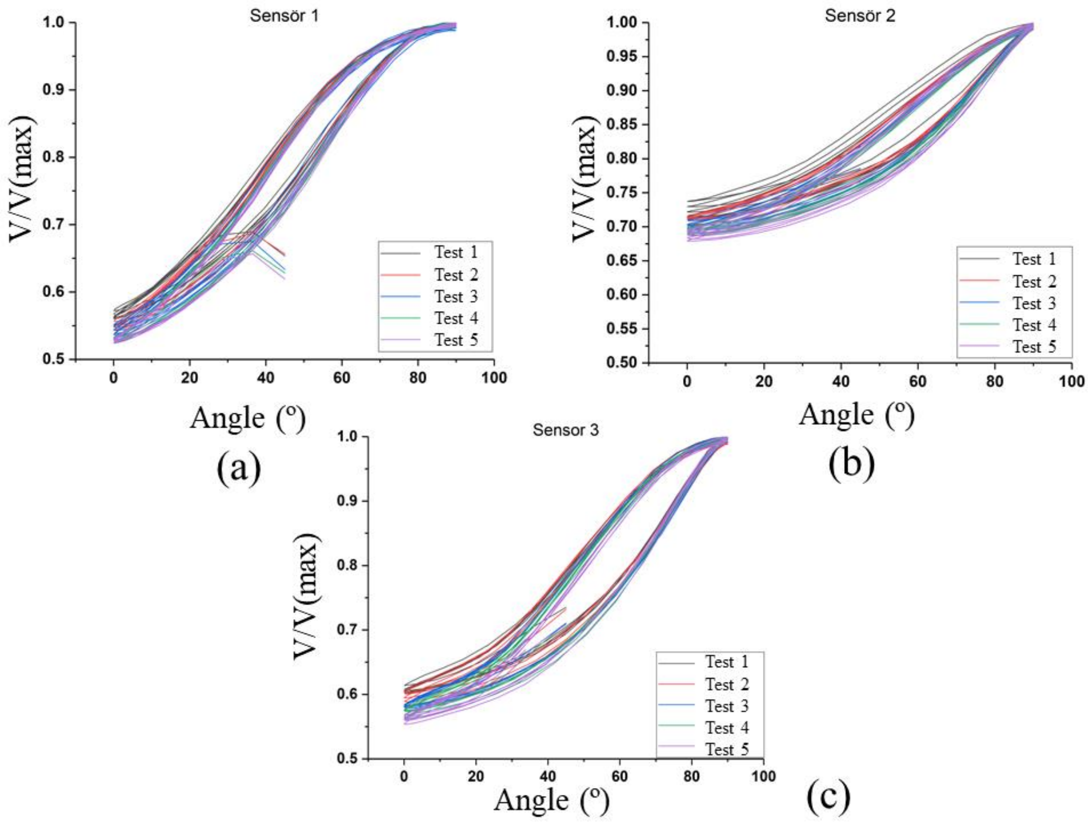

Figure 4.21 : Voltage – Angle curve of (a) sensor 1, (b) sensor 2 and (c) sensor 3. Three sensors are in the same Delta mechanism.

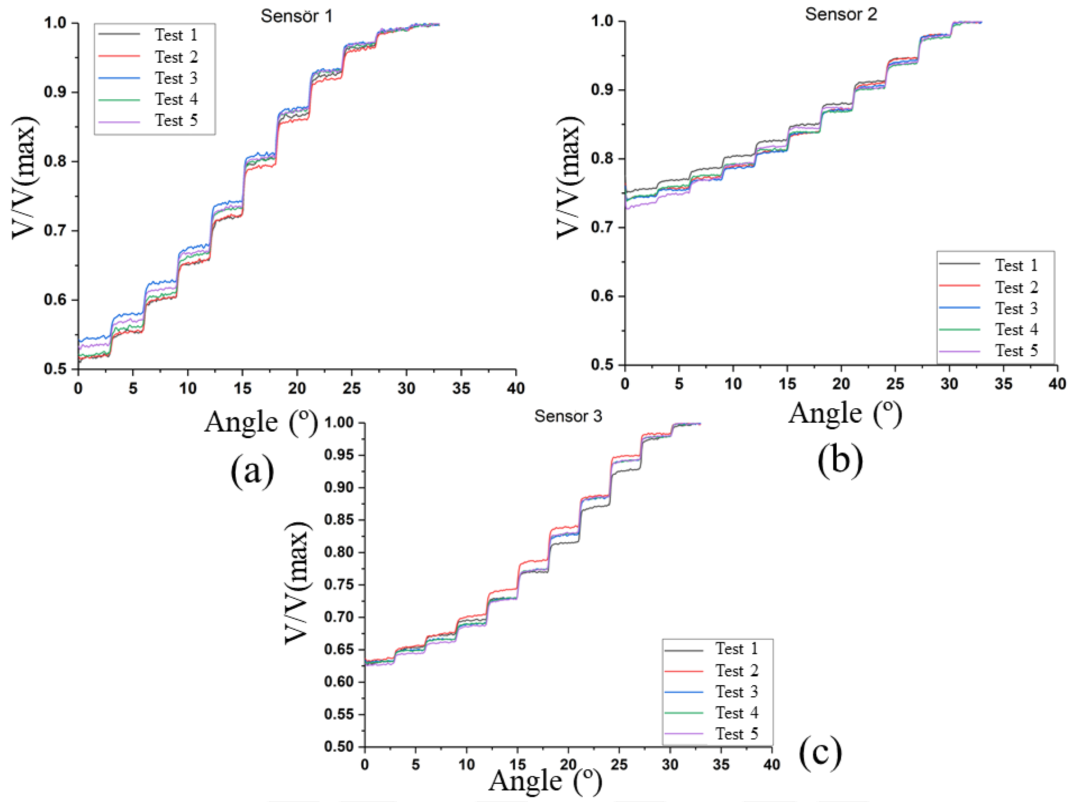

Figure 4.22 : Back to back step inputs starting from 0º to 90º degree with 9º degree increment. Total 15 test with five test for each sensor.

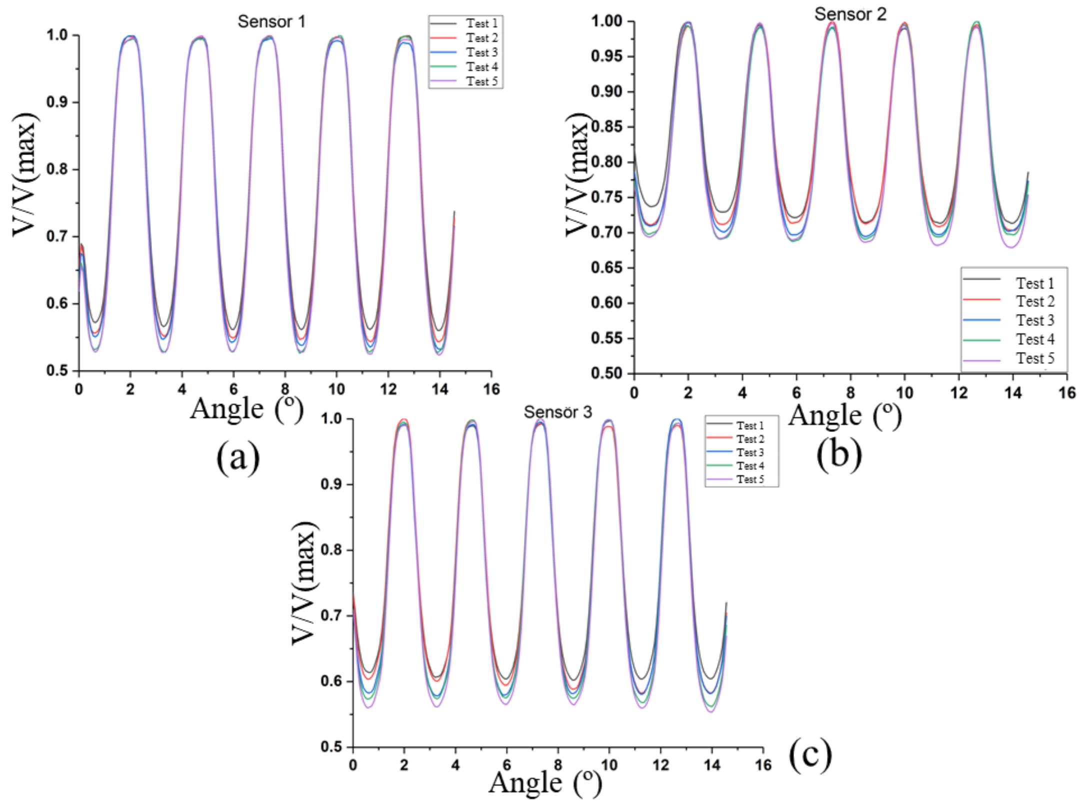

Figure 4.23 : Sinusoidal input with a magnitude of ±45º degree starting from 45º degree. Total 15 test with five test for each sensor.

In this sensor model, hysteresis curves appear to have closer profiles. However, for all three sensors, it can be said that the angle-dependent voltage change rate first increases and then decreases. In this design, it was seen that all 11 angle steps can be detected by the sensor, which corresponds to the lower than 9º angle. In the sine wave experiments, the reason for the same level of wave crests is because the normalization is done according to the maximum voltage value. Therefore, difference in the downward peaks of the sine waves means the sensor range changes with time. Also, in Figure 4.23, it can be seen that the lower peaks have a trend to go downwards. This chance in the range has been come across before in the Pantograph mechanism experiments. It seems that if the sensor is subjected to the longer period of action and heat (the temperature of sensor is increases with time) the resistance changes. There are other studies in the literature indicating the same phenomena (Enser et al., 2018). This problem could be dependent on the flexible material's fatigue and elasticity change with heat properties.

As a result of the experiments, it is found that the sensors are successful in detecting at least 9º degrees of angular changes. It is observed that the uncertainty in sensors number three is minimum and the uncertainty in sensors number 2 is maximum. Since the sensor numbers are given according to the sequence order in the mechanism, it is thought that the factors affecting the uncertainty may be errors in mechanism production and sensor placement or errors arising from experimental setup. It is estimated that the performance of the sensors can be further increased by improvements in these areas. In addition to that, the sensor has been shown to have a certain hysteresis problem and it has also been observed that the range of motion changes during long-time movements and as the sensor heats up. Alternatively, sensor performance can be improved by probabilistic estimation methods by determining sensor uncertainties.

The embedded sensor developed in Pantograph and Delta mechanisms is also designed for Stewart Platform mechanism. Since there are 6 legs in this mechanism, 6 sensor placements have been made for the base platform. The production method of the sensor is based on the sensor used in the Delta mechanism. Since detailed sensor studies are performed on the delta mechanism, only one example of the Stewart mechanism is given. However, sensor integration is made for six legs. Whether the sensors work or not has been tested after production using the DAQ card. In the first attempts, voltage change is measured from the 6 legs of the sensor. Figure 4.24 shows the data from one of these legs.

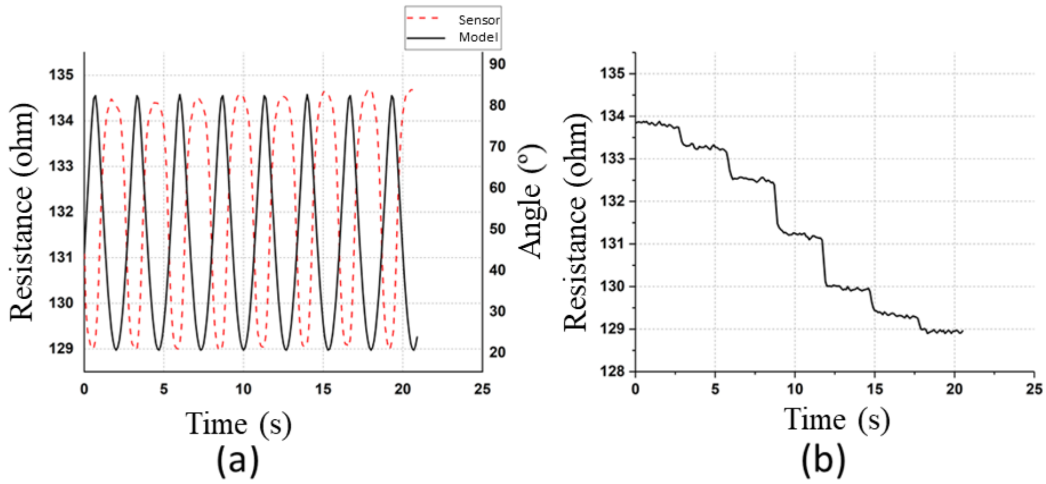

Figure 4.24 : Results of one embedded sensor in the Stewart mechanism. (a) Sinusoidal input, (b) step input starting from 20º to 80º degrees with 10º degrees increment.

The sinusoidal profile in Figure 4.24a was obtained by applying a sine wave on the Z axis to the moving platform. This time resistance values are considered as an output. As the given angle increases, the sensor contracts and the resistance values decrease because it works in the surface of compression. The point to be noted here is that the movement of the legs make a sinus-like motion not a true sinus wave. The differences between the hills that appear in the results are due to this reason. Figure 4.24b shows the results of the step experiment. The movements here are done in increments of 10º degrees from 20º to 80º degrees. As can be understood from these two results, the designed sensor and fabrication method can also be applied to the Stewart platform and give results similar to those in the Delta mechanism.

As a result, an embedded sensor that can measure the angle between two different rigid can be design with 2D fabrication methods for different parallel mechanism. The designed sensor is shown to be measure at least 9º degree step inputs. Given the noise in the sensor, it is expected the sensor to measure 4 – 5º degree changes with a low pass filter. However, at lower height the sensor can probably measure 1º with the correct equipment. If a software algorithm is developed for the sensor, it can be used to control the miniature DC motors. Therefore, an external sensor need could be resolved for the miniature origami inspired systems.

5. CONCLUSION AND FUTURE WORKS

The assembly problem in 2D fabrication methods for multi-material, low cost, small scale, origami inspired design is the main challenge for mass production of these systems. One of the solution of this challenge is making the systems have only basic operations that the fabrication method can provide and which they can be applied with the same machinery and process. In this research, three parallel mechanisms (Pantograph, Delta and Stewart mechanism) with origami inspired design and SCM 2D fabrication method is developed to have only the basic cut – bond – repeat cycle operations. Also, an embedded sensor, which measures the angle between two different links and compatible with the fabrication method is developed in order to eliminate the need for an external sensor for the small scale mechanisms. Table 5.1 shows the final scales of all three mechanisms.

Table 5.1 : Final values of all three mechanism. Base area means the maximum area when the mechanism is completely flat. "A" in RMS errors coulomb represents the constant radius at different Z planes with parallel motion. "B" represents the decreasing radiuses at constant Z plane experiments. "C" represents the rotational tests that are done for Stewart mechanism (specifically test 1 – 3).

Mechanism	DoF	Size [mm]		Workspace			Best Average RMS Errors		
		Base Area	Layer	X [mm]	Y [mm]	Z [mm]	A	B	C
Pantograph	1	15x160	11 Layer 2 mm	±25	±25	-	-	-	-
Delta	3	r = 96	11 Layer 2 mm	±10	±10	[40 - 60]	1.54	0.81	0
Stewart	6	r = 90	11 Layer 2 mm	±10	±10	[30 - 50]	1.61	0.72	0.93 (Max 1.79)

Initial analyzes of the fabrication and sensor methodologies are done on the pantograph mechanism. Later, results are applied to the more complicated mechanisms, which are Delta and Stewart mechanisms. The detailed design and fabrication processes are developed for these mechanisms to have no additional assembly steps. In the design process, the kinematic behaviors of existing mechanisms are considered. Therefore, it is shown that even though there arise new challenges, the classical mechanisms can be designed and fabricated using the layer by layer techniques. Also, these new mechanisms can follow the given trajectories continuously. The tests are conducted to measure the end effectors positions and find the trajectory following error without any control action. The position errors of the mechanisms are very similar to each other, around 2 mm RMS error. Moreover, the Delta platform had a parallel motion with a $\pm 4^o$ degree error and the Stewart platform could perform the rotational inputs with a small error like $\pm 2^o$ degrees.

While designing the mechanism, an embedded Stain gage sensor is developed simultaneously with it. The sensor has designed specifically for each mechanism considering their limitation factors. The main limitation was the placements of the sensors in their respective measurement areas. However, even though the number of sensors and their dimensions were different, the need was the same; angle measurement between two links, where the actuators are connected. The designed sensor is compatible with the fabrication process and it can be embedded using the same assembly steps as the mechanisms. The tests of the embedded sensor shown that it can track the continuous change in the angle between two links, but it has an innate hysteresis and nonlinearity due to the plastic flexible layer. Also, the step experiments showed that at least 9^o angle changes can be detected with the sensor. Nevertheless, the sensor also can detect a $4 – 5^o$ angles or even up to 1^o inside those steps.

In future works, the dynamical analyses can be done to understand the mechanism's behaviors deeply. The trajectory test can be conducted with control actions using the dynamics to improve the motion and reduce the error values. Moreover, a smaller DC motor can be used to control the mechanisms using the designed embedded sensor with a low pass filter and measuring algorithm. By doing so, the system can be completely integrated and does not depend any other sources externally. Also, the designed mechanisms are very suitable for smaller scales. Using better laser cutting machines, inkjet technologies and materials, the size of the mechanism can be reduced to the micro scales for the micro operations. In addition, the designs are suitable for mass production. If the necessary alterations and equipment is supplied the process can be automated as well as the errors can be reduced furthermore.

REFERENCES

Ando, B., & Baglio, S. (2013). All-inkjet printed strain sensors. *IEEE Sensors Journal*, *13*(12), 4874–4879. https://doi.org/10.1109/JSEN.2013.2276271

Andò, B., Baglio, S., Bulsara, A. R., Emery, T., Marletta, V., & Pistorio, A. (2017). Low-cost inkjet printing technology for the rapid prototyping of transducers. *Sensors (Switzerland)*, *17*(4), 1–11. https://doi.org/10.3390/s17040748

Aukes, D. M., Goldberg, B., Cutkosky, M. R., & Wood, R. J. (2014). An analytic framework for developing inherently-manufacturable pop-up laminate devices. *Smart Materials and Structures*, *23*(9). https://doi.org/10.1088/0964-1726/23/9/094013

Baisch, A. T., Ozcan, O., Goldberg, B., Ithier, D., & Wood, R. J. (2014). High speed locomotion for a quadrupedal microrobot. *International Journal of Robotics Research*, *33*(8), 1063–1082. https://doi.org/10.1177/0278364914521473

Birkmeyer, P., Peterson, K., & Fearing, R. S. (2009). DASH: A dynamic 16g hexapedal robot. *2009 IEEE/RSJ International Conference on Intelligent Robots and Systems, IROS 2009*, 2683–2689. https://doi.org/10.1109/IROS.2009.5354561

Chung, Y. H., & Lee, J. W. (2001). Design of a new 2 DOF parallel mechanism. *IEEE/ASME International Conference on Advanced Intelligent Mechatronics, AIM*, *1*, 129–134. https://doi.org/10.1109/aim.2001.936442

Correa, J. E., Toombs, J., Toombs, N., & Ferreira, P. M. (2016). Laminated micro-machine: Design and fabrication of a flexure-based Delta robot. *Journal of Manufacturing Processes*, *24*, 370–375. https://doi.org/10.1016/j.jmapro.2016.06.016

Correia, V., Caparros, C., Casellas, C., Francesch, L., Rocha, J. G., & Lanceros-Mendez, S. (2013). Development of inkjet printed strain sensors. *Smart Materials and Structures*, *22*(10). https://doi.org/10.1088/0964-1726/22/10/105028

Costantine, J., Tawk, Y., Maqueda, I., Sakovsky, M., Olson, G., Pellegrino, S., & Christodoulou, C. G. (2016). UHF Deployable Helical Antennas for CubeSats. *IEEE Transactions on Antennas and Propagation*, *64*(9), 3752–3759. https://doi.org/10.1109/TAP.2016.2583058

Demaurex, M.-O. (1999). The Delta Robot within the Industry. In C. R. Boër, L. Molinari-Tosatti, & K. S. Smith (Eds.), *Parallel Kinematic Machines* (pp. 395–399). Springer London. https://doi.org/10.1007/978-1-4471-0885-6

Doshi, N., Goldberg, B., Sahai, R., Jafferis, N., Aukes, D., Wood, R. J., & Paulson, J. A. (2015). Model driven design for flexure-based Microrobots. *IEEE International Conference on Intelligent Robots and Systems*, *2015-Decem*, 4119–4126. https://doi.org/10.1109/IROS.2015.7353959

Enser, H., Kulha, P., Sell, J. K., Schatzl-Linder, M., Strauß, B., Hilber, W., & Jakoby, B. (2018). Printed strain gauges embedded in organic coatings - Analysis of gauge factor and temperature dependence. *Sensors and Actuators, A: Physical*, *276*, 137–143. https://doi.org/10.1016/j.sna.2018.03.042

Evangelista, S. (2011). *The Delta robot – Swiss-made and fastest in the world!* EPFL News. https://actu.epfl.ch/news/the-delta-robot-swiss-made-and-fastest-in-the-worl/

Felton, S., Tolley, M., Demaine, E., Rus, D., & Wood, R. (2014). A method for building self-folding machines. *Science*, *345*(6197), 644–646. https://doi.org/10.1126/science.1252610

French, T. E. (1911). *A manual of engineering drawing for students and draftsmen*.

Gafford, J., Ranzani, T., Russo, S., Aihara, H., Thompson, C., Wood, R., & Walsh, C. (2016). Snap-on robotic wrist module for enhanced dexterity in endoscopic surgery. *Proceedings - IEEE International Conference on Robotics and Automation*, *2016-June*, 4398–4405. https://doi.org/10.1109/ICRA.2016.7487639

Jerançe, N., Vasiljević, D., Samardžić, N., & Stojanović, G. (2012). A compact inductive position sensor made by inkjet printing technology on a flexible substrate. *Sensors*, *12*(2), 1288–1298. https://doi.org/10.3390/s120201288

Koh, J. S., Yang, E., Jung, G. P., Jung, S. P., Son, J. H., Lee, S. I., Jablonski, P. G., Wood, R. J., Kim, H. Y., & Cho, K. J. (2015). Jumping on water: Surface tension-dominated jumping of water striders and robotic insects. *Science*, *349*(6247), 517–521. https://doi.org/10.1126/science.aab1637

Kosinska, A., Galicki, M., & Kedzior, K. (2003). Designing and optimization of parameters of Delta-4 parallel manipulator for a given workspace. *Journal of Robotic Systems*, *20*(9), 539–548. https://doi.org/10.1002/rob.10104

Kramer, R. K., Majidi, C., Sahai, R., & Wood, R. J. (2011). Soft curvature sensors for joint angle proprioception. *IEEE International Conference on Intelligent Robots and Systems*, *September*, 1919–1926. https://doi.org/10.1109/IROS.2011.6048270

Lee, G. Y., Kim, M. S., Yoon, H. S., Yang, J., Ihn, J. B., & Ahn, S. H. (2017). Direct Printing of Strain Sensors via Nanoparticle Printer for the Applications to Composite Structural Health Monitoring. *Procedia CIRP*, *66*, 238–242. https://doi.org/10.1016/j.procir.2017.03.279

López, M., Castillo, E., García, G., & Bashir, A. (2006). Delta robot: Inverse, direct, and intermediate Jacobians. *Proceedings of the Institution of Mechanical Engineers, Part C: Journal of Mechanical Engineering*

Science, *220*(1), 103–109. https://doi.org/10.1243/095440606X78263

McClintock, H., Temel, F. Z., Doshi, N., Koh, J. S., & Wood, R. J. (2018). The milliDelta: A high-bandwidth, high-precision, millimeter-scale Delta robot. *Science Robotics*, *3*(14). https://doi.org/10.1126/scirobotics.aar3018

Mintchev, S., Salerno, M., Cherpillod, A., Scaduto, S., & Paik, J. (2019). A portable three-degrees-of-freedom force feedback origami robot for human–robot interactions. *Nature Machine Intelligence*. https://doi.org/10.1038/s42256-019-0125-1

Pekarovicova, A., & Husovska, V. (2015). Printing Ink Formulations. In *Printing on Polymers: Fundamentals and Applications*. https://doi.org/10.1016/B978-0-323-37468-2.00003-8

Rey, L., & Clavel, R. (1999). The Delta Parallel Robot. In C. R. Boër, L. Molinari-Tosatti, & K. S. Smith (Eds.), *Parallel Kinematic Machines* (Vol. 53, Issue 9, pp. 401–417). Springer London. https://doi.org/10.1007/978-1-4471-0885-6

Rodriguez Leal, E., & Dai, J. S. (2007). From Origami to a New Class of Centralized 3-DOF Parallel Mechanisms. *Volume 8: 31st Mechanisms and Robotics Conference, Parts A and B*, 1183–1193. https://doi.org/10.1115/DETC2007-35516

Russo, S., Ranzani, T., Gafford, J., Walsh, C. J., & Wood, R. J. (2016). Soft pop-up mechanisms for micro surgical tools: Design and characterization of compliant millimeter-scale articulated structures. *Proceedings - IEEE International Conference on Robotics and Automation*, *2016-June*, 750–757. https://doi.org/10.1109/ICRA.2016.7487203

Salerno, M., Zhang, K., Menciassi, A., & Dai, J. S. (2014). A novel 4-DOFs origami enabled, SMA actuated, robotic end-effector for minimally invasive surgery. *Proceedings - IEEE International Conference on Robotics and Automation*, 2844–2849. https://doi.org/10.1109/ICRA.2014.6907267

Salerno, Marco, Firouzeh, A., & Paik, J. (2017). A low profile electromagnetic actuator design and model for an origami parallel platform. *Journal of Mechanisms and Robotics*, *9*(4), 1–11. https://doi.org/10.1115/1.4036425

Sonar, A. V., Burdick, K. D., Begin, R. R., Resch, E. M., Thompson, E. M., Thacher, E., Searleman, J., Fulk, G., & Carroll, J. J. (2005). Development of a virtual reality-based power wheel chair simulator. *IEEE International Conference Mechatronics and Automation, 2005*, *January*, 222–229. https://doi.org/10.1109/ICMA.2005.1626551

Sun, X., Felton, S. M., Wood, R. J., & Kim, S. (2015). Printing angle sensors for foldable robots. *2015 IEEE/RSJ International Conference on Intelligent Robots and Systems (IROS)*, *2015-Decem*, 1725–1731. https://doi.org/10.1109/IROS.2015.7353600

Tanikawa, T., Ukiana, M., Morita, K., Koseki, Y., Ohba, K., Fujii, K., & Arai, T. (2002). Design of 3DOF parallel mechanism with thin plate for micro finger module in micro manipulation. *IEEE International Conference* *on Intelligent Robots and Systems*, *2*(October), 1778–1783. https://doi.org/10.1109/irds.2002.1044013

Temel, F. Z., McClintock, H., Payne, C. J., Wamala, I., Walsh, C. J., Vasilyev, N. V., & Wood, R. J. (2017). Pop-up-inspired design of a septal anchor for a ventricular assist device. *Frontiers in Biomedical Devices, BIOMED - 2017 Design of Medical Devices Conference, DMD 2017*. https://doi.org/10.1115/DMD2017-3458

Tolley, M. T., Felton, S. M., Miyashita, S., Aukes, D., Rus, D., & Wood, R. J. (2014). Self-folding origami: shape memory composites activated by uniform heating. *Smart Materials and Structures*, *23*(9), 094006. https://doi.org/10.1088/0964-1726/23/9/094006

Überblick, E. (2018). *A survey of inkjet-printed low-cost sensors*. *85*, 504–514.

Whitney, J. P., Sreetharan, P. S., Ma, K. Y., & Wood, R. J. (2011). Pop-up book MEMS. *Journal of Micromechanics and Microengineering*, *21*(11), 115021. https://doi.org/10.1088/0960-1317/21/11/115021

Wood, R. J. (2008). The first takeoff of a biologically inspired at-scale robotic insect. *IEEE Transactions on Robotics*, *24*(2), 341–347. https://doi.org/10.1109/TRO.2008.916997

Wood, R. J., Avadhanula, S., Sahai, R., Steltz, E., & Fearing, R. S. (2008). Microrobot design using fiber reinforced composites. *Journal of Mechanical Design, Transactions of the ASME*, *130*(5), 1–11. https://doi.org/10.1115/1.2885509

Wood, R. J., Finio, B., Karpelson, M., Ma, K., Pérez-Arancibia, N. O., Sreetharan, P. S., Tanaka, H., & Whitney, J. P. (2012). Progress on “pico” air vehicles. *International Journal of Robotics Research*, *31*(11), 1292–1302. https://doi.org/10.1177/0278364912455073

Zhakypov, Z., Mete, M., Fiorentino, J., & Paik, J. (2019). Programmable fluidic networks design for robotic origami sequential self-folding. *RoboSoft 2019 - 2019 IEEE International Conference on Soft Robotics*, 814–820. https://doi.org/10.1109/ROBOSOFT.2019.8722798

Zhakypov, Z., & Paik, J. (2018). Design Methodology for Constructing Multimaterial Origami Robots and Machines. *IEEE Transactions on Robotics*, *34*(1), 151–165. https://doi.org/10.1109/TRO.2017.2775655

Zhang, K., & Dai, J. S. (2013). Classification of Origami-Enabled Foldable Linkages and Emerging Applications. *Volume 6B: 37th Mechanisms and Robotics Conference*, 1–9. https://doi.org/10.1115/DETC2013-12227

Zhang, Y., Anderson, N., Bland, S., Nutt, S., Jursich, G., & Joshi, S. (2017). All-printed strain sensors: Building blocks of the aircraft structural health monitoring system. *Sensors and Actuators, A: Physical*, *253*(2016), 165–172. https://doi.org/10.1016/j.sna.2016.10.007

CURRICULUM VITAE

Name Surname : Hasan Sevinç

Place and Date of Birth : Bursa/Turkey – 14.11.1993

E-Mail : hasan.sevinc.h@gmail.com

EDUCATION :

- **B.Sc.** : 2017, Istanbul Technical University, Mechanical Engineering Faculty, Mechanical Engineering

PUBLICATIONS, PRESENTATIONS AND PATENTS ON THE THESIS:

- **Sevinç, H., Samankan, S., Altınkaynak, A., Temel, Z., Acer, M**. 2019. Origami Tabanlı Sensör Entegreli Paralel Robot Tasarımı ve Üretimi, *ToRK 2019 - Turkey Robotics Conference*, 70 – 77.

OTHER PUBLICATIONS, PRESENTATIONS AND PATENTS:

- **Sevinç, H., Durgun, Ö. M., Önalan C., Acer M.** 2017. Mobile Robot Design with Shape Memory Alloys and Foldable Wheel, *TOK 2017 - Turkish National Conference on Automatic Control,* 336 – 341.
- **Aybakan A., Akkız A., Nalbant D., Sevinç H., Kahraman S., Sezer V.** 2018. Design and Control of Autonomous Mobile Security Robot**,** *TOK 2018 - Turkish National Conference on Automatic Control,* 330 – 335.